Gradient Polymers in Tissue Engineering

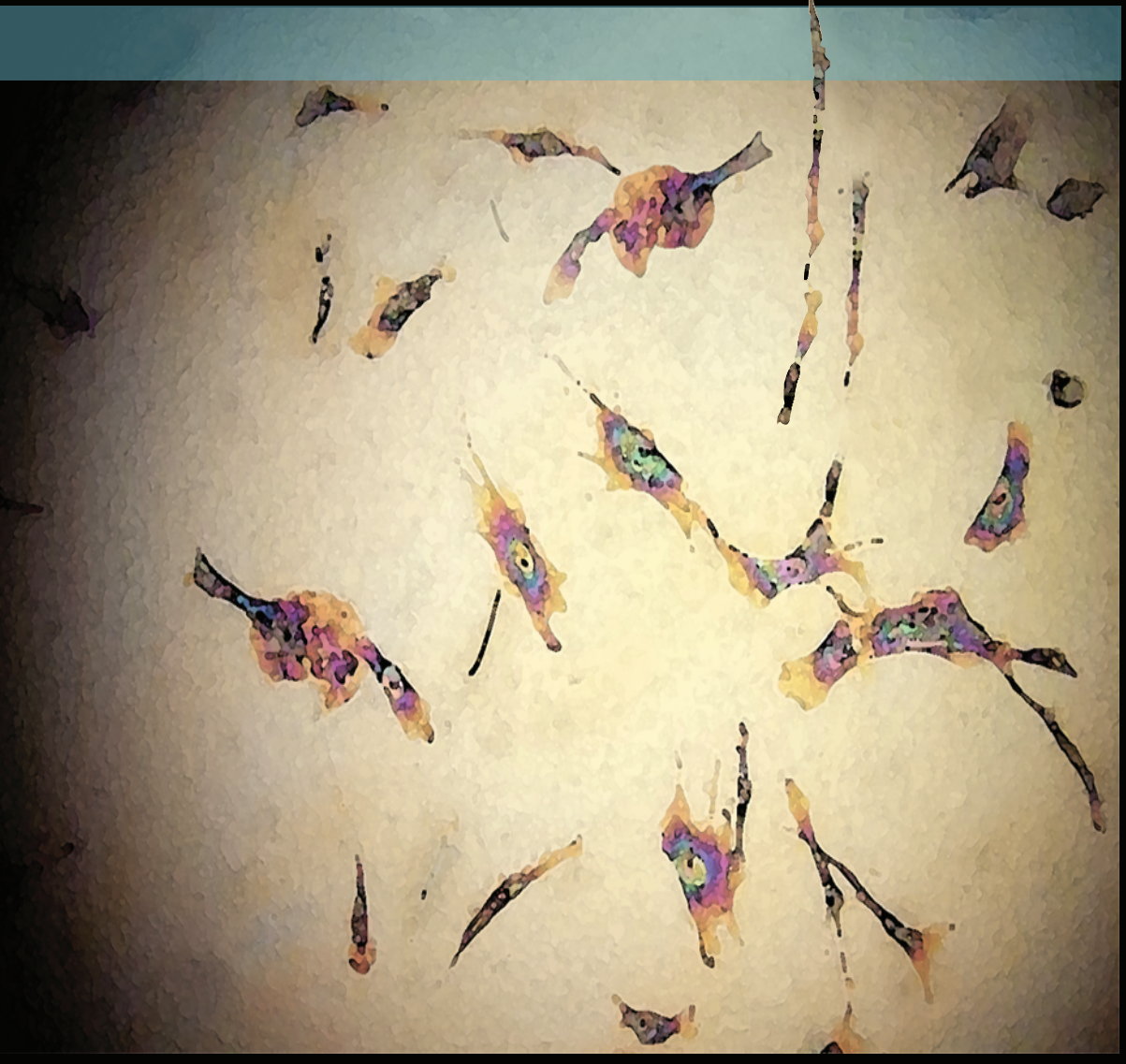

Michel Klein Gunnewiek

Gradient Polymers for Tissue Engineering

Michel Klein Gunnewiek

Members of the committee:

Chairman	Prof. dr. Ir. J.W.M. Hilgenkamp	University of Twente
Promotor	Prof. dr. G.J. Vancso	University of Twente
Assistant-promotor	Dr. E.M. Benetti	ETH Zürich
Members	Dr. L. Moroni	Maastricht University
	Prof. dr. J.J.L.M Cornelissen	University of Twente
	Prof. dr. D.W. Grijpma	University of Twente
	Prof. dr. H.A. Klok	EPFL Lausanne
	Prof. dr. B.M. Städler	Aarhus University
	Prof. dr. Ir. W.E. Hennink	Utrecht University

The work described in this thesis was performed at the Materials Science and Technology of Polymers (MTP) group, MESA+ Institute for Nanotechnology, Faculty of Science and Technology, University of Twente, PO Box 217, 7500 AE Enschede, the Netherlands.

This research was financially supported by the MESA+ Institute for Nanotechnology of the University of Twente and by the Dutch Technology Foundation STW, which is part of the Netherlands Organisation for Scientific Research (NWO) and partly funded by the Ministry of Economic Affairs (11135, Gradient Scaffolds for Tissue Engineering).

ISBN: 978-90-365-3841-1

DOI: 10.3990/1.9789036538411

© Cover design by GR-Artworks - Geneviève Rietveld

Printed by Ipskamp Drukkers in Enschede, the Netherlands

GRADIENT POLYMERS FOR TISSUE ENGINEERING

PROEFSCHRIFT

ter verkrijging van
de graad van doctor aan de Universiteit Twente,
op gezag van de rector magnificus,
prof. dr. H. Brinksma,
volgens besluit van het College voor Promoties,
in het openbaar te verdedigen
op woensdag 1 april 2015 om 14:45

door

Michel Klein Gunnewiek
geboren op 16 mei 1985
te Eibergen, Nederland

Dit proefschrift is goedgekeurd door:

Promotor	Prof. dr. G. Julius Vancso
Assistant-promotor	Dr. Edmondo M. Benetti

Table of Contents

General introduction

1.1 Introduction

With increasing life expectancy, there is an constant demand for finding solutions to restore damaged or diseased tissues and organs. Regenerative medicine holds the promise to create continuous body-part replacements through the combination of cells, biological factors, and synthetic scaffolds. However, a better control over cell-material interactions needs to be achieved to fabricate better performing and long-lasting supports for tissue engineering (TE). In particular, it is still crucial to control cell migration and differentiation into 3D scaffolds mimicking the physical and chemical gradients which naturally regulate and determine these processes within the human body.[1-2] In order to accomplish this, the modification of biomaterials' interfaces represent a potentially successful approach.[3] This encompasses the fabrication of synthetic extra-cellular matrices (ECMs) presenting interfacial gradients which can regulate the behavior of adhering cells.

This Thesis reports different strategies to engineer the surface of TE supports by using a combination of confined polymerizations and controlled functionalization. The materials obtained following these synthetic strategies were characterized by the state-of-the-art surface characterization techniques and they were subsequently applied in the presence of stem cells. The behavior of adhering cells was also studied, devoting particular attention to the influence of interfacial properties (physical) and surface composition (chemical) on stem cell adhesion and differentiation.

A versatile and powerful approach to fabricate physical and chemical surface gradients is by covalently attaching functional macromolecules to the surface of the support (or scaffold) that is meant to function as ECM.[4-5] Covalent attachment of synthetic polymers to form assemblies of tethered chains can be obtained by two

different fabrication methods, namely by “grafting-to” and “grafting-from” strategies (Scheme 1.1). The first technique is based on the covalent linking of functional polymer chains to an active surface.[6] In contrast, during the “grafting-from” approach the assemblies of polymer chains are grown from initiators that are covalently attached to the surface.[7] This last method, thus, encompasses the application of surface-initiated polymerizations (SIPs) which have been developed during the last two decades as confined polymerization reactions.[8] One advantage of SIPs is that in general a higher polymer surface grafting density can be obtained in comparison to the various “grafting-to” methods.[9] In addition, the development of controlled “living” polymerization techniques allowed a fine control over chain length and end group functionalities of the tethered macromolecules.[8-10]

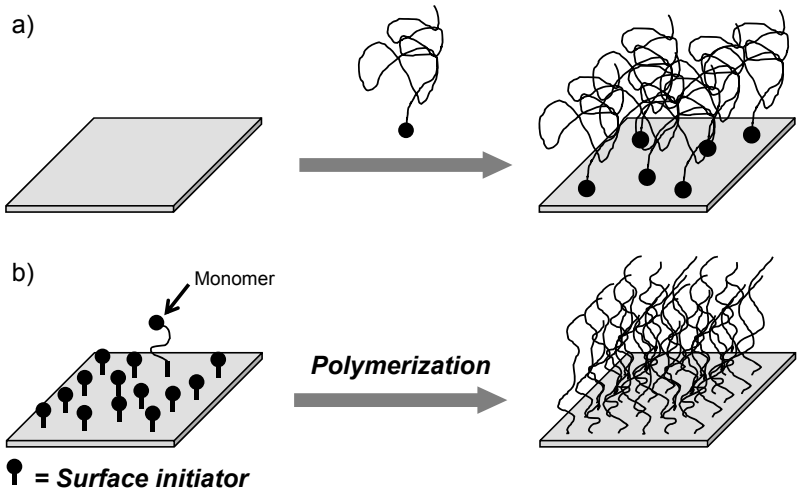

Scheme 1.1. Fabrication of polymer grafts using the “grafting-to” (A) or the “grafting-from” (B) approach.

One of the most reliable SIP methods is based on surface-initiated atom transfer radical polymerization (SI-ATRP). This technique was based on bulk and solution ATRP which was initially proposed by Sawamoto et al.[11] and Matyjaszewski et al.[12] As well and as the homogeneous processes, surface-confined ATRP is compatible to a wide variety of monomers and can be performed under mild reaction conditions (room temperature and aqueous solutions).

The surface-modification approaches which have been the subject of my PhD research and which are reported in this Thesis, focused on SI-ATRP-based modification of biomaterials. The surface tethered macromolecular assemblies which were created have been termed as "polymer brush" layers.[13] This particular nomenclature refers to the peculiar high surface density of macromolecules which could be obtained by SI-ATRP.[14] At relatively low grafting densities, surface-tethered polymer chains collapse on the underlying substrate, assuming a so-called mushroom or pancake regime.[15] However, when the spacing between the individual chains becomes smaller than their size (i.e. radius of gyration), these macromolecules stretch away from the surface as a result of the increased osmotic pressure or to avoid overlapping.[16] Densely packed end-grafted macromolecules in these particular chemico-physical conditions thus behave like "brushes", extending at the interface and maximizing the number of functions per unit area.

In the recent years, polymer brushes produced by SI-ATRP allowed to control different surface properties, such as adhesion, wettability, mechanical properties or bioactivity. The specific response of biomolecules or cells on polymer brush platforms presenting different chemico-physical properties was exploited to fabricate anti-biofouling coatings[17] but also to study the adhesion, migration and differentiation of various cell types.[18] All these processes could be directly modulated by the intrinsic composition of the polymers constituting the brush coating or, indirectly by specific bioconjugation. As an example, poly(*N*-isopropyl acrylamide) (PNIPAM)-based brushes can trigger different cellular responses depending on the temperature of the culture medium.[19-21] Above the lower critical solution temperature (LCST), the polymers collapse forming an hydrophobic layer which stimulate the adhesion of cells. On the contrary, below the LCST PNIPAM brushes showed bio-repellent character avoiding the unspecific adhesion of proteins and cells. As an alternative, antifouling polyethylene glycol (PEG)-based brush coatings can trigger different cell behaviors by opportune pre-functionalization with specific biomolecules.[17, 22]

The bioactivity of these polymer brush coatings have been investigate by using different types of solid substrates (silicon, gold, titanium).[8-9] However, as biocompatible polymers are more often used for polymer-based scaffolds in tissue engineering, poly(ε-caprolactone) (PCL) or other polyester based polymers are

becoming more of interest. Therefore, the research described in this Thesis is focused on the fabrication of polymer brush coatings on biodegradable polyester-based supports featuring both 2D and 3D scaffolds for TE and their application for stem-cells manipulation. SI-ATRP was employed to modify the chemical and physical properties of the scaffolds. In detail, poly(oligo(ethylene glycol) methacrylate) (POEGMA)-based brush layers are applied to drastically modify the effective surface topology and flexibility experienced by living cells. In addition, the wettability of POEGMA coatings was exploited to gradually vary the protein coverage throughout 3D porous structures.

1.2 Concept of the Thesis

Chapter 2 summarizes the application of polymer brush platforms for controlling the adhesion and differentiation of different cell types. Particular attention is devoted to thermoresponsive brush coatings applied for the fabrication of confluent cell sheets towards the development of artificial pre-tissues. Additionally, different polymer brush compositions to tune the response of cells through appropriate bio-conjugation are reviewed. This section highlights the effects of polymer architecture and other macromolecular parameters such as grafting density and biomolecule exposure on the behavior of adhered cells. Finally an overview on the application of polymer brushes for the fabrication of supports for tissue engineering is presented.

Chapter 3 discusses the fabrication of 2D and 3D supports presenting gradients in protein concentration. Firstly, the methods to fabricate protein gradients on flat substrates and on hydrogel surfaces is reviewed. In addition, the latest advances in the formation of protein gradients within 3D hydrogel supports and other porous polymeric scaffolds are presented. At the end of this Chapter, the employment of 2D and 3D gradients for stimulating cell differentiation is discussed.

Chapter 4 describes the surface-initiated polymerization of NIPAM from PCL flat films and the subsequent application of these surfaces for the formation of cell sheets. The chemical and physical properties of these brush supports were first

studied by Fourier transform infrared spectroscopy and atomic force microscopy (AFM). Finally, temperature-modulated cell adhesion and cell film formation are reported together with their reversible attachment onto the brush substrates.

Chapter 5 focuses on the effect of PCL semicrystalline topography on the behavior of adhering stem cells and on the decoupling effect of a thin polymer brush between substrate morphology and cell spreading. PCL films with variations in spherulite size were obtained by spincoating and controlling the parameters of the thermal processing, i.e. crystallization conditions. SI-ATRP of POEGMA and subsequent fibronectin immobilization was applied to mask the underlying PCL topology.

Chapter 6 focuses on the behavior of stem cells adhering on a brush layer containing a linear gradient in chain length (molecular weight). In this study, SI-ATRP of OEGMA was applied to generate functionalizable gradient brush layers from thin PCL films. Following fibronectin immobilization, these layers were applied to study the adhesion of stem cells, concentrating on the effect of brush length and polymer flexibility on the cellular morphology.

In C**hapter 7**, a novel method to introduce multi-directional variations of (bio)chemical environments inside 3D porous structures is introduced. Microporous PCL-based scaffolds constructed by rapid prototyping (RP) were modified by a POEGMA brush coatings to fabricate 3D gradients of different protein types within the constructs. These functional platforms were later on applied for the controlled manipulation of stem cells.

Finally in the **Outlook Chapter,** directions for future research are provided. For instance, options to improve the protein coupling efficiency as well as the activity of growth factors attached on the surface will be discussed. Furthermore, this Chapter will touch upon various brush systems to actively control the wettability of the 3D structure. And at last, the usage of other porous structures will be argued in terms of improving the protein attachment.

1.3 References

1 Lutolf, M. P.; Hubbell, J. A., *Nat Biotech* **2005,** *23,* 47-55.

2 Genzer, J.; Bhat, R. R., *Langmuir* **2008,** *24,* 2294-2317.

3 Tirrell, M.; Kokkoli, E.; Biesalski, M., *Surface Science* **2002,** *500,* 61-83.

4 Morgenthaler, S.; Zink, C.; Spencer, N. D., *Soft Matter* **2008,** *4,* 419-434.

5 Genzer, J., *Annual Review of Materials Research* **2012,** *42,* 435-468.

6 Zhao, B.; Brittain, W. J., *Progress in Polymer Science* **2000,** *25,* 677-710.

7 Tsujii, Y.; Ohno, K.; Yamamoto, S.; Goto, A.; Fukuda, T., Structure and Properties of High-Density Polymer Brushes Prepared by Surface-Initiated Living Radical Polymerization. In *Surface-Initiated Polymerization I*, Jordan, R., Ed. Springer Berlin Heidelberg: 2006; Vol. 197, pp 1-45.

8 Barbey, R.; Lavanant, L.; Paripovic, D.; Schuwer, N.; Sugnaux, C.; Tugulu, S.; Klok, H. A., *Chemical Reviews* **2009,** *109,* 5437-5527.

9 Edmondson, S.; Osborne, V. L.; Huck, W. T. S., *Chemical Society Reviews* **2004,** *33,* 14-22.

10 Matyjaszewski, K.; Tsarevsky, N. V., *Journal of the American Chemical Society* **2014,** *136,* 6513-6533.

11 Kato, M.; Kamigaito, M.; Sawamoto, M.; Higashimura, T., *Macromolecules* **1995,** *28,* 1721-1723.

12 Wang, J. S.; Matyjaszewski, K., *Macromolecules* **1995,** *28,* 7901-7910.

13 Milner, S. T., *Science* **1991,** *251,* 905-914.

14 Pyun, J.; Kowalewski, T.; Matyjaszewski, K., *Macromolecular Rapid Communications* **2003,** *24,* 1043-1059.

15 Brittain, W. J.; Minko, S., *Journal of Polymer Science Part a-Polymer Chemistry* **2007,** *45,* 3505-3512.

16 Bhat, R.; Tomlinson, M.; Wu, T.; Genzer, J., Surface-Grafted Polymer Gradients: Formation, Characterization, and Applications. In *Surface-Initiated Polymerization II*, Jordan, R., Ed. Springer Berlin Heidelberg: 2006; Vol. 198, pp 51-124.

17 Banerjee, I.; Pangule, R. C.; Kane, R. S., *Advanced Materials* **2011,** *23,* 690-718.

18 Raynor, J. E.; Capadona, J. R.; Collard, D. M.; Petrie, T. A.; Garcia, A. J., *Biointerphases* **2009,** *4,* FA3-FA16.

19 Cooperstein, M. A.; Canavan, H. E., *Langmuir* **2010,** *26,* 7695-7707.

20 da Silva, R. M. P.; Mano, J. F.; Reis, R. L., *Trends in Biotechnology* **2007,** *25,* 577-583.

21 Takahashi, H.; Nakayama, M.; Yamato, M.; Okano, T., *Biomacromolecules* **2010,** *11,* 1991-1999.

22 Ma, H.; Hyun, J.; Stiller, P.; Chilkoti, A., *Advanced Materials* **2004,** *16,* 338-341.

CHAPTER TWO

Polymer brush coatings regulating cell behavior: Passive interfaces turn into active

* This Chapter has been published in: L. Moroni, M. Klein Gunnewiek, E.M. Benetti; *Acta Biomaterialia* **2014**, 10, 2367-2378

2.1 Introduction

During the last two decades increasing efforts have been dedicated to tailor the chemical, biological and physical properties of supports and scaffolds meant to function as platform for the attachment, proliferation and differentiation of cells[1]. One of the main goals has been to design interfaces capable of triggering a specific cell response by including the appropriate biological functions and by mimicking the natural extracellular matrix (ECM) counterpart[2]. In addition, rising of tissue engineering (TE) approaches[3-4] stimulated the application of chemical surface modification approaches in order to mechanically support the regeneration of tissues in a biocompatible and naturally degradable environment[5]. This often encompassed fabrication strategies to control and precisely determine interfacial stiffness, wettability and loading of biological functions (such as cell adhesive units or growth factors)[6-9].

These objectives were applied on test surfaces and more structured supports by applying either chemical modification by physical treatment or self-assembled monolayers (SAMs) with variable chemistries. The first approaches could be applied to a variety of supports and often comprised physical and chemical oxidation in order to gain surface functions or simply tune wettability. SAMs were successfully proved as extremely versatile methods to precisely tailor surface chemistry of cell platform[10]. Nevertheless, SAMs suffered restricted applicability on most of the bio-degradable architectures used for housing cells manipulations. To overcome these limitations and concomitantly broaden both

chemical and physical surface modification possibilities, “macromolecular” approaches for the functionalization of bio-interfaces has recently risen as extremely promising methods[11]. This general strategy relied on the surface tethering of polymeric species which can be assembled, grown, or generally *grafted* onto the target surfaces via covalent or physical interactions[12-13]. These assemblies of macromolecules, also termed polymer brushes[14], were successfully applied to both metallic and organic surfaces, acting as versatile coatings for a wide variety of applications in biomaterials science. Dense polymer brush layers present a number of peculiar properties which justified their widespread application in the designing of bio-interfaces. The most relevant can be summarized as: (i) controlled swelling and wettability (which govern biofouling equilibrium), (ii) multifunctional character (to allow bio-conjugation), (iii) adjustable macro-molecular parameters (such as molar mass or grafting density), and (iv) full compatibility to most of support chemistries. Both *grafting-from*[15] and *grafting-to*[16] techniques have been studied and applied for the preparation of brush platforms for cell adhesion and proliferation. Nevertheless, *grafting-from* techniques allowed the generation of denser assemblies featuring fully tunable structural properties such as grafting density and film thickness. To this aim controlled polymerization initiated from surfaces (SIP) and radical processes, in particular, were increasingly developed and refined during the last decade providing “*living*” and “*quasi-living*” growths of macromolecules from surface immobilized initiators[12]. The impossibility to rely on direct methods for the chemical characterization of *grafted-from* polymer brushes often generated a certain uncertainty on the macromolecular parameters such as brush polydispersities and molar mass determination. Despite these drawbacks recently developed fabrication methods allowed the synthesis of *grafted-from* brushes from large area substrates (or specific areas) which, following chain detachment or etching, provided sufficient amounts of polymer solutions for characterization[17-20].

Thus, thanks to the ongoing advances in controlled SIP it could be possible to enable not only a precise control over brush chain length (brush thickness), but also over brush polydispersities and chain end-functions exposed at the interface[21-22]. Specifically, atom transfer radical (ATRP)[23-24], initiator-transfer agent terminator (INIFERTER)[25], and reversible addition-fragmentation chain transfer (RAFT)[26]

polymerizations have been the most applied for the modification of organic and inorganic supports. With these methods not only homopolymer but also block- and random-copolymer brushes[27-32] were successfully fabricated featuring a large number of chemistries and different macromolecular architectures, such as graft- or hyperbranched copolymers[33].

All these methods were used for the synthesis of polymer brush bio-interfaces to repel unspecific protein adsorption or successfully deplete bacteria attachment onto surfaces thanks to the excellent anti-biofouling properties of densely packed, highly hydrated brushes[34]. Some of these characteristics were also exploited to broaden the utilization of polymer brush coatings to form "intelligent" surfaces, closely mimicking ECM characteristics, for the manipulation of cells[35]. In this regard, here we focus on reviewing the fabrication and application of polymer brush layers as platform to study cell activity with the aim of integrating brush coatings within new formulations for the engineering of biomaterials.

The spotlight of this Chapter is centered on *grafting-from* methods for the synthesis of thick brushes given their versatility and universal effectiveness. Starting from poly(ethylene glycol) (PEG)-based brush systems by SIP, which have been historically among the first ones to be used for biomedical applications, we will summarize the most relevant brush surfaces presenting different chemistries and which were applied as cell-sensitive substrates. We will later on describe the latest developments in the synthesis of thermoresponsive brush interfaces, which have been successfully employed for reversible cell adhesion, cells separation and cell sheet engineering. The last section of this review finally reports the most recent advances in the designing of polymer brush coatings for stem cells manipulations. A particular attention in this last section will be devoted to the application of well determined brush chemistries and the employment of their peculiar physical properties for tissue engineering and regenerative medicine.

2.2 Bio-active polymer brushes: From PEGs to multifunctional grafts

With the adjective “bio-active” referred to polymer brush surfaces we define those assemblies of densely grafted macromolecules which, due to their peculiar chemistries and/or physical characteristics, are able to determine the response of adhering cells towards particular metabolic or morphological behavior. This high potential of brush coatings is a direct consequence of their tunable chemical and physical properties, which made them the ideal platforms to simulate distinct interfacial environments, which could mimic the ones of natural ECM.

Among the large variety of hydrophilic polymers, which have been tested up-to-date for the fabrication of brush bio-interfaces, the “gold standard” is represented by PEG and its derivatives, grafted through diverse strategies on a number of solid supports. Given its high hydrophilicity, PEG-based adsorbates were classically applied to confer a bio-passive character to metallic and non-metallic surfaces. Linear, hyperbranched and dendronized PEG films were thus produced in order to provide inert interfaces in biological media[36-38]. Nevertheless, the requirement of enhanced bio-conjugation of biological cues to promote bio-specific cell response on otherwise inert PEG surfaces increasingly triggered the use of radically polymerizable PEG- or oligo(ethylene glycol) (OEG)-containing (macro)monomers to be applied together with SIP in the synthesis of thick, dense and functional brush coatings[39]. These species, compared to end-functional or copolymer PEG-based adsorbates could be easily *grafted-from* initiator-activated supports either by surface-initiated aqueous ATRP or by other radical methods[39-48]. The use of hydroxyl-terminated OEG and PEG methacrylate/acrylate species thus allowed the fabrication of brush films with multiple anchoring points whose concentration can furthermore be adjusted by varying the degree of polymerization and thus chain length and brush film thickness[43]. In addition, the length of PEG side-unit could be varied by appropriately choosing the (macro)-monomer specie to obtain different swelling and mechanical properties of the films[41]. This modularity associated to its inert character resulted in a great interest in PEG-based brushes as a potential blank state onto which engineer different biological moieties and study how the biological microenvironment can be decoupled.

OEG-polymethacrylate (POEGMA) brushes were reported to form cell adhesive polymer bio-conjugates via either chain-ends or side chains coupling of cell-cues like RGD peptides or fibronectin (FN)[41], growth factors (GFs)[49], or collagen I[43]. On end-functionalized surface-grafted POEGMA brushes bio-adhesive proteins were exposed at the ECM interface keeping the underlying brush un-functionalized. By this method Klok et al. proved a relevant effect of the brush architecture, i.e.PEG side chain length, on the morphology of adhering human umbilical vascular endothelial cells (HUVECs)[41] (Figure 2.1). In this study RGD-functionalized POEGMA brushes featuring different OEG side chain lengths were reported to induce a different densities of focal adhesion (FA) complexes, and thus integrin-ligand affinities as a result of diverse brush swelling.

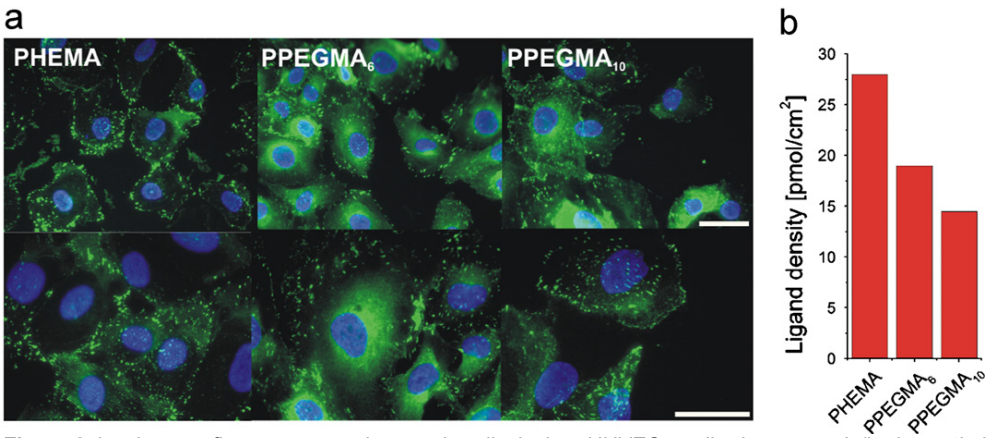

Figure 2.1. *Immunofluorescence micrographs displaying HUVECs adhering on poly(hydroxyethyl methacrylate) (PHEMA) and POEGMA brushes featuring different OEG side chains length. Given the increase of brush swelling with the increasing length of OEGs ligand-integrin affinity showed a reduction which resulted in a relative decrease of ligand density among the different brush surfaces tested. Reprinted from REF 41, Copyright 2007, with permission from Elsevier.*

In order to tune the physical properties and the cell adhesive character of POEGMA brushes the surface grafting density was also varied by diluting the initiator of the starting monolayers. By this approach, polymer grafting densities ranging from 0.02 to 0.35 chains/nm^2 were obtained. Subsequent physical adsorption of RGD-containing peptides showed a consequent variation of peptide loading within the brush from around 0.2 to 0 ng/mm^2 in the case of the most

diluted and densest brushes, respectively[45]. This variation of peptide concentration in the brush architecture thus translated into a different number of adhering MC3T3 cells among the different peptide-bearing films.

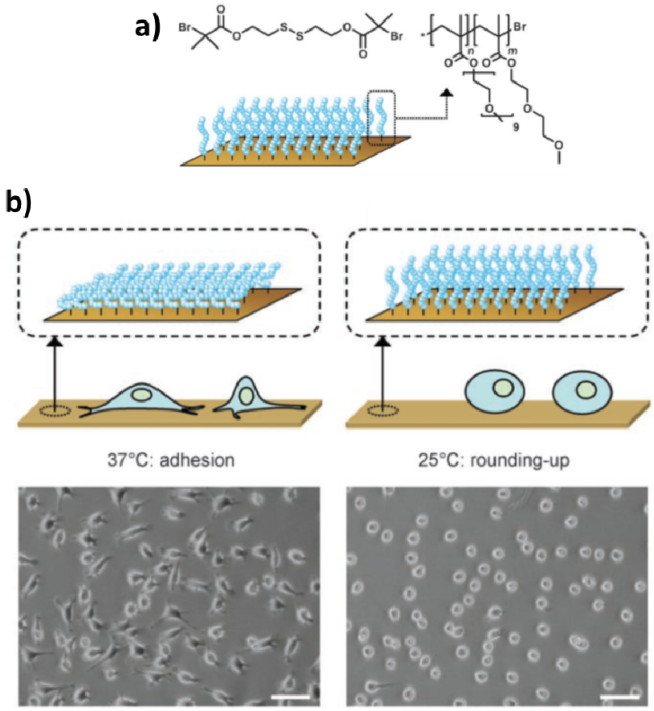

Figure 2.2. *The chemical composition of both ATRP initiator molecules assembled on Au surfaces and the subsequently grafted thermo-responsive OEGMA-based random co-polymer (a). The surface grafted POEGMA brushes were subsequently used for the reversible adhesion of L929 mouse fibroblasts across brush LCST as shown on the reported optical micrographs in (b). Adapted from REF 50.*

Following similar fabrications based on surface-initiated ATRP random copolymer brushes of 2-(2-methoxyethoxy)ethyl methacrylate (MEO_2MA) and OEGMA [50] were prepared to produce switchable fouling/non-fouling surfaces for the controlled adhesion and subsequent detachment of various cell types (Figure 2.2). These brush surfaces showed a sharp transition from the swollen hydrophilic to the collapsed hydrophobic state across a physiological temperature range (30-35°C)[51-52]. Thus, cells were harvested at 37°C allowing stable surface attachment

without the need of any adhesive cue, while they were released by lowering down the culture temperature at 25°C following a completely reversible process without any change of cell viability.

These temperature-responsive brushes were applied for the controlled attachment/detachment of both L929 mouse fibroblast and MCF-7 breast cancer cells demonstrating how different cell lines followed distinct adhesion and desorption mechanisms on brush coated surfaces[53].

The temperature-driven transition of some OEG-based amphiphilic brushes was subsequently exploited for the fabrication of cell sheets and their isolation, providing a potential study platform for the generation of artificial epidermis components[54]. This method allowed the formation of a confluent fibroblast film after 24h followed by uniform and ready lift off of the cell sheet by lowering the temperature below 20°C as depicted in Figure 2.3.

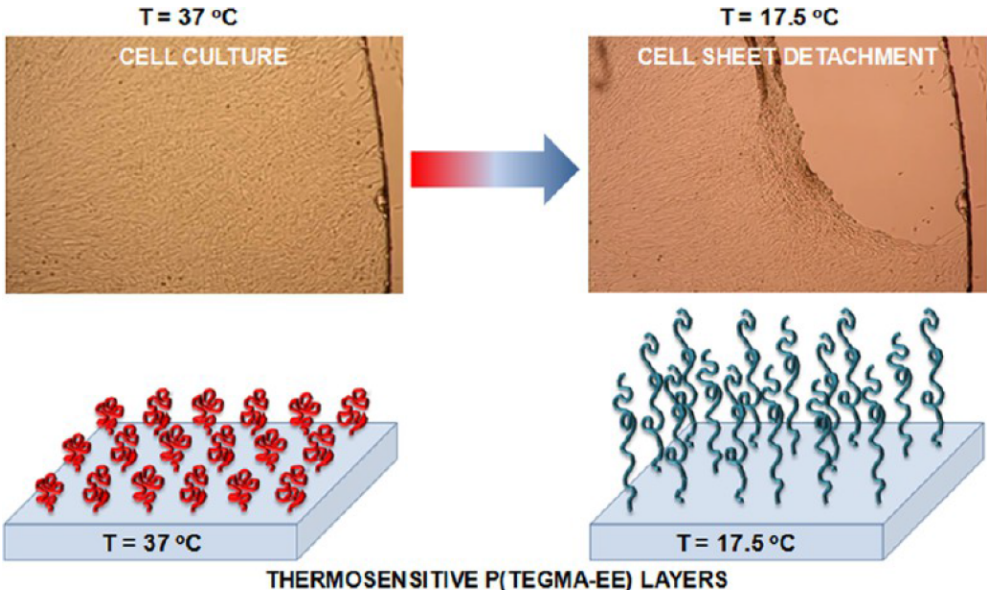

Figure 2.3. *Schematic depicting poly[tri(ethylene glycol) monoethyl ether methacrylate] (P(TEGMA-EE)) brushes thermo-responsive transition and subsequent formation of confluent fibroblast cell sheet. Adapted with permission from REF 54. Copyright 2013 American Chemical Society.*

It has to be mentioned that despite the widespread application of PEG-based coatings in the designing of biologically inert and highly functionalizable

brush coatings a new class of biocompatible polymers based on poly(2-oxazoline)s (POXs) has recently emerged[55-57]. These polymers were increasingly applied for the synthesis of drug delivery systems[58] and drug-conjugates and showed excellent biocompatibilities and stealth properties if compared to PEGs standards[59-60]. Consequently, POX-based brushes to fabricate bio-inert and functional coatings were also introduced in some recent reports by our group[61-64] and Jordan et al.[65-67]. In these specific applications POX coatings showed improved antifouling properties and stability against oxidative degradation compared to PEG analogues[63-64]. In addition a recent work by Jordan et al. demonstrated how POX-based *grafted-from* brushes featuring tunable chain-end chemistries and POX composition could effectively function as platforms for the controlled adhesion of cells[66].

In addition to PEG-based (macro)monomers several other methacrylate, acrylate and acrylamide-based species were efficiently grafted by controlled radical SIP in order to produce platforms for cell adhesion and proliferation. In many cases, these species allowed extensive conjugation of protein cues if compared to PEG-based monomers thus amplifying the cell response at the brush surface. Among the proposed chemistries poly(acrylic acid) (PAA) and poly(methacrylic acid) (PMAA) brushes[68-70], poly(glycidyl methacrylate) (PGMA)[71], poly(hydroxyethyl- and poly(hydroxypropyl methacrylate) (PHEMA and PHPMA)[72] brush films proved as efficient platforms for enhancing the bio-conjugation of cell adhesive cues and subsequent attachment of cells. Specifically, PAA and PMAA were applied to determine the effects of brush micro- and nano-architectures on the response of adhering cells. Ober et al.[68] studied PAA brush micropatterns on silicon oxide surfaces as platforms for the adhesion of RBL mast cells (as shown in Figure 2.4). In this report, unfunctionalized PAA grafts were shown to first repel cell spreading, which was initially concentrated at the silicon oxide surface. Later on, PAA brush patterns were shown to progressively accumulate the FN molecules secreted by RBL cells within the brush architecture, which induced an increasing spreading of cells membrane on the PAA brush over the incubation time. This platform also demonstrated the extraordinarily versatile character of brush films which, thanks to their multi-functionality, controlled swelling, and quasi-3D architecture, can efficiently function as study-boards for cell attachment and organization on synthetic ECM supports.

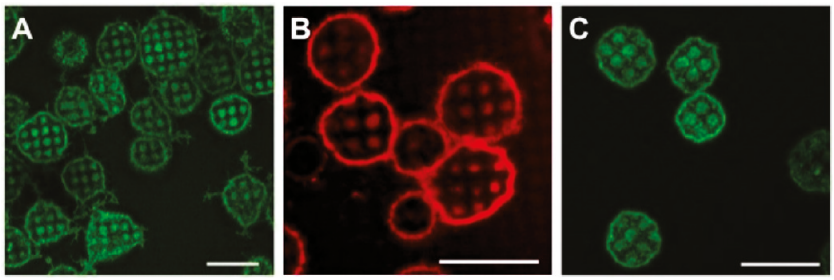

Figure 2.4. *RBL cells spreading on micro-patterned PAA brushes and accumulating plasma membrane on the brush structures. The fluorescent micrographs reports three different fluorescent markers specific for different membrane components, namely A488-IgE that binds to FcεRI (a) showed as green staining, TR-DPPE that partitions into the membrane lipid bilayer (b) (red staining) and A488-CTxB that binds to ganglioside GM1 (c) and it is evidenced as green staining. Adapted with permission from REF 68. Copyright 2011 American Chemical Society.*

In other reports multifunctional surfaces fabricated by *grafted-from* polymer brushes were exploited to mediate surface attachment of cells through reversible coupling of carbohydrate species. Glucose containing molecules and biopolymers are often playing a key role in cell-ECM interactions and they are specifically related to the metabolism of cancer cells. Since a typical ligand for carbohydrate-bearing species is boronic acid, boronate-containing polymer brushes featuring N-acrloyl-m-aminophenylboronic acid (NAAPBA) were thermally grafted from both flat and nano-structured silicon surfaces in order to complex glucose-based biomolecules and subsequently mediate the adhesion of various cells lineages. Specifically, the controlled attachment of both murine hybridoma (M2139), human acute myeloid leukaemia (KG1) and breast cancer cells (MCF-7) was successfully accomplished[73].

Multiple binding capability expressed by dense brushes proved as an effective mean to alternatively stimulate cell adhesion (with PBA in the anion form, at high pH values) through carbohydrate-mediated adhesion, and allowed subsequent “fast” release of the adhered cells in the presence of brush-capping glucose preparations complemented within the cell culture media. The rate of responsiveness of this particular brush-cell reversible interaction was increased by varying the pH of the medium, thus influencing the complexing ability of PBA moieties (Figure 2.5)[74-75]. Additionally, fully reversible and fast attachment-detachment cycles (which maintained high cell viability) were obtained by applying

these brush coatings on high aspect-ratio surfaces like silicon-oxide nanowires, previously proved to maximize cell-surface interactions and response (Figure 2.5)[73].

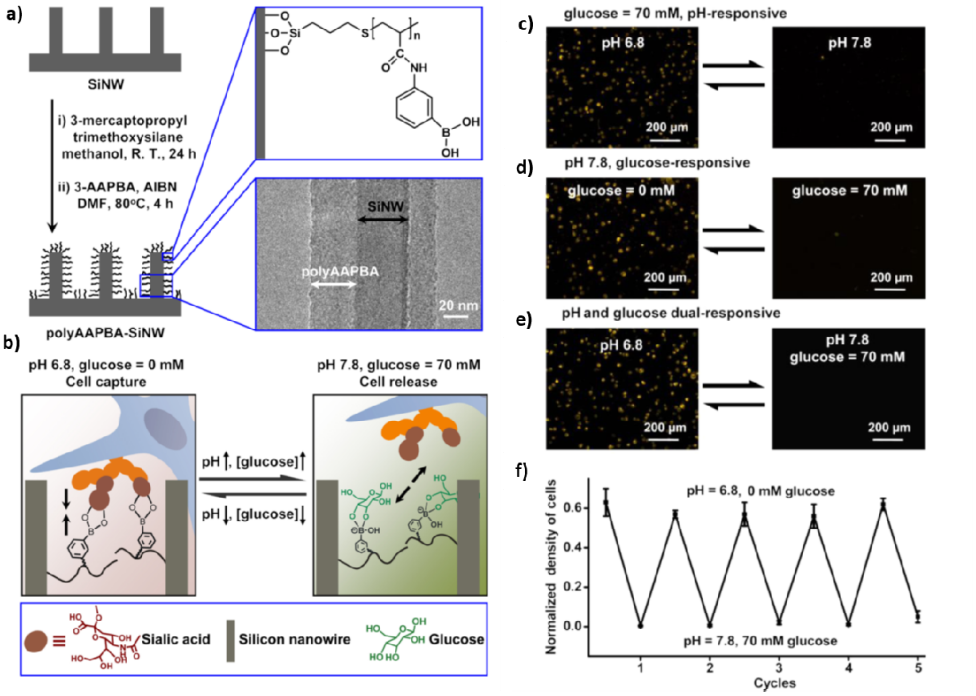

Figure 2.5. *The pH and glucose dual-responsive character of PAAPBA brushes grafted from silicon nanowire surfaces (a and b). At low pH values the uncharged boronic acid functions at the brush surface trigger cell adhesion via complexes with sialic acid at the cell membranes; at high pH values, instead, and/or in the presence of glucose species brush PBA functions are made unreactive towards membrane functions and cells are released from the surface. The dual-responsive nature of these cell sensitive surfaces is reported in c), d) and e), while the full reversibility of the process is exemplified by monitoring the cell density following consecutive pH and glucose concentration variations in f). Adapted from REF 73. Copyright 2013 American Chemical Society.*

The enhancement of bio-chemical interaction by multifunctional polymer brushes if compared to mono-molecular layers or SAMs was also exemplarily demonstrated by Sun and co-workers[76-77], who focused on the effects of chirality on cell behaviour at surfaces. In these studies, the authors first showed how cells respond to different stereochemistry of SAMs, modulating their adhesion due to the intrinsic chiral character of amino-acids constituting cells membrane proteins[76].

Secondly, they successfully demonstrated how the stereospecific adhesion of fibroblasts was substantially amplified by grafted-from brushes of poly-N-acryoyl-L(D)-amino acid. In particular, cells responded to L-films by enhancing spreading and attachment with lower apoptosis if compared to the corresponding D-films[77]. The concept of polymer brush multi-functionality was also applied and extended with the fabrication of layered brush structures and block-copolymer brushes as platforms for cell adhesion. These brush films were fabricated, as an example, by sequential photo-grafting of methacrylic acid (MA) to obtain vertically structured PMAA brushes by Navarro et al.[69].

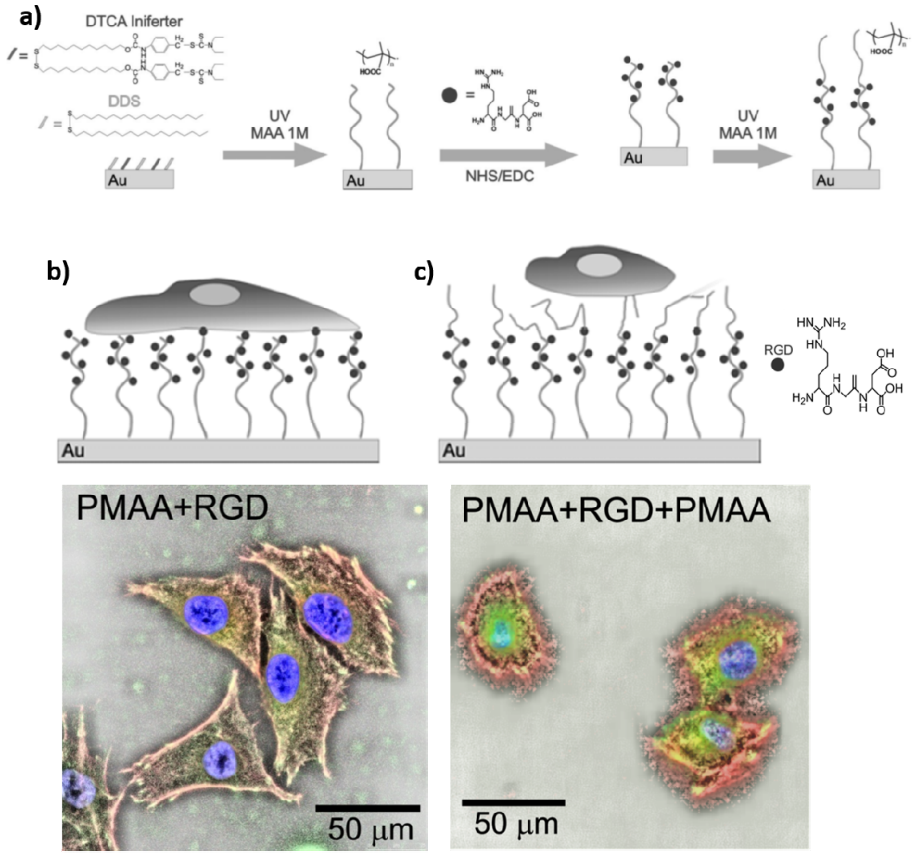

Figure 2.6. *Fabrication of stratified PMAA brushes by sequential INIFERTER SIP alternated by coupling of RGD sequences (a); the response of MC3T3 cells upon adhesion to PMAA-RGD interfaces (b) and PMAA brush layers "burying" the bio-functional films (c). The cells were shown to adapt their morphology in response to the accessibility of the ligands. Adapted from REF 69. Copyright 2008 American Chemical Society.*

PMAA brush films were first grafted by INIFERTER SIP method, and later on functionalized with cell-adhesive RGD sequences. By final re-initiation of SIP the cell-adhesive brush layer could be "buried" under an additional PMAA layer. The so-vertically-structured films were shown to induce different MC3T3 cell morphologies upon adhesion where cells spread uniformly on RGD-rich interfaces while re-adapt their morphologies to more rounded ones when adhering on brush-covered RGD-brush conjugates (Figure 2.6).

A step-forward in the application of brush platforms beyond the promotion of cell adhesion and proliferation was accomplished by incorporating functions and/or biological cues which stimulate cell differentiation towards determined tissue types. This strategy brought the already well-developed bio-conjugate brush films to more closely mimic ECM environments, thus stimulating the behaviour of adhering cells first on flat surfaces[43] and later on surface-structured implants[78]. Following these approaches GFs were covalently linked to poly(OEGMA-r-HEMA) brush surfaces along with cell adhesive cues in order to induce the differentiation of the preosteoblast MC3T3-E1 cells[49]. Alternatively, random-copolymer brushes presenting both functionalizable HEMA monomers for adhesive peptides immobilization and phosphate-bearing methacrylates (MEP) to promote matrix mineralization, were grafted and subsequently incubated in the presence of MC3T3-E1 (Figure 2.7). By adjusting co-monomers relative concentrations, poly(HEMA-r-MEP) brushes kept bio-specific characteristics and allowed efficient conjugation of GGGRGDS peptide sequences enabling cell attachment on the brush surface. MEP functions concomitantly stimulated matrix mineralization by mimicking the natural composition of bone ECM[79].

The development of multifunctional brush platforms capable of directing the differentiation of cells quickly developed towards the application of pluripotent stem cells. This encompassed the application of chemically structured polymer brushes and stem cells on both flat study platforms and 3D supports or implants for tissue regeneration. These topics are specifically addressed in Section 3 of this review.

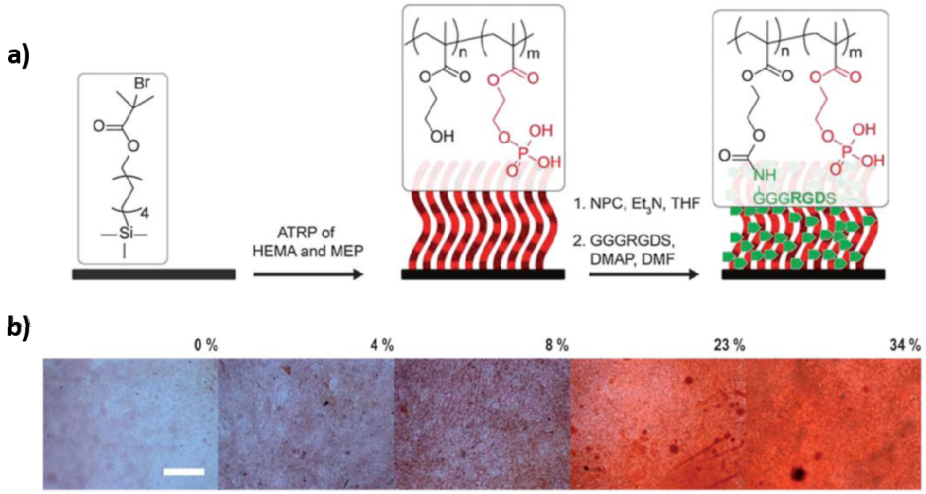

Figure 2.7. *Fabrication of "osteoconductive" P(HEMA-co-MEP) brushes by SI-ATRP (a) and Alzarin red assay showing an increase of matrix mineralization of MC3T3-E1 adhered on P(HEMA-co-MEP) brush surfaces with the relative concentration of MEP co-monomer (indicated by the percentage on top of the relative micrograph) (b). Adapted from REF 79 with permission of from The Royal Society of Chemistry.*

2.3 Thermo-responsive PNIPAM brushes for cell manipulations

The peculiar thermo-responsive properties of PNIPAM, i.e. a LCST within physiological conditions at 30-32°C, have been exploited to fabricate polymer brush films alternatively presenting hydrophilic and hydrophobic characters by varying the temperature of the incubation medium[21, 80-81]. Increase of temperature above LCST is accompanied by a coil-to-globule transition of PNIPAM grafted chains which allowed surface attachment of proteins from culture media[82-88]. Thus, PNIPAM brushes undergo a transition from anti-biofouling below their LCST, to biofouling above their LCST[89]. This transition was increasingly exploited during the last decade to control the adhesion of different cell types by producing reversibly adhesive substrates for culturing. Particularly, in the group of Okano PNIPAM brushes were applied to develop "cell sheet engineering"[90] providing an effective strategy to fabricate confluent assemblies of cells on thermally collapsed films which were subsequently released from the surface as self-standing sheets by

simply lowering down the culture temperature below LCST[91-99]. In these studies, the application of surface-grafted polymers presenting tunable cell-adhesive properties represented a substantial advance if compared to the commonly used enzymatic treatments which partially damage cells ECMs and cell-to-cell connections formed during culturing on solid substrates.

As proven in several recent reports and concomitantly theoretically described[91-100], cell attachment on PNIPAM brushes at 37°C (above LCST) was caused by the collapse of grafted chains which favor primary and ternary adsorption of cell adhesive protein cues present in the culture medium. This adsorption processes take place at the underlying substrate or SAM supporting the brush layer (also termed "grafting surface") and by chain-protein interaction within the brush, respectively (Figure 2.8)[101-102]. Furthermore these mechanism were found favored if compared to secondary adsorption, which involves protein attachment at the external brush-medium interface. Thus, adjustment of brush grafting density and chain length by surface dilution of initiator molecules, and application of controlled radical SIPs (such as RAFT[91] or ATRP[97]) allowed tuning of both cell attachment and detachment across the LCST.

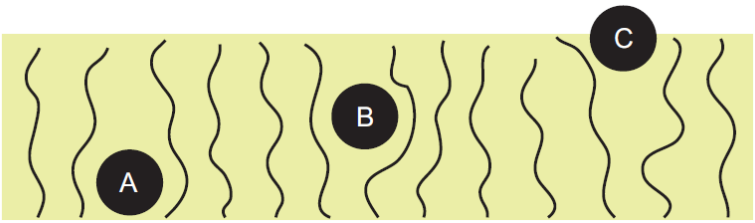

Figure 2.8. *Schematic depicting the different modes of protein adsorption on polymer brush surfaces: A) primary adsorption at the grafting surface; B) ternary adsorption due to polymer-protein interactions within the brush structure; C) secondary adsorption at the brush-medium interface. Reproduced from REF 100, Copyright 2012, with permission from Elsevier.*

Specifically, at high grafting densities protein adsorption is minimized both below and above LCST due to hydration and, generally, due to the osmotic pressure penalty that proteins have to overcome adhering to an unperturbed brush surface[100]. In these cases few cells could adhere on the collapsed PNIPAM brush unless long incubation times were performed, particularly when the fabrication of

confluent cell sheets is targeted. Oppositely, cells detachment at temperatures below LCST was favored by high grafting densities and longer chains due to the higher hydration and bio-repellency of these brush systems when they are completely swollen[91]. These brush-effects on cell adhesion and release across the LCST were all found dependent on the disjoining force between protein-mediated surface-attachments of cells and the osmotic pressure counterpart exerted by a reversibly collapsed or swollen brush interface[100]. The balance of these two forces thus determined the adhesion/release of cells from PNIPAM brushes.

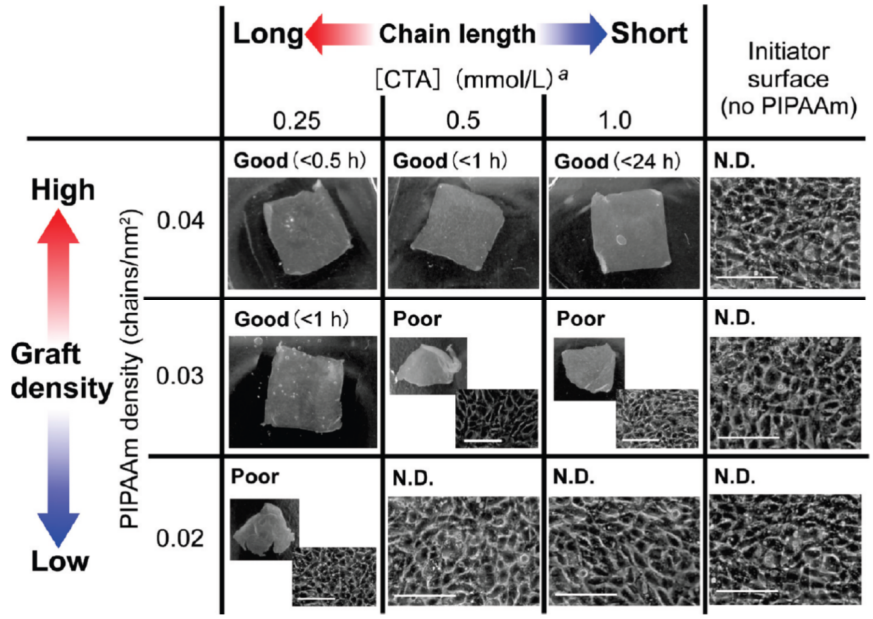

Figure 2.9. *The fabrication of cell sheets as reported in REF 91 from different PNIPAM brushes featuring various grafting densities. "Good" and "N.D." (not detached) indicate complete cell sheet harvest by reducing temperature (20 °C) and no cell sheet detachment within 24 h by reducing temperature, respectively. "Poor" indicates that some cell sheets showed complete harvest within 24 h but some of them could not. By varying the initiator surface concentration and the RAFT polymerization process PNIPAM brushes were shown to present variable grafting densities ranging from 0.02 to 0.04 chains/nm^2 and chain lengths (approximately between 20000 Da, for "short" brushes and 50000 Da for "long" brushes). Adapted with permission from REF 91. Copyright 2010 American Chemical Society.*

Following these fabrication methods, Okano et al. successfully assembled cell sheets featuring diverse cell types such as bovine carotid artery endothelial cells (BAECs)[91] and normal human dermal fibroblasts (NHDFs)[92], among others. Later on, epithelial cell sheets fabricated by PNIPAM brush-mediated attachment/proliferation/detachment were successfully applied for corneal reconstruction[103-104] and transplanted to treat oesophageal ulcerations (Figure 2.9)[105].

Reversible cell attachment on thermo-responsive brushes was also found dependent on the particular cell type. Specifically, if brush characteristics allowed indistinct adhesion of various cells, the rate of cell release from PNIPAM surface at low temperatures depended on the characteristics of that particular cell line[97]. Exploiting this different behavior and by carefully tuning brush length and grafting densities, different cells, co-cultured in the same medium, were shown to adhere onto collapsed PNIPAM brushes above the LCST and selectively be released by lowering down the temperature. In this way PNIPAM brush surfaces acted as effective cell separating surfaces[95, 97-98] (Figure 2.10).

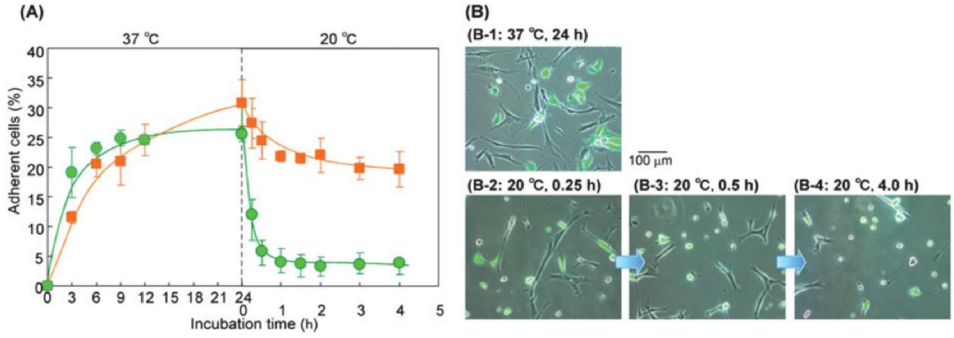

Figure 2.10. *Cell adhesion and detachment from a PNIPAM brush surface with optimized grafting density and chain length (A). The green circles and the orange squares in (A) represent human umbilical vein endothelial cells (HUVEC) and human skeletal muscle myoblast cells (HSMM), respectively, which adhered on the brush surface and later on detach following different rates at low temperatures. In the micrographs reported in (B), the co-cultured cells adhering indistinctively at 37°C (B-1) are shown, while at lower temperatures HSMMs are released faster than green fluorescent protein (GFP) expressing HUVECs (B-2 to B-4). Reproduced from REF 97 with permission from The Royal Society of chemistry.*

Several strategies were also applied to modify the chemical characteristics of PNIPAM brush layers in order to chemically tune the temperature driven attachment/detachment of cells. Specifically, block-copolymerization was applied to either introduce hydrophobic polystyrene segments at the outer brush interfaces[106] or co-monomers allowing coupling of cell adhesive cues[107]. Following similar synthetic strategies, RGD functionalized PNIPAM-PAA copolymer brushes showed enhanced adhesion of human hepatocellular liver carcinoma cells (HepG2), while co-polymerization of PNIPAM with 2-carboxyisopropylacrylamide (CIPAM) allowed the coupling of heparin functions on poly(NIPAM-co-CIPAM) brushes[99]. In this last case, the presence of heparin sites triggered the adhesion of cell-adhesive proteins and growth factors thus inducing steadily attachment and proliferation of mouse fibroblasts (NIH/3T3) above polymer LCST. Confluent cell sheets were subsequently released at lower culture temperature.

Co-polymerizations of NIPAM with more hydrophilic (such as CIPAM, acrylic acid AA or 3-acrylamidopropyl triethylammonium chloride APTAC) and hydrophobic monomers (as N-tertbutylacrylamide) were also applied from silica/glass micro-particles in order to form thermo-responsive dispersible microparticles for cell culture. These systems were subsequently applied for large scale culturing of mammalian cells (like Chinese hamster ovary cells; CHO-K1) on dispersed microcarriers and showed relevant enhancement of cells proliferation and subsequent viability in the absence of any sequential trypsinization[94, 96].

In summary, the application of PNIPAM-based brushes to produce a variety of reversible cell-adhesive platforms opened new possibilities not only for studying cell behavior at surfaces but also to engineer cell sheets ready to transplantation, separate different cell types and improve the efficiency of cell cultivation methods. These approaches, featuring the application of a relatively “old” polymer on “new” fabrications, are increasingly revealing new efficiencies for the development of “intelligent” biomaterials.

2.4 Polymer brushes directing stem cell behavior: Next generation coatings for regenerative medicine

As regenerative medicine strategies are focusing more and more on instructive biomaterials able to recruit cells *in situ* and steer their fate, polymer brushes can find a fertile ground in this field thanks to the flexibility with which they can be designed and synthesized on different substrates. We have previously discussed several examples where polymer brushes were used as smart linkers to present chemical moieties and biological cues to already specialized cells to influence their activity. This strategy could be even more powerful when applied to stem cells, which are known to be able to differentiate into several type of mature cells at the base of tissues and organs in our body. In this respect, polymer brushes could serve as a powerful platform that has the potential to steer which tissues are formed starting from a single cell source and depending on the intimate degree of interaction with the chosen stem cell population. A few recent studies showed, for example, that poly 2-(methacryloyloxy)ethyl]dimethyl-(3-sulfopropyl)ammoniumhydroxide (PMEDSAH) and POEGMA brushes can be used to selectively adhere bone marrow derived mesenchymal stem cells (MSCs)[108]. While PSBMA brushes were only used to show preliminarily selective adhesion of MSCs on the brush-functionalized culture substrates[109], POEGMA brushes were used to create functional linkers on medical grade titanium implants and covalent bind different FN domains that induced MSCs osteogenic differentiation through enhanced integrin-mediated adhesion[108]. When implanted in the tibia of rats, these functionalized implants results in a much better osteointegration than unfunctionalized titanium, thus proving that the brushes are also effective as smart linkers imparting instructive properties to biomaterials in vivo (Figure 2.11).

Polymer brushes could be also used to provide physico-chemical and biological cues to study fundamental biological processes. To obtain a large number of cells for tissue engineering and regenerative medicine applications, cells need to be expanded. To do this, it is of pivotal importance to use highly defined culture conditions when using stem cells, so that the original undifferentiated cell phenotype can be maintained during expansion. Polymer brushes can serve this purpose due to the high control that can be achieved when synthesizing them onto

a culture substrates. Poly(OEGMA-co-HEMA) and poly(L-lysine) brushes were used to culture human induced pluripotent stem cells and mouse fetal liver stem cells, respectively[110-111]. While the former brushes could maintain stem cell phenotype unaltered for at least 10 passages[110], the latter films could regulate stem cell maintenance or differentiation into hepatocytes depending on the brush density and consequently on the substrate stiffness[111]. PMEDSAH brushes were also applied to maintain human embryonic stem cells in defined culture. Results showed that this was possible for up to 15-20 passages and typical markers for stem cell undifferentiated state were expressed at similar level than when golden standard culture substrates like Matrigel were used[112]. Similarly, PSBMA grafting density was demonstrated to affect the degree of hydration of the underlying culture substrate and showed to maintain hematopoietic stem and progenitor cells undifferentiated at an optimal density of 0.1 mg/cm^2.[113]

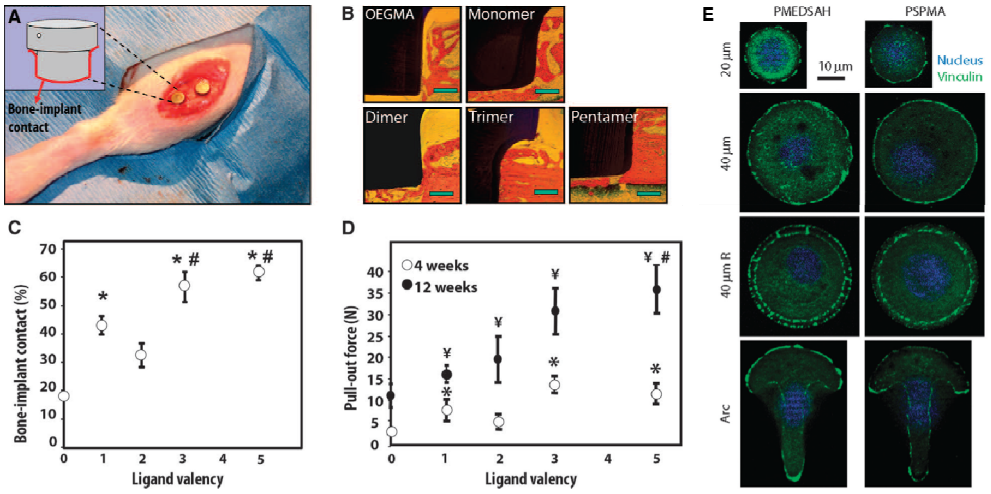

Figure 2.11. *Titanium implants (A) resulted in enhanced (B) integration with the surrounding tissues after fibronectin functionalization via POEGMA brushes. This was associated to a higher amount of (C) bone contact area and by (D) a higher interfacial strength, depending on the ligand valency of the fibronectin domains covalently bound to the PEOGMA brushes. From REF 108. Reprinted with permission from AAAS (E) The use of PMEDSAH and PSPMA modified substrates resulted in modulating focal adhesion patterns, as shown by vinculin staining after 24 hours from incubation, on different pattern geometries. Adapted from REF 114 with permission from The Royal Society of Chemistry.*

Tan et al.[114] proposed an elegant approach to micropattern defined geometrical domains with different polymer brush chemistries and studied the influence of selectively adsorbed ECM domains on epidermal stem cell adhesion, morphology, and differentiation. The authors showed that substrates with a negative potential were correlated with a higher degree of cell differentiation, which was connected to the formation of less focal adhesion despite no variations in cell morphology (Figure 2.11). A similar approach was used to create micro-engineered epidermis that can serve as an in vitro model to study drugs toxicity and the phenomena occurring in presence of disease cells, such as cancer cells[115].

Although studies showing the beneficial effect of polymer brushes to engineer the biological interface with stem cells are just starting to arise, the potential of polymer brushes is countless. By tailoring their chemistry, spatial arrangement, and length, we could envision to create new platform of biomaterials where more than a cell function can be accurately controlled and the biological function of more complex heterogeneous systems could be recapitulated in a synthetic manner. This would offer the tremendous possibility to decouple each variable at the base of cell-cell and cell-substrate interactions, thus allowing us to understand more in depth regenerative and degenerative phenomena and pose the basis for better therapies.

2.5 Conclusions and general perspectives

Surface modification strategies featuring the application of polymer brushes proved their versatility and applicability on a wide variety of biomaterials for the manipulation of cells. In this review Chapter we have summarized the most relevant examples of these applications. All these strategies have been shown to exploit a peculiar feature, common of all *grafted-from* polymer brush surfaces: high densities of multifunctional tethered macromolecules can be tuned to mimic the characteristics and functions of natural ECM.

If most of the presented approaches served to fabricate study-boards for cells behavior on specific bi-dimensional environments, the direct applications on 3D supports and ready-to-use implants are increasingly envisioned. A fundamental application in this respect will be surely represented by the engineering of scaffolds

for the regeneration of tissues. This will require the synthesis of brush coatings on 3D scaffolds to host and direct tissue (re)formation. This final goal will require new chemistries featuring bio-degradable and bio-compatible brushes. In addition, bio-conjugation with enzymatically degradable units and controlled functionalization will allow spatial and temporal definition over the interfacial activity of the brush films[116-121]. Moving towards more and more complex formulations holding the potential to recapitulate the heterogeneity of biological systems, polymer brushes could be also envisioned when biological gradients need to be implemented. This would open new horizons for the regeneration of functional tissues and organs where interfacial graded properties are required. Examples are the interfacial regions connecting tendons to muscles, ligaments to bones, and cartilage to subchondral bone for hard tissue regeneration, but also the graded variations within soft tissues such as in the composition of skin, arteries and veins, to mention a few. Ultimately, the application of mixed polymer brushes selectively exposing different biological cues could be further envisioned. In this way it would be possible to create biomaterials providing differential cues not only for a targeted tissue regeneration, but also for its innervation and vascularization, thus progressing from tissue to organ regeneration with a unique and universal material technology platform.

2.6 References

1 Hidalgo-Bastida, L. A.; Cartmell, S. H., *Tissue Eng Part B-Re* **2010,** *16,* 405-412.

2 von der Mark, K.; Park, J.; Bauer, S.; Schmuki, P., *Cell Tissue Res* **2010,** *339,* 131-153.

3 Langer, R.; Vacanti, J. P., *Science* **1993,** *260,* 920-926.

4 Vacanti, C. A., *Tissue Engineering* **2006,** *12,* 1137-1142.

5 Amass, W.; Amass, A.; Tighe, B., *Polym Int* **1998,** *47,* 89-144.

6 Fioretta, E. S.; Fledderus, J. O.; Burakowska-Meise, E. A.; Baaijens, F. P. T.; Verhaar, M. C.; Bouten, C. V. C., *Macromol Biosci* **2012,** *12,* 577-590.

7 Ravichandran, R.; Sundarrajan, S.; Venugopal, J. R.; Mukherjee, S.; Ramakrishna, S., *Macromol Biosci* **2012,** *12,* 286-311.

8 Shin, H.; Jo, S.; Mikos, A. G., *Biomaterials* **2003,** *24,* 4353-4364.

9 Chen, R.; Hunt, J. A., *J Mater Chem* **2007,** *17,* 3974-3979.

10 Senaratne, W.; Andruzzi, L.; Ober, C. K., *Biomacromolecules* **2005,** *6,* 2427-2448.

11 Raynor, J. E.; Capadona, J. R.; Collard, D. M.; Petrie, T. A.; Garcia, A. J., *Biointerphases* **2009,** *4,* Fa3-Fa16.

12 Edmondson, S.; Osborne, V. L.; Huck, W. T. S., *Chemical Society Reviews* **2004,** *33,* 14-22.

13 Zhao, B.; Brittain, W. J., *Prog Polym Sci* **2000,** *25,* 677-710.

14 Milner, S. T., *Science* **1991,** *251,* 905-914.

15 Husseman, M.; Malmstrom, E. E.; McNamara, M.; Mate, M.; Mecerreyes, D.; Benoit, D. G.; Hedrick, J. L.; Mansky, P.; Huang, E.; Russell, T. P.; Hawker, C. J., *Macromolecules* **1999,** *32,* 1424-1431.

16 Zdyrko, B.; Luzinov, I., *Macromolecular Rapid Communications* **2011,** *32,* 859-869.

17 Pasetto, P.; Blas, H.; Audouin, F.; Boissiere, C.; Sanchez, C.; Save, M.; Charleux, B., *Macromolecules* **2009,** *42,* 5983-5995.

18 Kruk, M.; Dufour, B.; Celer, E. B.; Kowalewski, T.; Jaroniec, M.; Matyjaszewski, K., *Macromolecules* **2008,** *41,* 8584-8591.

19 Xiang, P.; Petrie, K.; Kontopoulou, M.; Ye, Z. B.; Subramanian, R., *Polym Chem-Uk* **2013,** *4,* 1381-1395.

20 Koylu, D.; Carter, K. R., *Macromolecules* **2009,** *42,* 8655-8660.

21 Benetti, E. M.; Zapotoczny, S.; Vancso, J., *Adv Mater* **2007,** *19,* 268-271.

22 Li, A.; Benetti, E. M.; Tranchida, D.; Clasohm, J. N.; Schonherr, H.; Spencer, N. D., *Macromolecules* **2011,** *44,* 5344-5351.

23 Matyjaszewski, K.; Xia, J. H., *Chemical Reviews* **2001,** *101,* 2921-2990.

24 Siegwart, D. J.; Oh, J. K.; Matyjaszewski, K., *Prog Polym Sci* **2012,** *37,* 18-37.

25 Otsu, T., *Journal of Polymer Science Part a-Polymer Chemistry* **2000,** *38,* 2121-2136.

26 Chiefari, J.; Chong, Y. K.; Ercole, F.; Krstina, J.; Jeffery, J.; Le, T. P. T.; Mayadunne, R. T. A.; Meijs, G. F.; Moad, C. L.; Moad, G.; Rizzardo, E.; Thang, S. H., *Macromolecules* **1998,** *31,* 5559-5562.

27 Mansky, P.; Liu, Y.; Huang, E.; Russell, T. P.; Hawker, C. J., *Science* **1997,** *275,* 1458-1460.

28 Kim, J. B.; Huang, W. X.; Bruening, M. L.; Baker, G. L., *Macromolecules* **2002,** *35,* 5410-5416.

29 Boyes, S. G.; Akgun, B.; Brittain, W. J.; Foster, M. D., *Macromolecules* **2003,** *36,* 9539-9548.

30 Brittain, W. J.; Boyes, S. G.; Granville, A. M.; Baum, M.; Mirous, B. K.; Akgun, B.; Zhao, B.; Blickle, C.; Foster, M. D., *Surface- Initiated Polymerization Ii* **2006,** *198,* 125-147.

31 Wang, X.; Xiao, X.; Wang, X. H.; Zhou, J. J.; Li, L.; Xu, J., *Macromolecular Rapid Communications* **2007,** *28,* 828-833.

32 Rowe, M. A.; Hammer, B. A. G.; Boyes, S. G., *Macromolecules* **2008,** *41,* 4147-4157.

33 Ignatova, M.; Voccia, S.; Gabriel, S.; Gilbert, B.; Cossement, D.; Jerome, R.; Jerome, C., *Langmuir* **2009,** *25,* 891-902.

34 Banerjee, I.; Pangule, R. C.; Kane, R. S., *Adv Mater* **2011,** *23,* 690-718.

35 Advincula, R. C.; Brittain, W. J.; Caster, K. C.; Ruhe, J., *Polymer brushes: Synthesis, Characterization, Application*, Wiley-VCH Verlag GmbH & Co. KGaA: **2004**.

36 Gillich, T.; Benetti, E. M.; Rakhmatullina, E.; Konradi, R.; Li, W.; Zhang, A.; Schluter, A. D.; Textor, M., *J Am Chem Soc* **2011,** *133,* 10940-10950.

37 Duan, H. W.; Nie, S. M., *J Am Chem Soc* **2007,** *129,* 3333-3338.

38 Gudipati, C. S.; Finlay, J. A.; Callow, J. A.; Callow, M. E.; Wooley, K. L., *Langmuir* **2005,** *21,* 3044-3053.

39 Ma, H. W.; Hyun, J. H.; Stiller, P.; Chilkoti, A., *Adv Mater* **2004,** *16,* 338-341.

40 Brown, A. A.; Khan, N. S.; Steinbock, L.; Huck, W. T. S., *European Polymer Journal* **2005,** *41,* 1757-1765.

41 Tugulu, S.; Silacci, P.; Stergiopulos, N.; Klok, H. A., *Biomaterials* **2007,** *28,* 2536-2546.

42 Tugulu, S.; Klok, H. A., *Biomacromolecules* **2008,** *9,* 906-912.

43 Raynor, J. E.; Petrie, T. A.; Garcia, A. J.; Collard, D. M., *Adv Mater* **2007,** *19,* 1724-1728.

44 Singh, N.; Husson, S. M.; Cui, X. F.; Boland, T., *Abstr Pap Am Chem S* **2006,** *231*.

45 Singh, N.; Cui, X. F.; Boland, T.; Husson, S. M., *Biomaterials* **2007,** *28,* 763-771.

46 Klein Gunnewiek, M.; Benetti, E. M.; Di Luca, A.; van Blitterswijk, C. A.; Moroni, L.; Vancso, G. J., *Langmuir* **2013,** *29,* 13843–13852.

47 Andruzzi, L.; Senaratne, W.; Hexemer, A.; Sheets, E. D.; Ilic, B.; Kramer, E. J.; Baird, B.; Ober, C. K., *Langmuir* **2005,** *21,* 2495-2504.

48 Tria, M. C. R.; Grande, C. D. T.; Ponnapati, R. R.; Advincula, R. C., *Biomacromolecules* **2010,** *11,* 3422-3431.

49 Ren, X. S.; Wu, Y. Z.; Cheng, Y.; Ma, H. W.; Wei, S. C., *Langmuir* **2011,** *27,* 12069-12073.

50 Wischerhoff, E.; Uhlig, K.; Lankenau, A.; Borner, H. G.; Laschewsky, A.; Duschl, C.; Lutz, J. F., *Angewandte Chemie-International Edition* **2008,** *47,* 5666-5668.

51 Lutz, J. F.; Hoth, A., *Macromolecules* **2006,** *39,* 893-896.

52 Lutz, J. F.; Weichenhan, K.; Akdemir, O.; Hoth, A., *Macromolecules* **2007,** *40,* 2503-2508.

53 Uhlig, K.; Wischerhoff, E.; Lutz, J. F.; Laschewsky, A.; Jaeger, M. S.; Lankenau, A.; Duschl, C., *Soft Matter* **2010,** *6,* 4262-4267.

54 Dworak, A.; Utrata-Wesolek, A.; Szweda, D.; Kowalczuk, A.; Trzebicka, B.; Aniol, J.; Sieron, A. L.; Klama-Baryla, A.; Kawecki, M., *Acs Appl Mater Inter* **2013,** *5,* 2197-2207.

55 Hoogenboom, R., *Angew Chem Int Edit* **2009,** *48,* 7978-7994.

56 Tong, J.; Zimmerman, M. C.; Li, S. M.; Yi, X.; Luxenhofer, R.; Jordan, R.; Kabanov, A. V., *Biomaterials* **2011,** *32,* 3654-3665.

57 Tong, J.; Yi, X.; Luxenhofer, R.; Banks, W. A.; Jordan, R.; Zimmerman, M. C.; Kabanov, A. V., *Molecular Pharmaceutics* **2013,** *10,* 360-377.

58 Luxenhofer, R.; Han, Y. C.; Schulz, A.; Tong, J.; He, Z. J.; Kabanov, A. V.; Jordan, R., *Macromolecular Rapid Communications* **2012,** *33,* 1613-1631.

59 Viegas, T. X.; Bentley, M. D.; Harris, J. M.; Fang, Z. F.; Yoon, K.; Dizman, B.; Weimer, R.; Mero, A.; Pasut, G.; Veronese, F. M., *Bioconjugate Chemistry* **2011,** *22,* 976-986.

60 Mero, A.; Fang, Z. H.; Pasut, G.; Veronese, F. M.; Viegas, T. X., *J Control Release* **2012,** *159,* 353-361.

61 Konradi, R.; Pidhatika, B.; Muhlebach, A.; Textort, M., *Langmuir* **2008,** *24,* 613-616.

62 Pidhatika, B.; Moller, J.; Benetti, E. M.; Konradi, R.; Rakhmatullina, E.; Muhlebach, A.; Zimmermann, R.; Werner, C.; Vogel, V.; Textor, M., *Biomaterials* **2010,** *31,* 9462-9472.

63 Konradi, R.; Acikgoz, C.; Textor, M., *Macromolecular Rapid Communications* **2012,** *33,* 1663-1676.

64 Pidhatika, B.; Rodenstein, M.; Chen, Y.; Rakhmatullina, E.; Muhlebach, A.; Acikgoz, C.; Textor, M.; Konradi, R., *Biointerphases* **2012,** *7*.

65 Hutter, N. A.; Reitinger, A.; Garrido, J. A.; Jordan, R., *Abstr Pap Am Chem S* **2012,** *243*.

66 Zhang, N.; Pompe, T.; Amin, I.; Luxenhofer, R.; Werner, C.; Jordan, R., *Macromol Biosci* **2012,** *12,* 926-936.

67 Zhang, N.; Pompe, T.; Luxenhofer, R.; Werner, C.; Jordan, R., *Abstr Pap Am Chem S* **2012,** *243*.

68 Chiang, E. N.; Dong, R.; Ober, C. K.; Baird, B. A., *Langmuir* **2011,** *27,* 7016-7023.

69 Navarro, M.; Benetti, E. M.; Zapotoczny, S.; Planell, J. A.; Vancso, G. J., *Langmuir* **2008,** *24,* 10996-11002.

70 Yuan, S. J.; Xiong, G.; Wang, X. Y.; Zhang, S.; Choong, C., *J Mater Chem* **2012,** *22,* 13039-13049.

71 Yuan, S. J.; Xiong, G.; Roguin, A.; Choong, C., *Biointerphases* **2012,** *7*.

72 Ren, T. C.; Mao, Z. W.; Guo, J.; Gao, C. Y., *Langmuir* **2013,** *29,* 6386-6395.

73 Liu, H. L.; Li, Y. Y.; Sun, K.; Fan, J. B.; Zhang, P. C.; Meng, J. X.; Wang, S. T.; Jiang, L., *J Am Chem Soc* **2013,** *135,* 7603-7609.

74 Ivanov, A. E.; Eccles, J.; Panahi, H. A.; Kumar, A.; Kuzimenkova, M. V.; Nilsson, L.; Bergenstahl, B.; Long, N.; Phillips, G. J.; Mikhalovsky, S. V.; Galaev, I. Y.; Mattiasson, B., *J Biomed Mater Res A* **2009,** *88A,* 213-225.

75 Ivanov, A. E.; Kumar, A.; Nilsang, S.; Aguilar, M. R.; Mikhalovska, L. I.; Savina, I. N.; Nilsson, L.; Scheblykin, I. G.; Kuzimenkova, M. V.; Galaev, I. Y., *Colloid Surface B* **2010,** *75,* 510-519.

76 Sun, T. L.; Han, D.; Rhemann, K.; Chi, L. F.; Fuchs, H., *J Am Chem Soc* **2007,** *129,* 1496-1497.

77 Wang, X.; Gan, H.; Sun, T. L.; Su, B. L.; Fuchs, H.; Vestweber, D.; Butz, S., *Soft Matter* **2010,** *6,* 3851-3855.

78 Petrie, T. A.; Raynor, J. E.; Reyes, C. D.; Burns, K. L.; Collard, D. M.; Garcia, A. J., *Biomaterials* **2008,** *29,* 2849-2857.

79 Paripovic, D.; Hall-Bozic, H.; Klok, H. A., *J Mater Chem* **2012,** *22,* 19570-19578.

80 Yim, H.; Kent, M. S.; Mendez, S.; Balamurugan, S. S.; Balamurugan, S.; Lopez, G. P.; Satija, S., *Macromolecules* **2004,** *37,* 1994-1997.

81 Plunkett, K. N.; Zhu, X.; Moore, J. S.; Leckband, D. E., *Langmuir* **2006,** *22,* 4259-4266.

82 Jones, D. M.; Smith, J. R.; Huck, W. T. S.; Alexander, C., *Advanced Materials* **2002,** *14,* 1130-1134.

83 Kaholek, M.; Lee, W. K.; Ahn, S. J.; Ma, H. W.; Caster, K. C.; LaMattina, B.; Zauscher, S., *Chem Mater* **2004,** *16,* 3688-3696.

84 Canavan, H. E.; Cheng, X. H.; Graham, D. J.; Ratner, B. D.; Castner, D. G., *Langmuir* **2005,** *21,* 1949-1955.

85 Ista, L. K.; Mendez, S.; Perez-Luna, V. H.; Lopez, G. P., *Langmuir* **2001,** *17,* 2552-2555.

86 Cho, E. C.; Kim, Y. D.; Cho, K., *Polymer* **2004,** *45,* 3195-3204.

87 Magoshi, T.; Ziani-Cherif, H.; Ohya, S.; Nakayama, Y.; Matsuda, T., *Langmuir* **2002,** *18,* 4862-4872.

88 Xue, C. Y.; Yonet-Tanyeri, N.; Brouette, N.; Sferrazza, M.; Braun, P. V.; Leckband, D. E., *Langmuir* **2011,** *27,* 8810-8818.

89 Alarcon, C. D. H.; Farhan, T.; Osborne, V. L.; Huck, W. T. S.; Alexander, C., *J Mater Chem* **2005,** *15,* 2089-2094.

90 Yang, J.; Yamato, M.; Kohno, C.; Nishimoto, A.; Sekine, H.; Fukai, F.; Okano, T., *Biomaterials* **2005,** *26,* 6415-6422.

91 Takahashi, H.; Nakayama, M.; Yamato, M.; Okano, T., *Biomacromolecules* **2010,** *11,* 1991-1999.

92 Takahashi, H.; Nakayama, M.; Itoga, K.; Yamato, M.; Okano, T., *Biomacromolecules* **2011,** *12,* 1414-1418.

93 Nagase, K.; Watanabe, M.; Kikuchi, A.; Yamato, M.; Okano, T., *Macromol Biosci* **2011,** *11,* 400-409.

94 Tamura, A.; Nishi, M.; Kobayashi, J.; Nagase, K.; Yajima, H.; Yamato, M.; Okano, T., *Biomacromolecules* **2012,** *13,* 1765-1773.

95 Nagase, K.; Mukae, N.; Kikuchi, A.; Okano, T., *Macromol Biosci* **2012,** *12,* 333-340.

96 Tamura, A.; Kobayashi, J.; Yamato, M.; Okano, T., *Acta biomaterialia* **2012,** *8,* 3904-3913.

97 Nagase, K.; Kimura, A.; Shimizu, T.; Matsuura, K.; Yamato, M.; Takeda, N.; Okano, T., *J Mater Chem* **2012,** *22,* 19514-19522.

98 Nagase, K.; Hatakeyama, Y.; Shimizu, T.; Matsuura, K.; Yamato, M.; Takeda, N.; Okano, T., *Biomacromolecules* **2013,** *14,* 3423-3433.

99 Arisaka, Y.; Kobayashi, J.; Yamato, M.; Akiyama, Y.; Okano, T., *Biomaterials* **2013,** *34,* 4214-4222.

100 Halperin, A.; Kroger, M., *Biomaterials* **2012,** *33,* 4975-4987.

101 Choi, S.; Choi, B. C.; Xue, C. Y.; Leckband, D., *Biomacromolecules* **2013,** *14,* 92-100.

102 Xue, C. Y.; Choi, B. C.; Choi, S.; Braun, P. V.; Leckband, D. E., *Adv Funct Mater* **2012,** *22,* 2394-2401.

103 Nishida, K.; Yamato, M.; Hayashida, Y.; Watanabe, K.; Yamamoto, K.; Adachi, E.; Nagai, S.; Kikuchi, A.; Maeda, N.; Watanabe, H.; Okano, T.; Tano, Y., *New Engl J Med* **2004,** *351,* 1187-1196.

104 Kobayashi, T.; Kan, K.; Nishida, K.; Yamato, M.; Okano, T., *Biomaterials* **2013,** *34,* 9010-9017.

105 Ohki, T.; Yamato, M.; Murakami, D.; Takagi, R.; Yang, J.; Namiki, H.; Okano, T.; Takasaki, K., *Gut* **2006,** *55,* 1704-1710.

106 Yu, Q.; Zhang, Y. X.; Chen, H.; Zhou, F.; Wu, Z. Q.; Huang, H.; Brash, J. L., *Langmuir* **2010,** *26,* 8582-8588.

107 Li, L. H.; Wu, J. D.; Gao, C. Y., *Colloid Surface B* **2011,** *85,* 12-18.

108 Petrie, T. A.; Raynor, J. E.; Dumbauld, D. W.; Lee, T. T.; Jagtap, S.; Templeman, K. L.; Collard, D. M.; Garcia, A. J., *Science translational medicine* **2010,** *2,* 45ra60.

109 Steinbach, A.; Tautzenberger, A.; Ignatius, A.; Pluntke, M.; Marti, O.; Volkmer, D., *J Mater Sci-Mater M* **2012,** *23,* 573-579.

110 Deng, Y.; Zhang, X.; Zhao, X.; Li, Q.; Ye, Z.; Li, Z.; Liu, Y.; Zhou, Y.; Ma, H.; Pan, G.; Pei, D.; Fang, J.; Wei, S., *Acta biomaterialia* **2013,** *9,* 8840-50.

111 Tsai, H. A.; Shen, C. N.; Chang, Y. C., *Biomacromolecules* **2012,** *13,* 3483-93.

112 Villa-Diaz, L. G.; Nandivada, H.; Ding, J.; Nogueira-de-Souza, N. C.; Krebsbach, P. H.; O'Shea, K. S.; Lahann, J.; Smith, G. D., *Nat Biotechnol* **2010,** *28,* 581-3.

113 Chang, Y.; Higuchi, A.; Shih, Y. J.; Li, P. T.; Chen, W. Y.; Tsai, E. M.; Hsiue, G. H., *Langmuir* **2012,** *28,* 4309-17.

114 Tan, K. Y.; Lin, H.; Ramstedt, M.; Watt, F. M.; Huck, W. T.; Gautrot, J. E., *Integrative biology : quantitative biosciences from nano to macro* **2013,** *5,* 899-910.

115 Gautrot, J. E.; Wang, C.; Liu, X.; Goldie, S. J.; Trappmann, B.; Huck, W. T.; Watt, F. M., *Biomaterials* **2012,** *33,* 5221-9.

116 Kloxin, A. M.; Kasko, A. M.; Salinas, C. N.; Anseth, K. S., *Science* **2009,** *324,* 59-63.

117 Hahn, M. S.; Miller, J. S.; West, J. L., *Adv Mater* **2006,** *18,* 2679-2684.

118 Lutolf, M. R.; Weber, F. E.; Schmoekel, H. G.; Schense, J. C.; Kohler, T.; Muller, R.; Hubbell, J. A., *Nature Biotechnol* **2003,** *21,* 513-518.

119 Lutolf, M. P.; Hubbell, J. A., *Nature Biotechnol* **2005,** *23,* 47-55.

120 Lutolf, M. P.; Lauer-Fields, J. L.; Schmoekel, H. G.; Metters, A. T.; Weber, F. E.; Fields, G. B.; Hubbell, J. A., *P Natl Acad Sci USA* **2003,** *100,* 5413-5418.

121 Wylie, R. G.; Ahsan, S.; Aizawa, Y.; Maxwell, K. L.; Morshead, C. M.; Shoichet, M. S., *Nat Mater* **2011,** *10,* 799-806.

Proteins gradients for tissue engineering: From 2D to 3D

3.1 Introduction

Current research activities in polymer and biomaterials science have been devoted to design and engineer two-dimensional (2D) and three-dimensional (3D) supports presenting a gradual variation of (bio)chemical composition and physical properties. This general strategy is being followed in order to closely mimic the intrinsic characteristics of the natural extra-cellular matrix (ECM).[1-2] Synthetic platforms presenting gradient-like properties possess the capability of triggering several biological processes like migration via haptotaxis[3] and durotaxis[4]. In addition, biomaterials presenting chemical gradients were also applied at the interface between different tissue types, such as bone and cartilage.[1, 5] The fabrication of such synthetic ECMs generally encompassed the spatial variation of at least one matrix characteristic, either chemical (e.g. protein concentration[6-7] or hydrophilicity[8]) or physical (e.g. matrix stiffness[9]).

Among different materials, 2D platforms on silicon, titanium or gold surfaces were used to fabricate protein gradients by physisorption or covalent attachment.[2, 10] These functionalizations featured the employment of functional linkers to the metal/metal oxide surface, such as silanes, thiols and polymer brushes[11]. Alternatively, 3D supports presenting gradient morphologies and/or compositions encompassed the application of functional hydrogels, which more closely resemble the native ECM among other biomaterial compositions.[12-14] When hydrogels were composed of bio-inert compounds (such as poly(ethylene glycol)s (PEGs) derivatives), they did not trigger or affect any biological process[14-15] while still offering the possibility to incorporate bio-active cues to direct cellular behavior.[16-17]

Similar hydrogels were not only applied to fabricate 3D scaffolds but also to coat 2D surfaces. In both cases, the functional components used for hydrogel preparation allowed the subsequent formation of gradients, within their porous structure[6-7, 18] or at their outer interfaces[19-21].

Materials presenting porous morphologies and a biodegradable character have been particularly attractive in tissue engineering (TE) as 3D scaffolds to support cell adhesion, proliferation, and differentiation.[22-26] Within these scaffolds both cell differentiation and subsequent tissue formation are accompanied by synthetic matrix degradation. During this process, the intrinsic macro, micro, and, where applicable nano porosity of the supports assure the efficient diffusion of nutrients and removal of cellular waste product.[27]

These and others fabrication strategies to create “intelligent” supports for cell manipulations and TE applications will be reviewed in this Chapter, with a particular attention posed on the most recent advances in the formation of surface (2D) gradients and 3D biomaterials with gradient-like characteristics. Specifically I will first address the application of polymer brush coatings as functional platforms to immobilize protein gradients. Subsequently I will concentrate on the most prominent techniques used for designing hydrogel-based supports as porous synthetic ECMs in TE applications. Finally In the last section of this Chapter, I will discuss the specific applications of 2D and 3D polymeric materials for cell manipulation.

3.2 Surface gradients

3.2.1 Polymer brush-assisted 2D gradients

Over the last two decades, several methods have been proposed to fabricate chemical gradients on 2D substrates. The first method to fabricate unidirectional chemical gradients on a 2D silicon substrate was presented in 1992 by Chaudhury and Whitesides.[28] Specifically the authors exploited vapor deposition of silane species on silicon surfaces to form a gradient-like surface concentration of hydrophobic adsorbates. A similar strategy, which was based on the formation of mixed self-assembled monolayers (SAMs), allowed the formation of protein gradients on gold substrates by coupling protein adsorption and spatially-controlled

electrochemical desorption of the thiol-based adsorbates.[29] The application of a potential window across the surface enabled the formation of a gradient density of a thiol-based SAMs.[29-32] This process was followed by backfilling of a second, oligoethylene glycol-bearing thiol, which formed protein resistant SAMs. In this way, a monodirectional compositional gradient within the SAM was obtained. Finally, adsorption of proteins on hydrophobic thiol species allowed the fabrication of a surface protein density gradient across the mixed SAM.[33-34]

SAMs presenting gradient-like compositions or morphologies on silicon and gold substrates were also applied for the subsequent "surface-initiated" polymerization (SIP) to form polymer brush grafting density gradients.[35-39] These strategies rely on the pre-formation of an initiator SAM presenting gradient-like coverage at the surface (Figure 3.1a). Subsequent SIP (Figure 3.1b) produced a graded variation of polymer grafting density along the sample, obtaining assemblies of grafted polymers varying their conformation from mushroom to brush regimes (Figure 3.1c).[40-42] Similar gradients of grafting densities were used to study cell adhesion or protein adsorption on morphologically different polymeric grafts.[43-48] As an example, poly(2-hydroxyethyl methacrylate) (PHEMA) grafts presenting graded grafting densities were fabricated to vary the concentration of physisorbed fibronectin (FN).[43] In this particular case, FN coverage decreased significantly from 550 to 0 ng/cm^2 on PHEMA films presenting grafting density values ranging from 0 to 0.03 chains/nm^2, respectively. Above this last grafting density, the antifouling character of more densely grafted PHEMA chains significantly inhibited the adsorption of FN.

A different method to form a gradient of polymer brush grafting density was presented by Morgenthaler et al. using poly(L-lysine)(20 kDa)-g-PEG(2 kDa) graft-copolymers (PLL-g-PEG) adsorbing on titanium oxide (TiO_2) surfaces.[49] Due to the electrostatic interactions between positively charged PLL backbones and negatively charged TiO_2 surface and by varying the exposure time along the substrate, a gradient in surface coverage of PEG chains was obtained. This method allowed to assemble surface gradients of EG units density (nEG) ranging from 0 to around 17 units/nm^2 along a single TiO2 support. These platforms were subsequently applied to spatially control the adsorption of bovine serum albumin (BSA) and fibrinogen (Fgn) on the graft-copolymer surfaces.[50] Although the

adsorption of both proteins gradually decreased with increasing nEG, inhibition of Fgn adsorption required higher EG density (12.8 ± 0.6/nm^2) compared to BSA (8.3 ± 0.8/nm^2) (due to the different protein size). These differences in adsorption behavior were attributed to a lower energy cost for Fgn to adhere between PEG chains, which enabled the selective Fgn immobilization on higher EG density regions.

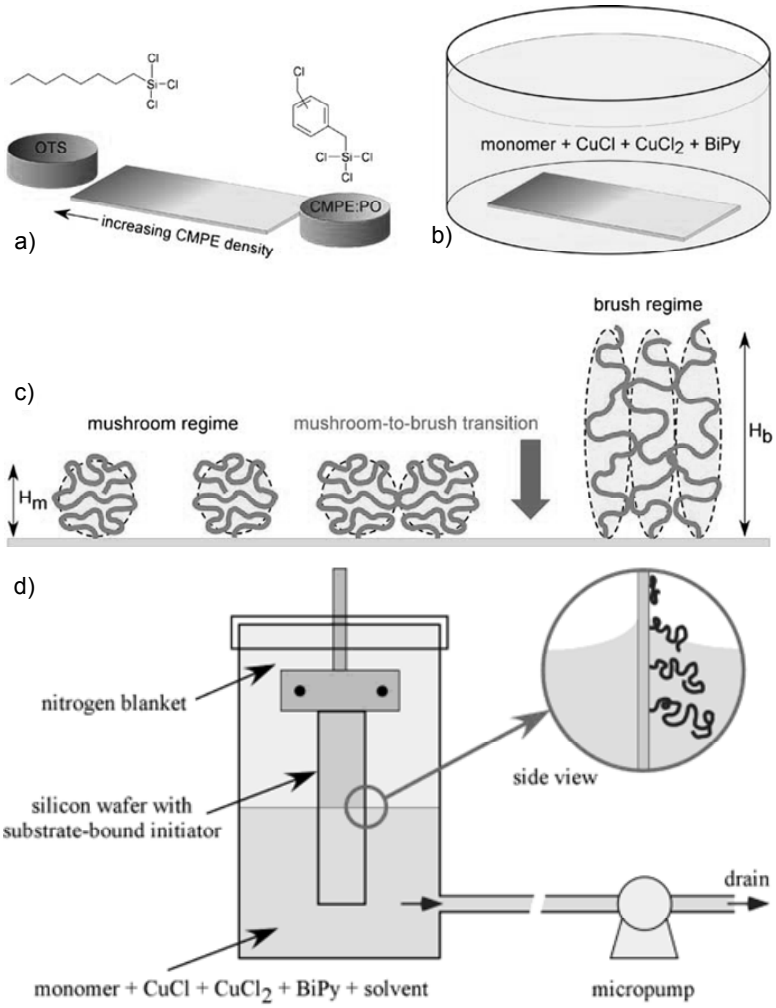

Figure 3.1. *(a) Method of preparing gradients in grafting density of an ATRP initiator on a solid substrate. (b) Surface-grafted polymer brushes are formed on the substrates by using SI-ATRP. (c) Schematic illustrating polymer conformations in the mushroom (height H_m) and brush (height H_b) regimes and the mushroom-to-brush transition. Adapted with permission from REF 51. (d) Schematic of the setup for creating surface grafted polymer brushes with a gradient in molecular weight. Adapted with permission from REF 52. Copyright 2003 American Chemical Society.*

Polymer brushes presenting gradual variation of film thickness (i.e. molar mass of grafted chains) in one direction along the substrate[52] were synthesized by varying the exposure time to SIP solution of an initiator-covered substrate (Figure 3.1d).[52-54] Following this strategy one could actively control the thickness of a polymer brush film. Thus, the morphology of the gradient along the sample could be effectively tuned .[54]

A different method to fabricate a gradient of brush thickness was introduced by Huck and coworkers.[55-56] In this case, electrochemical-induced SI-ATRP[57-58] was used to introduce a surface gradient of "active" initiator species along a substrate. As an example, a platinum gauze working electrode, a platinum wire counter electrode, and a saturated calomel reference electrode (SCE) could be employed to gradually vary the thickness of poly(sulfopropyl methacrylate) (PSPMA) brushes.[55] An alternative technique made use of a sacrificial metal surface (working as anode) to reduce the dormant Cu(II) species to the active Cu(I) species.[56] Positioning of the working electrode with a specific tilting angle above the initiator-functionalized substrate altered the relative concentration of active and dormant species, and therefore the rate of polymerization across the surface. Light-mediated living polymerization in combination with a photomask was also proposed as an alternative procedure to produce thickness gradients of polymer brushes or, to spatially confine the brush growth on specific areas at the substrate.[59] Similarly, sophisticated (and more expensive) lithographic techniques were employed to create brush thickness gradients presenting spatial resolutions down to few hundred of nanometers. These last methods were recently reviewed by Li and coworkers.[60]

It is worth to mention that several of the above mentioned preparations could be also combined to form orthogonal gradients of both brush thickness and polymer grafting density. These samples were subsequently employed as comprehensive study boards to investigate the physical and covalent surface attachment of different proteins.[61-66]

All the above mentioned brush systems can be used to spatially control the protein concentration onto solid substrates. However, in order to more closely mimic the natural ECM, 2D gradients supported by hydrogels will be discussed in the following section.

3.2.2 Hydrogel-supported 2D gradients

One of the recently introduced methods to fabricate chemical gradients on the surface of functional hydrogels is based on microfluidics. The formation of lamellar flows of protein solutions inside micro-channels[67-68] was specifically applied to selectively physisorb or chemisorb protein species onto hydrogel surfaces (as shown in Figure 3.2a).[67-71] Alternatively, the progressive depletion of proteins in the fluid due to adsorption onto a PDMS substrate[67, 72] produced a surface concentration gradient of proteins ranging from sub-micrometer to centimeters in length.[73] In a similar manner, yet employing multi-channel systems, different protein patterns can be created, such as multiple gradient-like arrays and double gradients featuring two different protein species.[72]

Protein gradients on hydrogels can be fabricated also along the width of microchannels by injecting two or more protein solutions into a fluidic-based system composed of alternated splitting and mixing units.[18, 68, 74] When two inlets were used, one containing a protein solution and the second just a buffer solution, a single gradient of one protein type is formed between the walls. Alternatively, the addition of a solution of a second protein through an additional inlet allowed the fabrication of hydrogels featuring concentration gradients of two different protein species.[75] The designing of microfluidic devices presenting three or more inlets was also reported and shown to enable the fabrication of more complex, multiple-protein concentration profiles.[68]

Another technique based on microfluidics was presented by Cosson et al. and was based on hydrodynamic flow focusing (HFF) (Figure 3.2c).[20] PEG-based hydrogels and specific protein binding via NeutrAvidin were used to generate gradients of tethered biotinylated biomolecules. In this case, a microchannel presenting three independently controlled inlets was applied. Width and position of protein solution streams could be precisely controlled by adjusting the flow rates of the individual channels.[20-21]

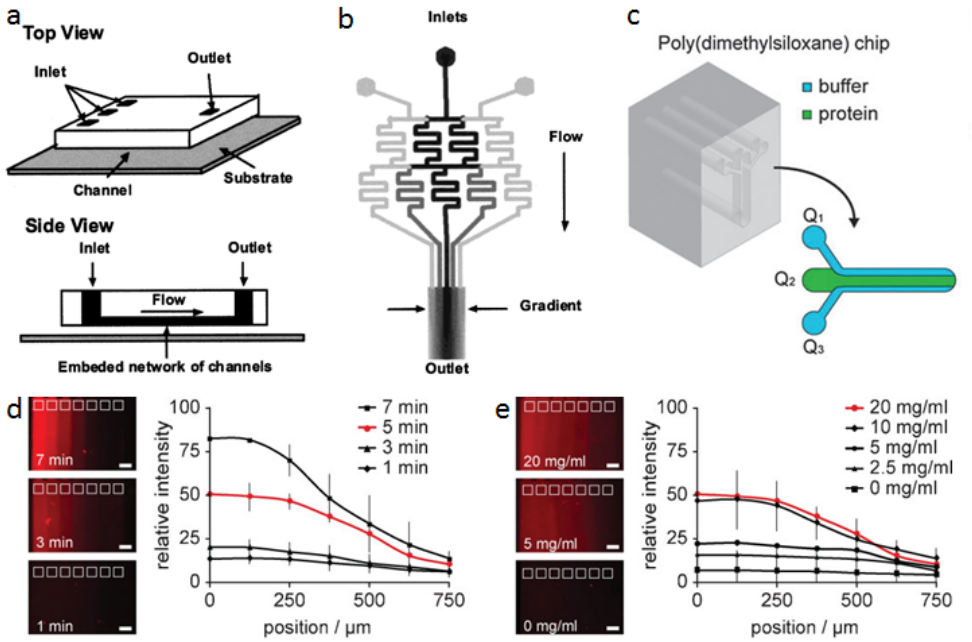

Figure 3.2. *(a) Scheme of a microfluidic gradient generator setup and (b) the schematic design of a representative gradient-generating microfluidic network using three inlets. Adapted with permission from REF 68. Copyright 2000 American Chemical Society (c) Schematic representation of a microfluidic chip used for hydrodynamic flow focusing. Adapted with permission from REF 20 with permission from The Royal Society of Chemistry. (d, e) Fluorescent micrographs and the representative intensity plots of a fluorescent protein bound to a hydrogel surface as a result of different (d) exposure times and (e) starting concentrations. Adapted with permission from REF 19.*

All the above mentioned fabrications relied on variations of exposure times by one or more protein solutions on an hydrogel substrate (Figure 3.2d). Alternatively, gradual variation of protein concentration within the flowing stream was exploited (Figure 3.2e).[19] More complex patterns could be formed by applying the microfluidic chips on different proteins in following subsequent steps [19-21] (Figure 3.3). As an example, Lutolf and coworkers created a pattern of 4 parallel linear gradients of fluorescently-labeled human imunoglobin (hIgG) (Figure 3.3a, b). Simple rotation of the pre-functionalized chip by 90 degrees (Figure 3.3c) allowed the formation of 4 additional patterns of BSA-biotin concentration gradients, finally obtaining an array of orthogonally intersecting gradient patterns (Figure 3.3d, e).

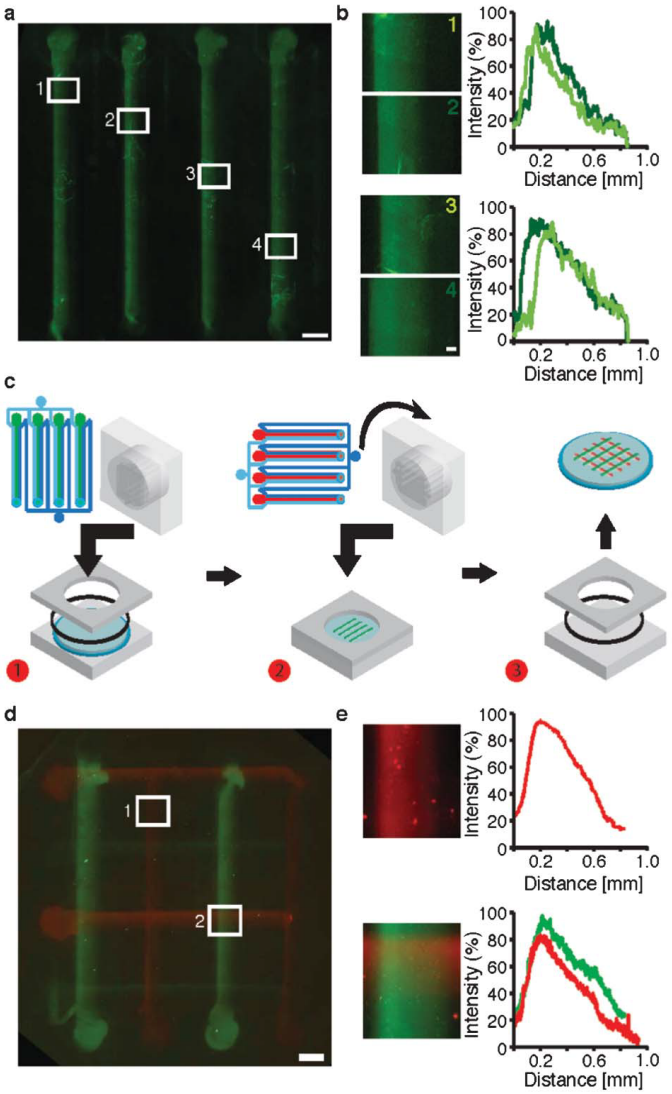

Figure 3.3. *(a) Stitched micrographs of a pattern of four parallel arrayed protein gradients. (b) Micrographs showing the magnification of individual gradients (white frames) and a graphical representation of their respective intensity profiles (scale bar = 100 mm). (c) A scheme showing the patterning of arrays of overlapping gradients. Step 1: The microfluidic device is assembled and the first set of four gradients is patterned. Step 2: The microfluidic device is partially disassembled with the patterned hydrogel remaining fixed to ensure good alignment. The microfluidic chip is turned by 90° and the second set of parallel gradients is patterned. Step 3: The patterned hydrogel is recovered. (d) Stitched micrographs of a four-by-four gradient array of two different proteins. (Scale bar = 900 mm). (e) Micrographs of regions of interest of the gradient array (white frames) and a graphical representation of the corresponding intensity profiles. Reprinted with permission from REF 21 with permission from The Royal Society of Chemistry.*

3.3 3D gradient biomaterials

3.3.1 Hydrogel supports

In addition to planar surfaces, the investigation of cellular behavior within 3D hydrogels is gaining interest since such supports more closely mimic natural ECM environments. One technique to fabricate hydrogels presenting 3D gradient properties is based on the so called "gradient maker".[6] This technique consists of an apparatus made of two chambers containing different solutions which are interconnected through a narrow tube (Figure 3.4a). As the solution in chamber 1 is drained from the gradient maker into a mold it is concomitantly re-filled with the solution coming from chamber 2. While chamber 1 is continuously stirred, it is progressively diluted with the solution from chamber 2 until the outflowing material is basically the same composition of this last chamber. By using polymer solutions that can crosslink upon UV irradiation, an hydrogel matrix presenting a gradient composition could be thus formed. This technique was used to gradually vary the physical properties[76-77] as well as the chemical composition[78] (Figure 3.4b) of hydrogels across their 3D architecture. Using a similar technique, Langer et al. applied a multichannel microfluidic device to gradually vary the cell adhering RGD (Arg-Gly-Asp) concentration within a precursor solution for hydrogel fabrication. Subsequent photopolymerization of the pre-polymer mixture was used "to fix" the RGD gradient within the hydrogel support.[18] The same technique was applied by Guarnieri et al. to fabricate a unidirectional concentration gradient of RGD within a PEG-based hydrogel scaffold.[79] The amount of RGD measured at the highest concentration was around 10 μM and it linearly decreased till nearly 0 μM through the matrix.

Similarly to the "gradient maker" method, hydrogels with a 3D variation of composition could be fabricated using a multiple syringe setup.[80-82] Gradual variation of pre-polymer solution feed from each individual syringe and subsequent photocrosslinking enabled the fabrication of a protein concentration gradient inside the support.

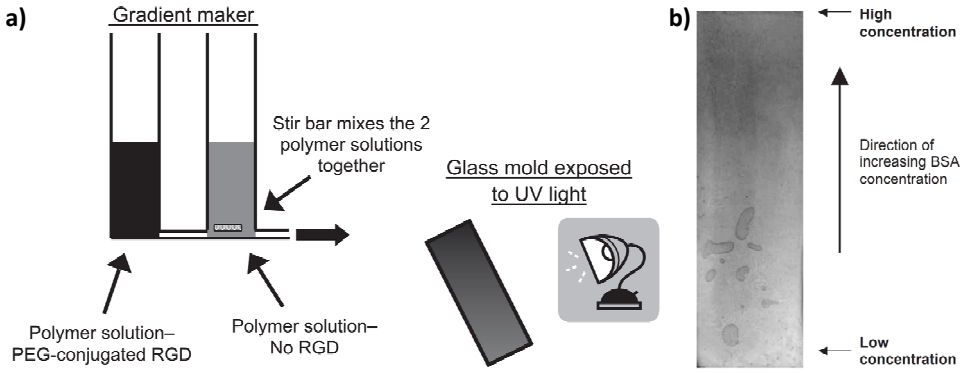

Figure 3.4. *(a) Schematic representation of a gradient maker used to gradually vary the concentration of RGD inside a PEG solution The resulting polymer solution is pumped into a mold where it is photopolymerized. (b) Representative image of a BSA-gradient hydrogel stained with Coomassie brilliant blue. Staining intensity increased with increasing concentrations of BSA. Reprinted from REF 6, Copyright 2005, with permission from Elsevier.*

In addition to these controlled fabrication methods photochemical patterning was introduced to spatially control in 3D the concentration of proteins throughout hydrogels. This was achieved by locally photoactivating a specific chemical reaction in pre-determined positions within the matrix. This method was applied to couple peptides or proteins at specific volumes within an hydrogel either with the aid of a photoinitator,[83-86] by thiol-ene photocoupling,[87-89] by enzymatic reactions,[90] or thorough thiol/amine-maleimide chemistry.[91-92]

In addition, UV-triggered reactions could be alternatively exploited to pattern 3D supports by locally cleaving proteins conjugates within a hydrogel matrix.[88-89] A continuous 3D gradient of RGD concentration (Figure 3.5a, d) could thus be fabricated within PEG hydrogels by varying the exposure time of the samples to UV light. (Figure 3.5a). In alternative pre-selected volumes of a PEG hydrogel scaffold presenting a constant peptide concentration were intercalated with regions of decreasing concentration (Figure 3.5b), finally forming linearly patterned supports (c-e). Due to the versatility of photochemical activation, multiple gradient designs and specific protein patterns could be finally fabricated and combined.[93]

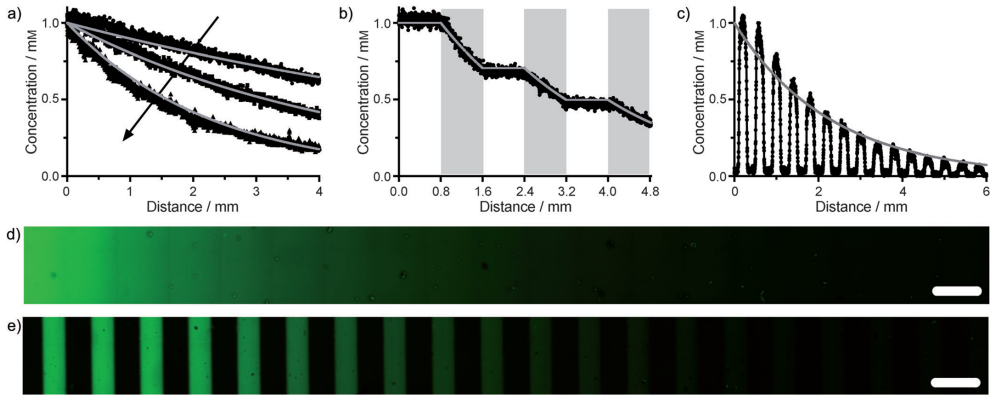

Figure 3.5. *(a) Concentration profiles of hydrogels exposed to gradients of UV light generated by a moving opaque photomask at different speeds (1.6, 0.8, or 0.4 mm/min). Concentration profiles of hydrogels exposed by shuttering the light (b) or releasing pre-patterned lines (c), unique gradients in the peptide concentration were generated across the network. Scale bars = 400 mm. Reprinted with permission from REF 89.*

Ehrbar et al. introduced a fabrication technique which combined electrochemistry with pH-dependent enzymatic polymerization to fabricate PEG hydrogels featuring 3D gradients of protein content.[94] By inserting electrodes into a transglutaminase (TG) - PEG precursor solution, the local pH was precisely varied at the anode–electrolyte and the cathode–electrolyte interfaces, forming a continuous pH variation between the two electrodes. Thus, enzymatic polymerization could be confined at the anode or the cathode and gradually suppressed towards the opposite electrode. Organizing the electrodes in a specific pattern design and using multiple protein solutions resulted in hydrogel scaffolds presenting 3D gradient concentrations of different proteins.

The formation of more complex systems featuring spatially-controlled organization of cells, matrix components, and biological cues was proposed by Weber et al. who combined 3D printing techniques with layer-by-layer patterning (Figure 3.6).[95] This process consisted of a sequential deposition of a PDMS mold that contained the precursor solutions, a layer of PEG hydrogel (Figure 3.6a) and a patterned or uniform layer consisting of a combinations of cells, biomolecules and hydrogel material (Figure 3.6b). By this process, a synthetic ECM featuring a 3D variation of bio-components and synthetic materials was obtained.

Although hydrogels resemble the natural ECM environment, they lack the structural integrity. Therefore in the following section, protein gradients inside porous polymer scaffolds will be reviewed.

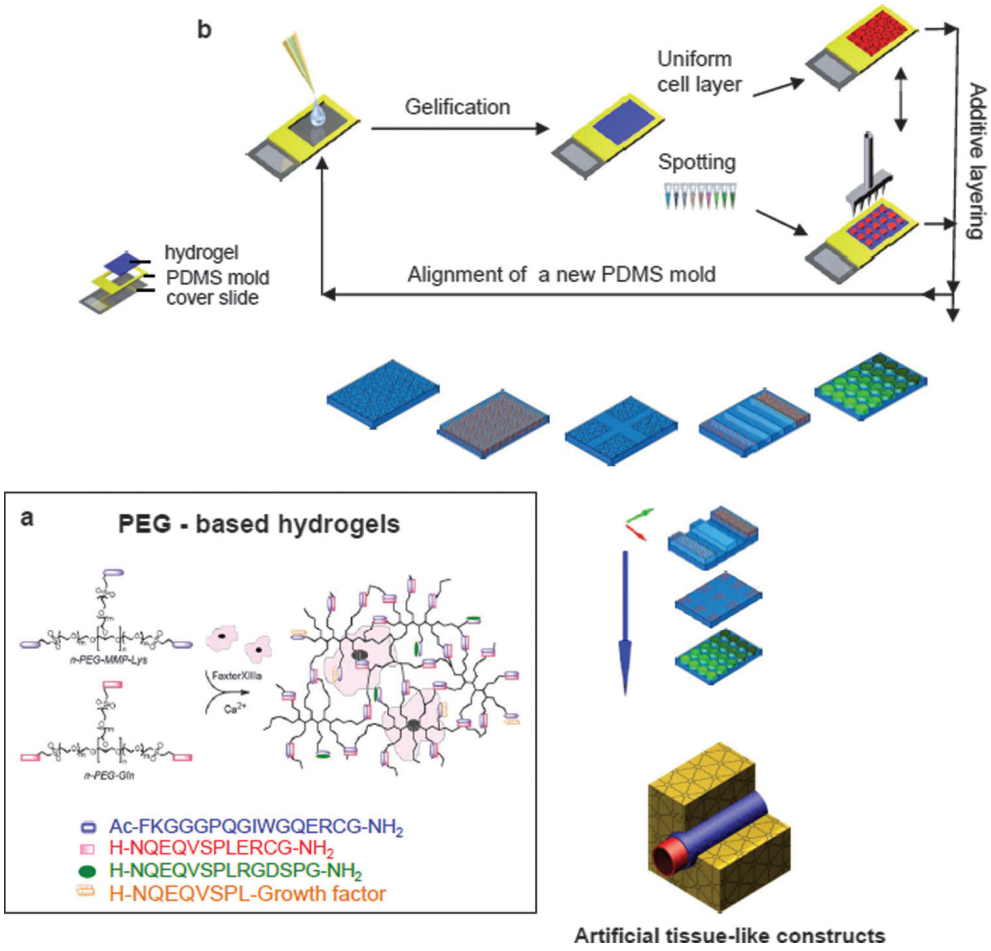

Figure 3.6. *Scheme of the artificial tissue-like construct formation proposed by Weber and coworkers. (a) Scheme of the synthetic artificial extracellular matrix system (aECM). (b) Presentation of the fabrication procedure. A first layer of modular designed PEG-based hydrogel is casted with the help of a PDMS mask, then combinations of cells, molecules, and hydrogels are deposited as either uniform or patterned layers. By repetitive alignment of PDMS molds and deposition of new layers, constructs with different heterogeneous designs are formed. Layer-by-layer assembly of individually patterned layers results in a tissue-like construct. Reproduced with permission from REF 95 with permission from The Royal Society of Chemistry.*

3.3.2 3D Gradients within porous scaffolds

Due to the increasing application of porous scaffolds in TE, the controlled functionalization of these supports by (bio)chemical gradients has been developed. A well-known method to fabricate porous constructs is based on electrospinning. Here, a high voltage is used to create an electrically charged flow of a polymer solution or melt from a nozzle to a collector plate.[96] As the polymer solidifies, it forms an interconnected porous web of fibers. Several methods to gradually vary the composition of the electrospinning solution at a single nozzle included a "gradient maker",[97] a microfluidic device (Figure 3.7a)[98] or, alternatively, a setup where two solutions mix at a T-junction.[99] Compositional gradients of electrospun fiber mats can also be fabricated using the double electrospinning process, as shown in Figure 3.7b.[100] Here two spinnerets were placed at the opposite side of a rotating drum and the flow rate of both solutions was varied independently.[101-102] Keeping steady the collector plate or the rotating drum at a certain position, a compositional gradient along the vertical axis of the final matrix could be fabricated. Additional lateral movement of the platforms allowed the deposition of a gradient of fiber composition also along the horizontal axis of the scaffold.[103-104] Using similar setups, different types of gradient scaffolds were fabricated featuring proteins incorporated inside the fibers. The cues could be subsequently released in the surrounding solution,[97-98, 103, 105] or, alternatively, remained anchored to the surface of the fibers via specific binding (e.g. through heparin-based linkages).[104]

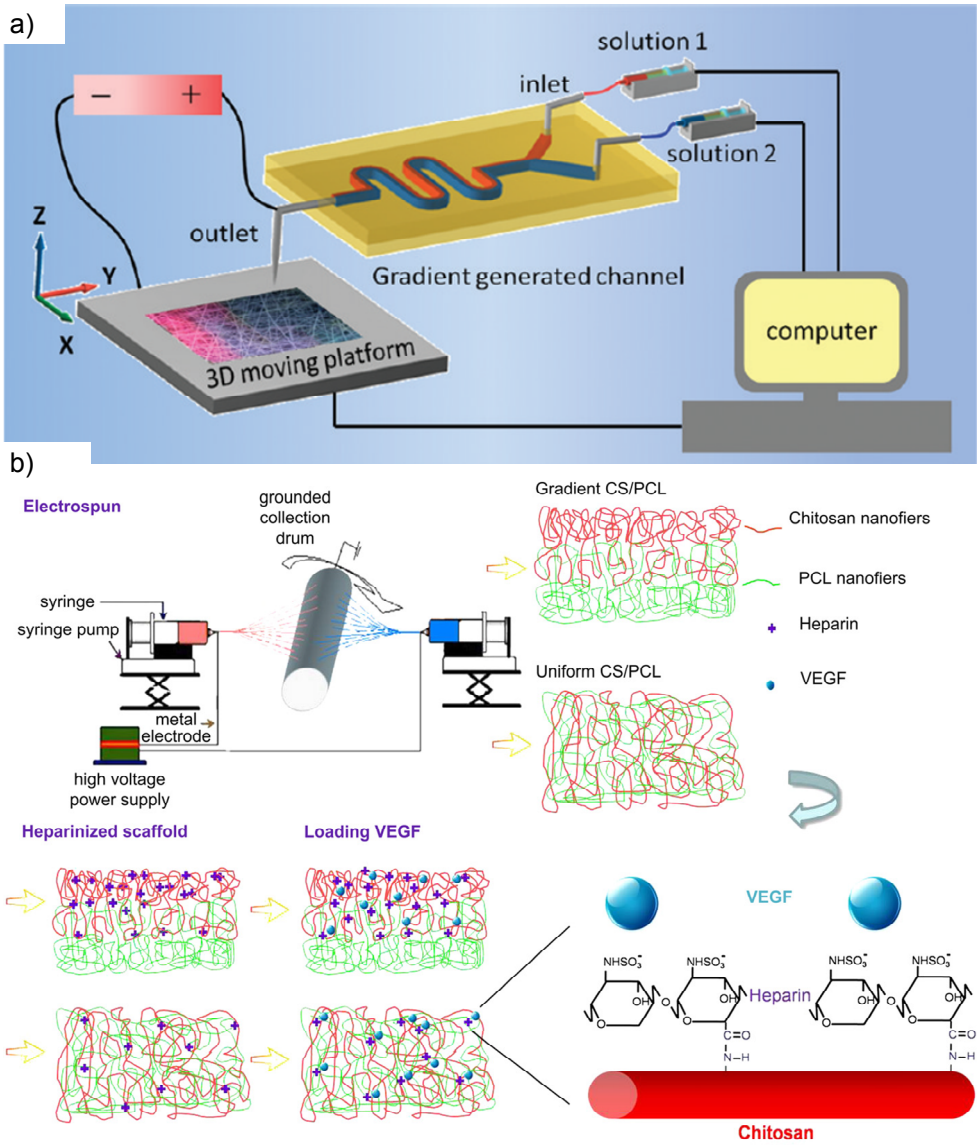

Figure 3.7. *(a) Schematic representation of a two inlet microfluidic device in combination with an electrospinning nozzle on a 3-D controllable platform to generate gradient electrospun fibrous scaffolds. Reprinted with permission from REF 98. Copyright 2012 American Chemical Society. (b) Schematic diagram of a double electrospinning process used to fabricate gradient and uniform nano-fibrous scaffolds for vascular tissue engineering. Reprinted from REF 104, Copyright 2012, with permission from Elsevier.*

Gradual diffusion of mineral[106], protein[107], or aminolysis[108] solutions within pre-formed electrospun supports allowed selective activation of the matrix following a gradient morphology. Due to the porous character of the fiber mats, solutions could diffuse into the scaffold and create a unidirectional compositional gradient throughout the 3D structure. Following this method Shi et al. demonstrated the effective fabrication of FN gradients by protein physisorption onto poly(methyl glutarimide) (PMGI) fibers.[107] Using this "controlled filling method" and by varying the diffusion speed as well as the FN concentration in the solutions, different FN concentration gradients within the support could be controlled and produced. In a similar way, Zou et al. created a gradient of amino groups at the fibers' surface by varying the aminolysis time across the structure of a poly(DL-lactide) (PDLLA) electrospun fiber mat.[108] The surface-exposed amino groups were subsequently coupled to gelatin units finally forming a gradient of biomolecules within the 3D support.

Protein gradients within 3D scaffolds could be also obtained by simple, controlled diffusion of different protein solutions into matrices, as shown by Lee et al. (

Figure ***3.8***a).[109] By this procedure, a PCL/Pluronic F127-based porous membrane was modified with a double gradient of platelet-derived growth factor-β (PDGF-BB) and bone morphogenetic protein 2 (BMP-2) presented in opposite direction across the scaffold. The growth factors (GFs) where immobilized on the structure via hydrogen bonding between heparin and Pluronic F127 and the subsequent ionic interaction of the proteins with heparin.

Complementing protein diffusion methods with centrifugation during scaffold fabrication enabled the fabrication of morphological and chemical gradients within PCL/ Pluronic F127-based 3D scaffolds (

Figure ***3.8***b).[110-112] Fibril-like PCL accumulated in a cylindrical mold and created a density gradient (i.e. a gradient in available surface area) by the gradual increment of the centrifugal force along the main axis of the mold. Later on, the surface of PCL/ Pluronic F127 fibrils could be chemically modified by heparin adsorption, thus forming a unidirectional gradient of biomolecule concentration which followed the density variation within the scaffold.[113]

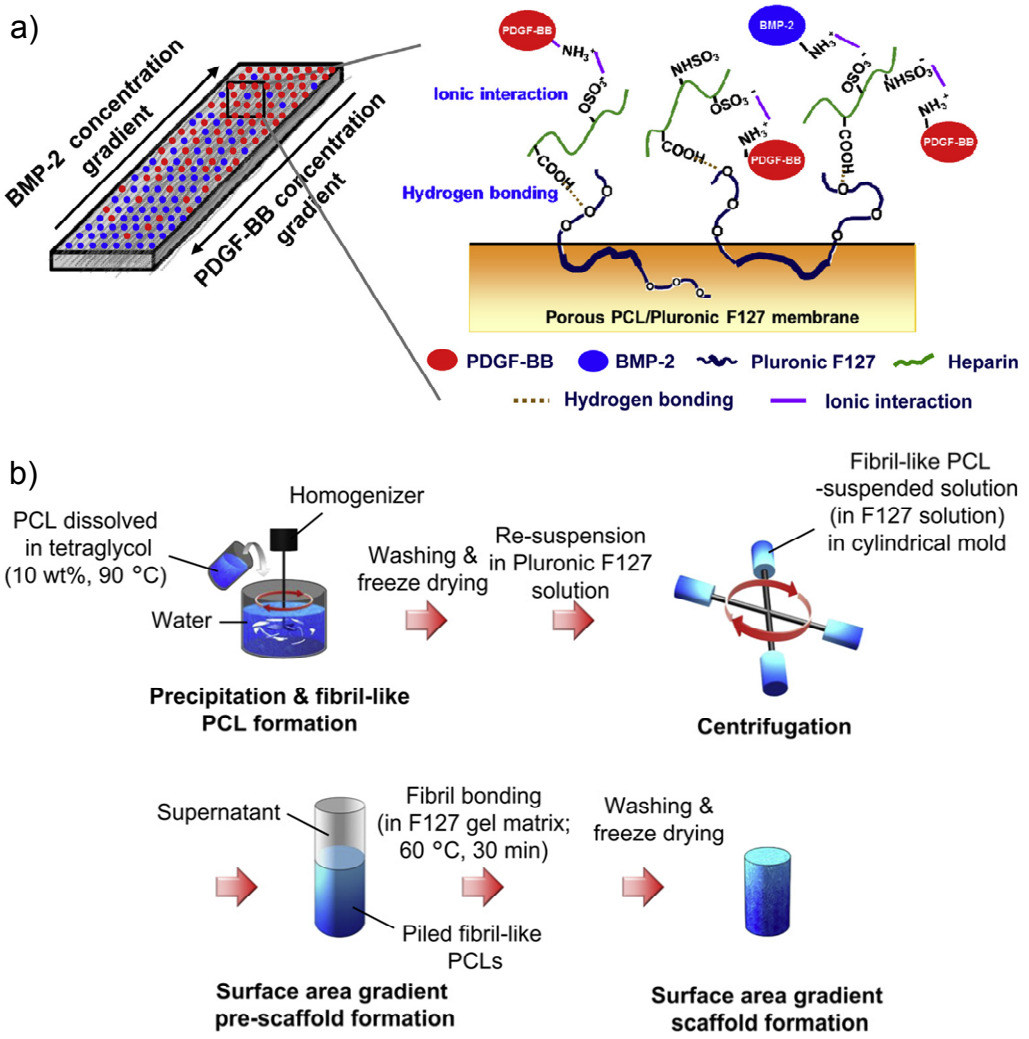

Figure 3.8. *Schematic diagram (a) illustrating the formation of PCL/Pluronic F127 membrane with reverse gradients of PDGF-BB and BMP-2 and the successive binding of heparin and growth factors onto the membrane surface. Reprinted from REF 109, Copyright 2014, with permission from Elsevier. Schematic diagram (b) showing the fabrication process of the surface area gradient porous scaffold by a centrifugation method. Reprinted from REF 113, Copyright 2011, with permission from Elsevier.*

3.4 Cellular response on gradient-like supports

It is generally known that cells anchor to a surface or to the surrounding ECM via cellular receptors like integrins and through other adhesions proteins.[114-115] These receptors probe the ECM and trigger a specific response depending on the environment, inducing adhesion, proliferation, migration or differentiation.[116-118] Specifically, cell adhesion significantly depends on the concentration of ligands at the surface and a critical ligand spacing should be maintained in order to maximize cell spreading and obtain a stable attachment. Several reports measured the maximum spacing between RGD units on surfaces necessary to allow fibroblast attachment and formation of focal points. These values ranged from 20 to 60 nm.[119-122] These findings were in line with the measured maximal surface density of fibrinogen (Fgn) to allow fibroblast adhesion, which, on PLL-g-PEG-based films was calculated as 47 ± 3 nm.[50] Following a similar trend, the adhesion of fibroblasts on PHEMA-brush supported FN showed the highest fibroblast adhesion and maximum cell spreading for protein coverages of 50 and 100 ng/cm^2, respectively.[44]

In addition to adhesion, cell migration was also found very sensitive to surface coverage of protein and cues. In 1989 Brandley and Schnaar were the first to investigate the effect of a linear and an exponential gradient of RGD surface coverage on cell adhesion and migration.[123] They showed that cell migration was always taking place in the direction of higher peptide surface densities and, thus, towards areas with higher cell-adhesive character. In addition, the steepness of the protein gradient on the surface was also proven to alter the movement of cells.[6, 79] Namely, steeper surface gradients of adhesive cues stimulated longer and faster fibroblasts migrations.[6, 79]

Besides the cell adhesive RGD peptides and RGD-derivatives, also surface-immobilized growth factors (GF) induced cell migration, as shown in case of fibroblasts. A gradient-like surface concentration of basic fibroblast growth factors (bFGF) on PEG-RGD-based hydrogels induced, for example, a marked migration by vascular smooth muscle cells (VSMCs).[7] Specifically, VSCMs showed an aligned morphology and moved in the direction of increasing bFGF concentration.[7]

When cells are cultured within hydrogels and 3D supports, different mechanisms of migration take place compared to planar substrates.[124-125] Composition and concentration of biological cues in combination with the degree of cross-linking of the polymeric matrix are crucial parameters which determine the ability of cells to migrate.[126] Kyburz et al. showed that hydrogels with low crosslink density (0.18 ± 0.02 mM) and high RGD concentration (1 mM CRGDS) allowed relatively high migration rates (17.6 ± 0.9 μm/h).[127] Wylie et al. fabricated a linear gradient of sonic hedgehog (SHH) concentration inside the structure of an agarose hydrogel.[91] A graded variation of SHH, a protein that stimulates cell differentiation and migration,[128-130] influenced the behavior of neural precursor cells (NPCs) cultured at the outer surface of the hydrogel support. NPCs were in fact observed to migrate through the hydrogel, reaching the depth of maximal SHH concentration during 14 days of culture. On the contrary, the same cells cultured on a similar hydrogel without any SHH function did not show any diffusion within the scaffold, remaining at its outer surface.

The differentiation of cells was also studied on supports which presented protein gradients. Depending on the protein/growth factor coverage and the morphology (steepness) of the gradients, the differentiation towards different cell lineages was investigated. As an example, Guo et al. fabricated electrospun fibrous scaffolds based on poly(lactide-co-glycolide) (PLGA) that featured a unidirectional gradient of encapsulated bFGF (Figure 3.9). The effect of bFGF release from the support was spatially modulated by the GF coverage and the scaffold morphology also influenced the migration and differentiation of mouse dermal fibroblasts. By increasing the non-gradient (NG) concentration of bFGF (NG0.7 > NG0.1) within the scaffold enhanced fibroblast migration compared to the unfunctionalized scaffold. The depth of cell migration was further determined by the steepness of the concentration profile of bFGF gradient (Figure 3.9A). bFGF gradient coverage *in vivo* was additionally showed to control the density of mature blood vessels (positive to both CD31 and α-SMA) within the constructs (Figure 3.9B). These fabrication strategies were effective to generate artificial blood vessels which displayed a functional character by the presence of blood cells in their interior following 10 days of implantation (Figure 3.9C).

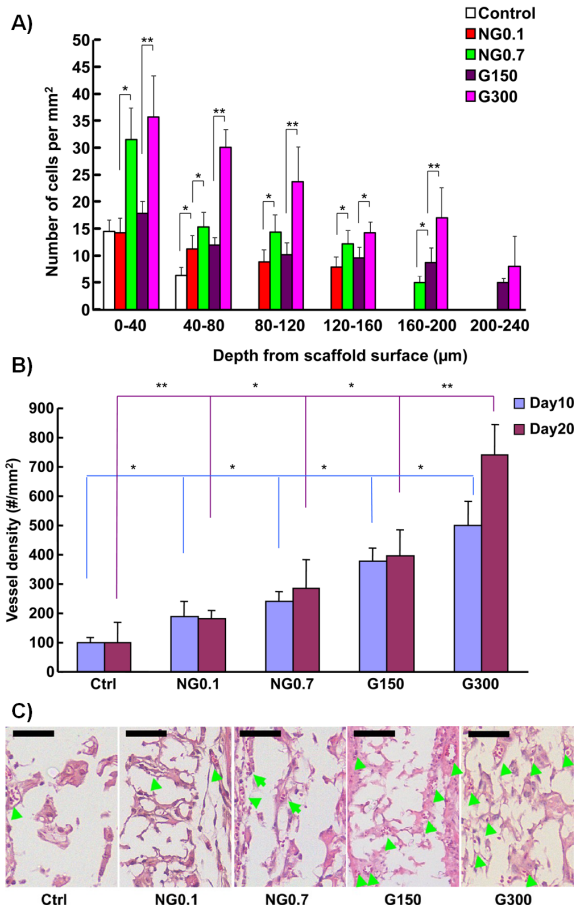

Figure 3.9. *(A) In vitro study of cell migration into scaffolds with bFGF gradients. After 14 days of culture, scaffolds were sectioned (each section covered the entire scaffold thickness), stained with rhodamine phalloidin for F-actin. Cell number at different depth of the scaffold was quantified. Five samples for each scaffold type were used. Values represent the mean and standard deviation. *p < 0.01, **p < 0.001. (B) Vessel numbers within the scaffolds after 10 and 20 days of subcutaneous implantation. Values are presented as mean ± standard deviation (n = 5). *p < 0.01, **p < 0.001. (C) Blood vessels within the scaffolds after 10 days of implantation. The functional vessels that contain well-defined lumens and blood cells are indicated by green arrows. Scale bar = 50 μm. Reprinted with permission from REF 105. Copyright 2012 American Chemical Society.*

Synthetic ECMs presenting gradient of bio-chemical cues were also applied to control osteogenic differentiation in bone/cartilage engineering implants.[131] In this research area, Li et al. fabricated a gradient of gelatin and hydroxyapatite (HA) along a poly(DL-lactide) (PDLLA) electrospun scaffold and subsequently showed that both the viability as well as the cell density of pre-osteoblast (MC-3T3 E1)

increased in the direction of the gradient.[108] In addition, both alkaline phosphatase activity and collagen type-I expression showed a similar trend, indicating the presence of a gradient in osteogenic differentiation along the scaffold architecture. In order to create a gradient tissue, Zhang et al. fabricated a scaffold based on PLGA containing a dexamethasone (Dex) gradient by gradually changing the Dex concentration in the electrospinning solution from 10^{-4} mol/L (100 %) to 2 x 10^{-5} mol/L (20 %).[98] Mesenchymal stem cells (MSCs) cultured on these scaffold adhered, proliferated (Figure 3.10A) as well as differentiated into a specific lineage. The higher Dex concentration induced adipocyte formation while a lower Dex concentration induced osteogenic differentiation (Figure 3.10B).

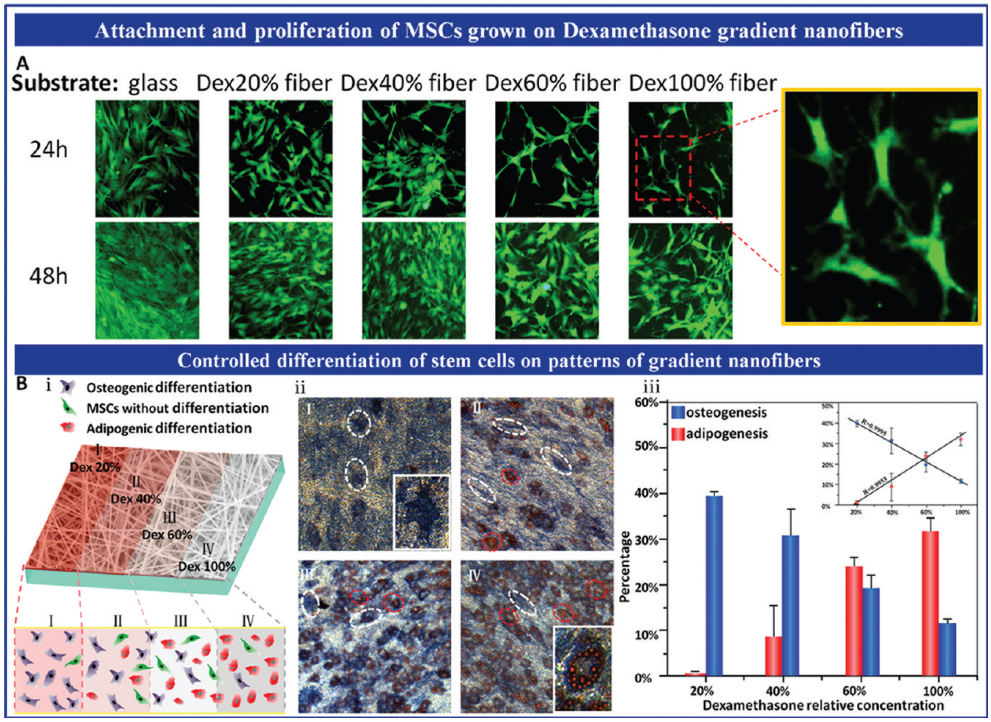

Figure 3.10. *Nanofibers with dexamethasone concentration gradient induce MSC differentiation. (A) Fluorescent images of MSC attachment and proliferation grown on dexamethasone gradient nanofibers. (B) Schematic diagram of MSC specific differentiation induced by substrate (i). ALP (osteocyte) and red-oil (adipocyte) staining images of MSCs growth on nanofibers with dexamethasone concentration gradient (ii). Differentiation proportion of MSCs induced by substrate with different dexamethasone concentrations (iii). Reprinted with permission from REF 98. Copyright 2012 American Chemical Society.*

Aiming at a similar tissue construct, Lee et al. created a porous membrane containing a double gradient of platelet-derived growth factor-b (PDGF-BB) and bone morphogenetic protein 2 (BMP-2).[109] The growth factors where immobilized on the membrane via hydrogen bonding of heparin and Pluronic F127 and the subsequent ionic interaction of the proteins with heparin, as discussed before. The highest concentration of the growth factors in the structure was measured around 65 ng and it decreases linearly to around 5 ng per membrane section (5 mm x 10 mm x 0.4 mm). Adipose-derived stem cells (ASCs) cultured on this structure showed an upregulation of different tenogenic markers at membrane sections loaded with higher concentrations of PDGF-BB, while different osteogenic markers where upregulated in sections with higher concentrations of BMP-2. ASCs differentiation was also visualized via selective staining with antibodies against tenomodulin (for tenogenesis) and bone sialoprotein (osteogenesis).

3.5 Future outlook

As we continue to shed light on the complexity of cellular signaling and organization from a single cell level to populations of different cells forming tissues and organs in our body, the need for further controlling and replicating such biological functions at the interface with biomaterials is of paramount importance to regenerate fully functional tissue substitutes. New material technology platforms should aim at multiplexing the different signals at the base of the targeted cell activity in a more dynamic manner. In this respect supramolecular chemistry could be a promising route. Host-guest chemistry based on noncovalent interactions (electrostatic, hydrogen bonding, van der Waals and hydrophobic),[132] in combination with SAMs, have been applied to engineer reversible and stimuli-responsive 2D biointerfaces.[133] Additionally, 3D supramolecular polymeric hydrogels and scaffolds are also gaining interest as they are easily prepared via a modular approach.[134-135] Cyclodextrins (CD), cucurbiturils (CB) and calixaranes are examples of host molecules that can include specific guests via molecular recognition.[132, 136-138] Additionally, ureido-pyrimidinone (UPy) unites are self-complementary which interact via hydrogen bonding.[132, 139-142]

Using these various principles different proteins, ranging from small peptides[137-138, 142-143] to large proteins[136, 144-146] and growth factors[147], have been dynamically bound to solid surfaces and into 3D structures. Although most supramolecular biointerfaces and biomaterials are homogeneous, recently, the group of Huskens obtained a gradient in protein concentration across a solid substrate using gel-state supported lipid bilayers (SLB).[148] Such SLBs show negligible movement around room temperature, while above their melting temperature, a gradient can be achieved via electrophoresis. However, other gradient systems can be envisioned when supramolecular chemistry is combined with the previously mentioned gradient fabrication methods. As an example, one could use the gradient SAMs or polymer brushes to gradually vary the CD concentration along a substrate. Varying the CB concentration in the opposite direction would create a double gradient of proteins that specifically bind to either CD or CB. This will allow for the fabrication of a dynamic 2D double gradient surface. With the same principle of varying the CD or CB concentration, the gradient maker setup could be used to fabricate a single or a multigradient supramolecular and bioactive hydrogel. The development of such artificial and spatially controlled biofunctional materials with dynamic capabilities together with more in-depth *in vitro* and *in vivo* studies seems a promising route for future biomaterial-based tissue regeneration strategies.

3.6 References

1 Seidi, A.; Ramalingam, M.; Elloumi-Hannachi, I.; Ostrovidov, S.; Khademhosseini, A., *Acta Biomaterialia* **2011,** *7,* 1441-1451.

2 Genzer, J., *Annual Review of Materials Research* **2012,** *42,* 435-468.

3 Carter, S. B., *Nature* **1967,** *213,* 256-260.

4 Plotnikov, S. V.; Waterman, C. M., *Current Opinion in Cell Biology* **2013,** *25,* 619-626.

5 Castro, N.; Hacking, S. A.; Zhang, L., *Ann Biomed Eng* **2012,** *40,* 1628-1640.

6 DeLong, S. A.; Gobin, A. S.; West, J. L., *Journal of Controlled Release* **2005,** *109,* 139-148.

7 DeLong, S. A.; Moon, J. J.; West, J. L., *Biomaterials* **2005,** *26,* 3227-3234.
8 Kennedy, S. B.; Washburn, N. R.; Simon Jr, C. G.; Amis, E. J., *Biomaterials* **2006,** *27,* 3817-3824.
9 Engler, A. J.; Sen, S.; Sweeney, H. L.; Discher, D. E., *Cell* **2006,** *126,* 677-689.
10 Morgenthaler, S.; Zink, C.; Spencer, N. D., *Soft Matter* **2008,** *4,* 419-434.
11 Senaratne, W.; Andruzzi, L.; Ober, C. K., *Biomacromolecules* **2005,** *6,* 2427-2448.
12 Alcantar, N. A.; Aydil, E. S.; Israelachvili, J. N., *Journal of Biomedical Materials Research* **2000,** *51,* 343-351.
13 Banerjee, I.; Pangule, R. C.; Kane, R. S., *Advanced Materials* **2011,** *23,* 690-718.
14 Jain, A.; Jain, S. K., **2008,** *25,* 403-447.
15 Veronese, F. M.; Pasut, G., *Drug Discovery Today* **2005,** *10,* 1451-1458.
16 Zalipsky, S., *Advanced Drug Delivery Reviews* **1995,** *16,* 157-182.
17 Zhu, J., *Biomaterials* **2010,** *31,* 4639-4656.
18 Burdick, J. A.; Khademhosseini, A.; Langer, R., *Langmuir* **2004,** *20,* 5153-5156.
19 Cosson, S.; Kobel, S. A.; Lutolf, M. P., *Advanced Functional Materials* **2009,** *19,* 3411-3419.
20 Allazetta, S.; Cosson, S.; Lutolf, M. P., *Chemical Communications* **2011,** *47,* 191-193.
21 Cosson, S.; Allazetta, S.; Lutolf, M. P., *Lab on a Chip* **2013,** *13,* 2099-2105.
22 Hutmacher, D. W., *Biomaterials* **2000,** *21,* 2529-2543.
23 Hollister, S. J., *Nature Materials* **2005,** *4,* 518-524.
24 Pham, Q. P.; Sharma, U.; Mikos, A. G., *Tissue Engineering* **2006,** *12,* 1197-1211.
25 Rezwan, K.; Chen, Q. Z.; Blaker, J. J.; Boccaccini, A. R., *Biomaterials* **2006,** *27,* 3413-3431.
26 Sill, T. J.; von Recum, H. A., *Biomaterials* **2008,** *29,* 1989-2006.
27 Hutmacher, D. W., *J Biomat Sci-Polym E* **2001,** *12,* 107-124.
28 Chaudhury, M. K.; Whitesides, G. M., *Science* **1992,** *256,* 1539-1541.

29 Terrill, R. H.; Balss, K. M.; Zhang, Y.; Bohn, P. W., *Journal of the American Chemical Society* **2000,** *122,* 988-989.

30 Wang, Q.; Bohn, P. W., *The Journal of Physical Chemistry B* **2003,** *107,* 12578-12584.

31 Plummer, S. T.; Bohn, P. W., *Langmuir* **2002,** *18,* 4142-4149.

32 Love, J. C.; Estroff, L. A.; Kriebel, J. K.; Nuzzo, R. G.; Whitesides, G. M., *Chemical Reviews* **2005,** *105,* 1103-1170.

33 Plummer, S. T.; Wang, Q.; Bohn, P. W.; Stockton, R.; Schwartz, M. A., *Langmuir* **2003,** *19,* 7528-7536.

34 Wang, Q.; Bohn, P. W., *Thin Solid Films* **2006,** *513,* 338-346.

35 Wu, T.; Efimenko, K.; Vlček, P.; Šubr, V.; Genzer, J., *Macromolecules* **2003,** *36,* 2448-2453.

36 Edmondson, S.; Osborne, V. L.; Huck, W. T. S., *Chemical Society Reviews* **2004,** *33,* 14-22.

37 Wang, X.; Tu, H.; Braun, P. V.; Bohn, P. W., *Langmuir* **2006,** *22,* 817-823.

38 Barbey, R.; Lavanant, L.; Paripovic, D.; Schuwer, N.; Sugnaux, C.; Tugulu, S.; Klok, H. A., *Chemical Reviews* **2009,** *109,* 5437-5527.

39 Wu, T.; Gong, P.; Szleifer, I.; Vlček, P.; Šubr, V.; Genzer, J., *Macromolecules* **2007,** *40,* 8756-8764.

40 De Gennes, P. G., *Macromolecules* **1980,** *13,* 1069-1075.

41 Brittain, W. J.; Minko, S., *Journal of Polymer Science Part a-Polymer Chemistry* **2007,** *45,* 3505-3512.

42 Wu, T.; Efimenko, K.; Genzer, J., *Journal of the American Chemical Society* **2002,** *124,* 9394-9395.

43 Mei, Y.; Wu, T.; Xu, C.; Langenbach, K. J.; Elliott, J. T.; Vogt, B. D.; Beers, K. L.; Amis, E. J.; Washburn, N. R., *Langmuir* **2005,** *21,* 12309-12314.

44 Mei, Y.; Elliott, J. T.; Smith, J. R.; Langenbach, K. J.; Wu, T.; Xu, C.; Beers, K. L.; Amis, E. J.; Henderson, L., *Journal of Biomedical Materials Research Part A* **2006,** *79A,* 974-988.

45 Ren, T.; Yu, S.; Mao, Z.; Moya, S. E.; Han, L.; Gao, C., *Biomacromolecules* **2014,** *15,* 2256-2264.

46 Choi, S.; Choi, B. C.; Xue, C.; Leckband, D., *Biomacromolecules* **2013,** *14,* 92-100.

47 Vasilev, K.; Mierczynska, A.; Hook, A. L.; Chan, J.; Voelcker, N. H.; Short, R. D., *Biomaterials* **2010,** *31,* 392-397.

48 Wu, J.; Mao, Z.; Gao, C., *Biomaterials* **2012,** *33,* 810-820.

49 Morgenthaler, S.; Zink, C.; Städler, B.; Vörös, J.; Lee, S.; Spencer, N. D.; Tosatti, S. G. P., *Biointerphases* **2006,** *1,* 156-165.

50 Pei, J.; Hall, H.; Spencer, N. D., *Biomaterials* **2011,** *32,* 8968-8978.

51 Bhat, R.; Tomlinson, M.; Wu, T.; Genzer, J., Surface-Grafted Polymer Gradients: Formation, Characterization, and Applications. In *Surface-Initiated Polymerization II*, Jordan, R., Ed. Springer Berlin Heidelberg: 2006; Vol. 198, pp 51-124.

52 Tomlinson, M. R.; Genzer, J., *Macromolecules* **2003,** *36,* 3449-3451.

53 Li, L.; Zhu, Y.; Li, B.; Gao, C., *Langmuir* **2008,** *24,* 13632-13639.

54 Ren, T.; Mao, Z.; Guo, J.; Gao, C., *Langmuir* **2013,** *29,* 6386-6395.

55 Li, B.; Yu, B.; Huck, W. T. S.; Liu, W.; Zhou, F., *Journal of the American Chemical Society* **2013,** *135,* 1708-1710.

56 Yan, J.; Li, B.; Yu, B.; Huck, W. T. S.; Liu, W.; Zhou, F., *Angewandte Chemie International Edition* **2013,** *52,* 9125-9129.

57 Magenau, A. J. D.; Strandwitz, N. C.; Gennaro, A.; Matyjaszewski, K., *Science* **2011,** *332,* 81-84.

58 Li, B.; Yu, B.; Huck, W. T. S.; Zhou, F.; Liu, W., *Angewandte Chemie* **2012,** *124,* 5182-5185.

59 Poelma, J. E.; Fors, B. P.; Meyers, G. F.; Kramer, J. W.; Hawker, C. J., *Angewandte Chemie International Edition* **2013,** *52,* 6844-6848.

60 Lin, X.; He, Q.; Li, J., *Chemical Society Reviews* **2012,** *41,* 3584-3593.

61 Bhat, R. R.; Chaney, B. N.; Rowley, J.; Liebmann-Vinson, A.; Genzer, J., *Advanced Materials* **2005,** *17,* 2802-+.

62 Bhat, R. R.; Tomlinson, M. R.; Genzer, J., *Journal of Polymer Science Part B-Polymer Physics* **2005,** *43,* 3384-3394.

63 Harris, B. P.; Kutty, J. K.; Fritz, E. W.; Webb, C. K.; Burg, K. J. L.; Metters, A. T., *Langmuir* **2006,** *22,* 4467-4471.

64 Harris, B. P.; Metters, A. T., *Macromolecules* **2006,** *39,* 2764-2772.

65 Hutter, N. A.; Steenackers, M.; Reitinger, A.; Williams, O. A.; Garrido, J. A.; Jordan, R., *Soft Matter* **2011,** *7,* 4861-4867.

66 Li, L.; Wu, J.; Gao, C., *Colloid Surface B* **2011,** *85,* 12-18.

67 Caelen, I.; Bernard, A.; Juncker, D.; Michel, B.; Heinzelmann, H.; Delamarche, E., *Langmuir* **2000,** *16,* 9125-9130.

68 Jeon, N. L.; Dertinger, S. K. W.; Chiu, D. T.; Choi, I. S.; Stroock, A. D.; Whitesides, G. M., *Langmuir* **2000,** *16,* 8311-8316.

69 Gunawan, R. C.; Choban, E. R.; Conour, J. E.; Silvestre, J.; Schook, L. B.; Gaskins, H. R.; Leckband, D. E.; Kenis, P. J. A., *Langmuir* **2005,** *21,* 3061-3068.

70 Kim, S.; Kim, H. J.; Jeon, N. L., *Integrative Biology* **2010,** *2,* 584-603.

71 Toh, A. G.; Wang, Z. P.; Yang, C.; Nguyen, N.-T., *Microfluid Nanofluid* **2014,** *16,* 1-18.

72 Fosser, K. A.; Nuzzo, R. G., *Analytical Chemistry* **2003,** *75,* 5775-5782.

73 He, J.; Du, Y.; Villa-Uribe, J. L.; Hwang, C.; Li, D.; Khademhosseini, A., *Advanced Functional Materials* **2010,** *20,* 131-137.

74 Jiang, X.; Xu, Q.; Dertinger, S. K. W.; Stroock, A. D.; Fu, T.-m.; Whitesides, G. M., *Analytical Chemistry* **2005,** *77,* 2338-2347.

75 Gunawan, R. C.; Silvestre, J.; Gaskins, H. R.; Kenis, P. J. A.; Leckband, D. E., *Langmuir* **2006,** *22,* 4250-4258.

76 Chatterjee, K.; Lin-Gibson, S.; Wallace, W. E.; Parekh, S. H.; Lee, Y. J.; Cicerone, M. T.; Young, M. F.; Simon Jr, C. G., *Biomaterials* **2010,** *31,* 5051-5062.

77 Nemir, S.; Hayenga, H. N.; West, J. L., *Biotechnology and Bioengineering* **2010,** *105,* 636-644.

78 Wang, X.; Wenk, E.; Zhang, X.; Meinel, L.; Vunjak-Novakovic, G.; Kaplan, D. L., *Journal of Controlled Release* **2009,** *134,* 81-90.

79 Guarnieri, D.; De Capua, A.; Ventre, M.; Borzacchiello, A.; Pedone, C.; Marasco, D.; Ruvo, M.; Netti, P. A., *Acta Biomaterialia* **2010,** *6,* 2532-2539.

80 Smith Callahan, L. A.; Childers, E. P.; Bernard, S. L.; Weiner, S. D.; Becker, M. L., *Acta Biomaterialia* **2013,** *9,* 7420-7428.

81 Smith Callahan, L. A.; Ganios, A. M.; Childers, E. P.; Weiner, S. D.; Becker, M. L., *Acta Biomaterialia* **2013,** *9,* 6095-6104.

82 Smith Callahan, L. A.; Policastro, G. M.; Bernard, S. L.; Childers, E. P.; Boettcher, R.; Becker, M. L., *Biomacromolecules* **2013,** *14,* 3047-3054.

83 Hahn, M. S.; Miller, J. S.; West, J. L., *Advanced Materials* **2005,** *17,* 2939-2942.

84 Hahn, M. S.; Miller, J. S.; West, J. L., *Advanced Materials* **2006,** *18,* 2679-2684.

85 Hahn, M. S.; Taite, L. J.; Moon, J. J.; Rowland, M. C.; Ruffino, K. A.; West, J. L., *Biomaterials* **2006,** *27,* 2519-2524.

86 Hoffmann, J. C.; West, J. L., *Soft Matter* **2010,** *6,* 5056-5063.

87 Polizzotti, B. D.; Fairbanks, B. D.; Anseth, K. S., *Biomacromolecules* **2008,** *9,* 1084-1087.

88 DeForest, C. A.; Anseth, K. S., *Nat Chem* **2011,** *3,* 925-931.

89 DeForest, C. A.; Anseth, K. S., *Angewandte Chemie International Edition* **2012,** *51,* 1816-1819.

90 Mosiewicz, K. A.; Kolb, L.; van der Vlies, A. J.; Martino, M. M.; Lienemann, P. S.; Hubbell, J. A.; Ehrbar, M.; Lutolf, M. P., *Nat Mater* **2013,** *12,* 1072-1078.

91 Wylie, R. G.; Ahsan, S.; Aizawa, Y.; Maxwell, K. L.; Morshead, C. M.; Shoichet, M. S., *Nat Mater* **2011,** *10,* 799-806.

92 Wylie, R. G.; Shoichet, M. S., *Biomacromolecules* **2011,** *12,* 3789-3796.

93 Khetan, S.; Burdick, J. A., *Soft Matter* **2011,** *7,* 830-838.

94 Milleret, V.; Simona, B. R.; Lienemann, P. S.; Vörös, J.; Ehrbar, M., *Advanced Healthcare Materials* **2014,** *3,* 508-514.

95 Sala, A.; Hanseler, P.; Ranga, A.; Lutolf, M. P.; Vörös, J.; Ehrbar, M.; Weber, F. E., *Integrative Biology* **2011,** *3,* 1102-1111.

96 Huang, Z. M.; Zhang, Y. Z.; Kotaki, M.; Ramakrishna, S., *Composites Science and Technology* **2003,** *63,* 2223-2253.

97 Handarmin; Tan, G. J. Y.; Sundaray, B.; Marcy, G. T.; Goh, E. L. K.; Chew, S. Y., *Drug Deliv. and Transl. Res.* **2011,** *1,* 147-160.

98 Zhang, X.; Gao, X.; Jiang, L.; Qin, J., *Langmuir* **2012,** *28,* 10026-10032.

99 Sundararaghavan, H. G.; Burdick, J. A., *Biomacromolecules* **2011,** *12,* 2344-2350.

100 Samavedi, S.; Olsen Horton, C.; Guelcher, S. A.; Goldstein, A. S.; Whittington, A. R., *Acta Biomaterialia* **2011,** *7,* 4131-4138.

101 Bonani, W.; Maniglio, D.; Motta, A.; Tan, W.; Migliaresi, C., *Journal of Biomedical Materials Research Part B: Applied Biomaterials* **2011,** *96B,* 276-286.

102 Samavedi, S.; Guelcher, S. A.; Goldstein, A. S.; Whittington, A. R., *Biomaterials* **2012,** *33,* 7727-7735.

103 Bonani, W.; Motta, A.; Migliaresi, C.; Tan, W., *Langmuir* **2012,** *28,* 13675-13687.

104 Du, F.; Wang, H.; Zhao, W.; Li, D.; Kong, D.; Yang, J.; Zhang, Y., *Biomaterials* **2012,** *33,* 762-770.

105 Guo, X.; Elliott, C. G.; Li, Z.; Xu, Y.; Hamilton, D. W.; Guan, J., *Biomacromolecules* **2012,** *13,* 3262-3271.

106 Li, X.; Xie, J.; Lipner, J.; Yuan, X.; Thomopoulos, S.; Xia, Y., *Nano Letters* **2009,** *9,* 2763-2768.

107 Shi, J.; Wang, L.; Zhang, F.; Li, H.; Lei, L.; Liu, L.; Chen, Y., *ACS Applied Materials & Interfaces* **2010,** *2,* 1025-1030.

108 Zou, B.; Liu, Y.; Luo, X.; Chen, F.; Guo, X.; Li, X., *Acta Biomaterialia* **2012,** *8,* 1576-1585.

109 Min, H. K.; Oh, S. H.; Lee, J. M.; Im, G. I.; Lee, J. H., *Acta Biomaterialia* **2014,** *10,* 1272-1279.

110 Oh, S. H.; Park, I. K.; Kim, J. M.; Lee, J. H., *Biomaterials* **2007,** *28,* 1664-1671.

111 Oh, S. H.; Kim, T. H.; Im, G. I.; Lee, J. H., *Biomacromolecules* **2010,** *11,* 1948-1955.

112 Kim, T.; Oh, S.; Kwon, E.; Lee, J.; Lee, J., *Macromol. Res.* **2013,** *21,* 878-885.

113 Oh, S. H.; Kim, T. H.; Lee, J. H., *Biomaterials* **2011,** *32,* 8254-8260.

114 Geiger, B.; Spatz, J. P.; Bershadsky, A. D., *Nature Reviews Molecular Cell Biology* **2009,** *10,* 21-33.

115 Prager-Khoutorsky, M.; Lichtenstein, A.; Krishnan, R.; Rajendran, K.; Mayo, A.; Kam, Z.; Geiger, B.; Bershadsky, A. D., *Nat Cell Biol* **2011,** *13,* 1457-1465.

116 Cukierman, E.; Pankov, R.; Yamada, K. M., *Current Opinion in Cell Biology* **2002,** *14,* 633-640.

117 Wozniak, M. A.; Modzelewska, K.; Kwong, L.; Keely, P. J., *Biochimica et Biophysica Acta (BBA) - Molecular Cell Research* **2004,** *1692,* 103-119.

118 Fraley, S. I.; Feng, Y.; Krishnamurthy, R.; Kim, D. H.; Celedon, A.; Longmore, G. D.; Wirtz, D., *Nature Cell Biology* **2010,** *12,* 598-604.

119 Cavalcanti-Adam, E. A.; Micoulet, A.; Blümmel, J.; Auernheimer, J.; Kessler, H.; Spatz, J. P., *European Journal of Cell Biology* **2006,** *85,* 219-224.

120 Cavalcanti-Adam, E. A.; Volberg, T.; Micoulet, A.; Kessler, H.; Geiger, B.; Spatz, J. P., *Biophysical Journal* **2007,** *92,* 2964-2974.

121 Underwood, P. A.; Bennett, F. A., *Journal of Cell Science* **1989,** *93,* 641-649.

122 Danilov, Y. N.; Juliano, R. L., *Experimental Cell Research* **1989,** *182,* 186-196.

123 Brandley, B. K.; Schnaar, R. L., *Developmental Biology* **1989,** *135,* 74-86.

124 Cukierman, E.; Pankov, R.; Stevens, D. R.; Yamada, K. M., *Science* **2001,** *294,* 1708-1712.

125 Petrie, R. J.; Gavara, N.; Chadwick, R. S.; Yamada, K. M., *The Journal of Cell Biology* **2012,** *197,* 439-455.

126 Even-Ram, S.; Yamada, K. M., *Current Opinion in Cell Biology* **2005,** *17,* 524-532.

127 Kyburz, K. A.; Anseth, K. S., *Acta Biomaterialia* **2013,** *9,* 6381-6392.

128 Levine, E. M.; Roelink, H.; Turner, J.; Reh, T. A., *Journal of Neuroscience* **1997,** *17,* 6277-6288.

129 Fu, M.; Lui, V. C. H.; Sham, M. H.; Pachnis, V.; Tam, P. K. H., *Journal of Cell Biology* **2004,** *166,* 673-684.

130 Angot, E.; Loulier, K.; Nguyen-Ba-Charvet, K. T.; Gadeau, A. P.; Ruat, M.; Traiffort, E., *Stem Cells* **2008,** *26,* 2311-2320.

131 Bessa, P. C.; Casal, M.; Reis, R. L., *Journal of Tissue Engineering and Regenerative Medicine* **2008,** *2,* 81-96.

132 Schneider, H. J., *Angew Chem Int Edit* **2009,** *48,* 3924-3977.

133 Yang, H.; Yuan, B.; Zhang, X.; Scherman, O. A., *Accounts Chem Res* **2014,** *47,* 2106-2115.

134 Dankers, P. Y. W.; Meijer, E. W., *B Chem Soc Jpn* **2007,** *80,* 2047-2073.

135 Appel, E. A.; del Barrio, J.; Loh, X. J.; Scherman, O. A., *Chemical Society Reviews* **2012,** *41,* 6195-6214.

136 Gonzalez-Campo, A.; Brasch, M.; Uhlenheuer, D. A.; Gomez-Casado, A.; Yang, L. T.; Brunsveld, L.; Huskens, J.; Jonkheijm, P., *Langmuir* **2012,** *28,* 16364-16371.

137 Neirynck, P.; Brinkmann, J.; An, Q.; van der Schaft, D. W. J.; Milroy, L.-G.; Jonkheijm, P.; Brunsveld, L., *Chemical Communications* **2013,** *49,* 3679-3681.

138 Neirynck, P.; Schimer, J.; Jonkheijm, P.; Milroy, L. G.; Cigler, P.; Brunsveld, L., *J Mater Chem B* **2015,** *3,* 539-545.

139 Guo, M. Y.; Pitet, L. M.; Wyss, H. M.; Vos, M.; Dankers, P. Y. W.; Meijer, E. W., *Journal of the American Chemical Society* **2014,** *136,* 6969-6977.

140 Appel, W. P. J.; Meijer, E. W.; Dankers, P. Y. W., *Macromol Biosci* **2011,** *11,* 1706-1712.

141 Dankers, P. Y. W.; van Leeuwen, E. N. M.; van Gemert, G. M. L.; Spiering, A. J. H.; Harmsen, M. C.; Brouwer, L. A.; Janssen, H. M.; Bosman, A. W.; van Luyn, M. J. A.; Meijer, E. W., *Biomaterials* **2006,** *27,* 5490-5501.

142 Dankers, P. Y. W.; Harmsen, M. C.; Brouwer, L. A.; Van Luyn, M. J. A.; Meijer, E. W., *Nature Materials* **2005,** *4,* 568-574.

143 An, Q.; Brinkmann, J.; Huskens, J.; Krabbenborg, S.; de Boer, J.; Jonkheijm, P., *Angew Chem Int Edit* **2012,** *51,* 12233-12237.

144 Young , J. F.; Nguyen , H. D.; Yang, L.; Huskens, J.; Jonkheijm, P.; Brunsveld , L., *ChemBioChem* **2010,** *11,* 180-183.

145 Hwang, I.; Baek, K.; Jung, M.; Kim, Y.; Park, K. M.; Lee, D.-W.; Selvapalam, N.; Kim, K., *Journal of the American Chemical Society* **2007,** *129,* 4170-4171.

146 Wan, P.; Wang, Y.; Jiang, Y.; Xu, H.; Zhang, X., *Advanced Materials* **2009,** *21,* 4362-4365.

147 Cabanas-Danés, J.; Rodrigues, E. D.; Landman, E.; van Weerd, J.; van Blitterswijk, C.; Verrips, T.; Huskens, J.; Karperien, M.; Jonkheijm, P., *Journal of the American Chemical Society* **2014,** *136,* 12675-12681.

148 Krabbenborg, S. O.; van Weerd, J.; Karperien, M.; Jonkheijm, P.; Huskens, J., *ChemPhysChem* **2014,** *15,* 3460-3465.

Controlled surface initiated polymerization of N-isopropylacrylamide from polycaprolactone substrates for regulating cell adhesion

In this Chapter SI-ATRP from polyester based substrates is introduced. For this study poly(ε-caprolactone) (PCL) thin films were modified with thermoresponsive poly(N-isopropylacrylamide) (PNIPAM) brushes to direct and control cellular attachment and detachment. Prior to brush growth, the surface of PCL was activated by a diamine to allow for initiator coupling. Infra-red spectra taken before and after cell culturing demonstrated the covalently attached nature of the PNIPAM brushes. PCL is a biocompatible polymer and to prove that the modifications described above did not change this characteristic property, a cell attachment / detachment study was carried out. The modified substrates showed a lower cell attachment when compared to PCL alone and to PCL films modified with the initiator. The possibility to detach the cells in the form of a sheet was proved using PNIPAM-modified PCL films by lowering the temperature to 25°C. No relevant detachment was shown by the unmodified or by the initiator modified surfaces. This confirmed that the detachment was temperature dependent and not connected to other factors such as polymer swelling. These functionalized polymeric films can find applications as smart cell culture systems in regenerative medicine applications.

* This Chapter has been published in: M. Klein Gunnewiek, A. Di Luca, X. Sui, C.A. van Blitterswijk, L. Moroni, G.J. Vancso; *Israel Journal of Chemistry* **2012**, 52, 339-346

4.1 Introduction

Atom Transfer Radical Polymerization (ATRP), pioneered by Krzysztof Matyjaszewski, is one of the most successful methods to create polymer brushes with control over molar mass and molar mass distributions.[1-8] The discovery of ATRP initiated more and more research activities in many different areas in the field of polymer technology, ranging from understanding the underlying mechanism and kinetics of ATRP,[1-2] and the surface-initiated polymerization of polymer brushes,[9-12] to the growth and use of thermoresponsive polymers.[13-14] In recent years, studies of cell and bacteria behavior on polymers grown by ATRP were also performed to control cell adhesion, proliferation, migration and growth.[15-19] Surface-initiated ATRP was used with great success to obtain designed surfaces exhibiting coatings with thicknesses in the nanoscale with targeted and controlled properties.[1-4] Gold and silicon were most often employed as substrates for polymerization[3-4, 20-28], although tissue culture polystyrene (TCPS)[29-31] or titanium[32-36] were also investigated as substrates for biomedical applications. In the specific case of polymer-based scaffolds for tissue engineering, the use of biocompatible polymer substrates, such as poly(ε-caprolactone) (PCL) or other polyester based polymers, is desirable.[37-39] In these settings, the aim of this Chapter is to provide results obtained on the SI-ATRP from PCL films of a poly(*N*-isopropylacrylamide) (PNIPAM) layer.

PNIPAM[4-5, 40-44] is a well know polymer that triggers a different cellular response above and below its critical solution temperature (LCST) due to a change in chain conformation and variations in intra- and intermolecular interactions around the LCST. Above the LCST, the polymer assumes a dehydrated collapsed and more hydrophobic state resulting in a cell adhesive brush. When lowering the temperature below the LCST, these polymers assume a highly hydrophilic state resulting in swelling and non-biofouling. The effect of LCST has been well studied and explained in terms of cell detachment and cell sheet harvesting from different substrates (e.g silicon, glass or TCPS).[27, 40, 45-52] Cell sheet harvesting is a branch within the tissue engineering field, in which cells are expanded at 37 °C on top of PNIPAM grafted culture dishes.[40, 50] After reaching confluency, cells are harvested as intact sheets by simply reducing the temperature to below the LCST.

In 1995, Okano *et al.*[53] proposed a mechanism for cell detachment on PNIPAM surfaces upon lowering the working temperature below LCST. It was shown that the metabolism of the cultured cells plays an important role in the detachment. By lowering the temperature to 20°C, PNIPAM becomes hydrated and cell metabolic activity is correspondingly decreased. A subsequent increase of the temperature to an optimal value but still below the LCST, will enhance the detachment as a result of increased cell metabolic activity. As the cellular metabolism is different for every cell type, this optimum temperature will change, as well. Later, other researchers also studied the detachment mechanism of cells on thermoresponsive brushes.[45, 54-55] Using Total Internal Reflection Fluorescence (TIRF) microscopy, Uhlig *et al.*[54] confirmed that the detachment mechanism was cell type dependent and that cells play an active role in this mechanism. Cooperstein *et al.* also discussed this mechanism.[45] They proposed a two-step detachment mechanism from PNIPAM brushes. Their model includes a passive step involving the hydration of polymer chains and an active step involving cell shape change and detachment from the surface driven by cytoskeletal action and metabolic processes.

The attachment and detachment of a cell from a thermoresponsive substrate is not only affected by the type of cell, but also by the length and the grafting density of the polymer brush. Both the length and density of brushes determine the extent and rate of hydration. For example, Xu *et al.* grew PNIPAM brushes on silicon substrates with a variable length between 3 and 31 nm and showed that thicker brushes resulted in enhanced fibroblast attachment and growth.[56] However, Akigama *et al.*[57], found an optimum brush length around 20 nm for bovine endothelial cells when PNIPAM brushes were grown on TCPS. This difference in results might be due to the more hydrophobic nature of TCPS that enhances the hydration.[57] Mizutani *et al.*[31] showed a decrease in endothelial cell attachment for PNIPAM brushes grown on TCPS. When the brush length exceeded 60 nm, cell adhesion was negligible. PNIPAM grown on glass substrates showed an optimal cell attachment and detachment of fibroblasts with brush length estimated to 11-13 nm.[58] These studies all reported that cell attachment occurred at short brush lengths. However, Sui *et al.*[59] has recently shown that cell attachment can occur for brush lengths up to 220 nm. Whereas low density polymer brush with a dry

thickness of ~ 10 nm showed the highest cell adhesion with elongated morphology, increasing the brush density and dry thickness resulted in decreased cell density and elongation. A general consensus on the effect of brush length on cell adhesion is still missing. The results we obtained suggest a way to modulate cell adhesion and shape by changing the length of the brushes and opening new application of this surface modification.

As mentioned previously, the effect of brushes on cell behavior has been well studied. However, polymeric scaffolds have seldom been used as substrate.[37-39, 60-61] The possibility to modify polymeric materials with brushes in order to improve their properties, is an appealing strategy to expand their applications in different fields of tissue engineering. Therefore, in this study the thermoresponsive effect of PNIPAM grown from PCL substrates with respect to film and cell behavior was investigated.

4.2 Results and discussion

4.2.1 Fabrication and characterization

PCL films were prepared by spin-coating a 5 wt% polymer solution onto silicon or glass substrates with a thickness in the order of 1 µm. After spin-coating, the PCL films were annealed to release the stress in the film. The spin-coated PCL film was subsequently modified in three steps with PNIPAM brushes, as shown in Scheme 4.1. First, PCL was aminolysed with ethylenediamine (EDA), after which the ATRP initiator (BIBB) was attached to the film. NIPAM was subsequently polymerized to a thickness of around 200 nm according to a procedure presented in previous work.[59]

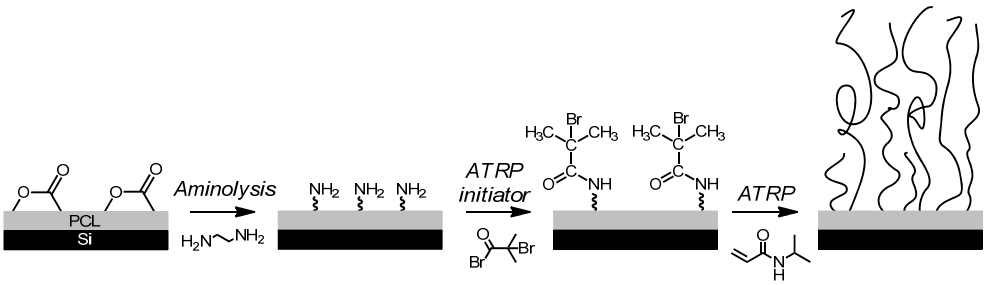

Scheme 4.1. *Reaction diagram for the modification of PCL films using aminolysis and surface-initiated-ATRP of NIPAM to produce surface tethered PNIPAM brushes.*

The surface morphology of the modified substrates was determined at each different step by capturing Atomic Force Microscopy (AFM) images (Figure 4.1). AFM is a powerful analytical tool for both the characterization and the fabrication of polymer brush structures. The application of AFM in the field of polymer brushes is described in detail by Sui *et al.*[62] From the AFM images it was clear that the roughness did not change significantly by modifying PCL with either EDA, or the initiator. This implied that modification of PCL with EDA - i.e. breaking the ester bonds of the polymer chains - was sufficient enough for the formation of polymer brushes without introducing significant surface roughness. As shown in Figure 4.1d, the brush coating formed uniformly, covering and enhancing the PCL topological features.

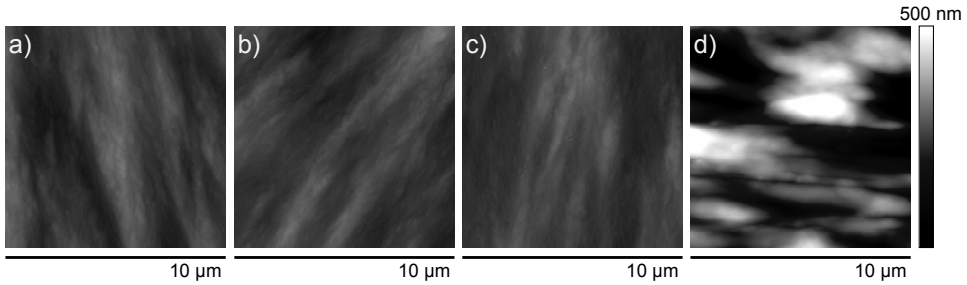

Figure 4.1. *Surface morphologies of (a) PCL, (b) aminolysed PCL, (c) initiator covered PCL and (d) PNIPAM brushes grown from PCL by AFM.*

The presence of PNIPAM on the surface of the PCL films was also confirmed by Attenuated Total Reflection Fourier Transform Infrared (ATR-FTIR) measurements (Figure 4.2). The spectra of unmodified PCL clearly showed the characteristic ester peak at 1721 cm^{-1}. After the modification with PNIPAM, this peak was significantly reduced and the two characteristic amide peaks at 1637 and 1535 cm^{-1} of PNIPAM were present. The spectra after cell culturing showed the same characteristic peaks for unmodified PCL as well as for PNIPAM, indicating the stable and covalent attachment of PNIPAM to the PCL film. However, ATR-FTIR spectra of PCL films modified with either EDA or the initiator did not show any significant difference, due to modification of only a thin surface layer. After subjecting these two films to the polymerization mixture, no amide peaks where shown in the FTIR spectra, indicating that PNIPAM could have only grown due to

the coupling of initiator to the PCL films by the EDA modification. Also static contact angle measurements on these samples showed a significant decrease in contact angle values from 83° for unmodified PCL to 69° for PCL modified with EDA, due to the formation of extra amine and alcohol groups on the surface.

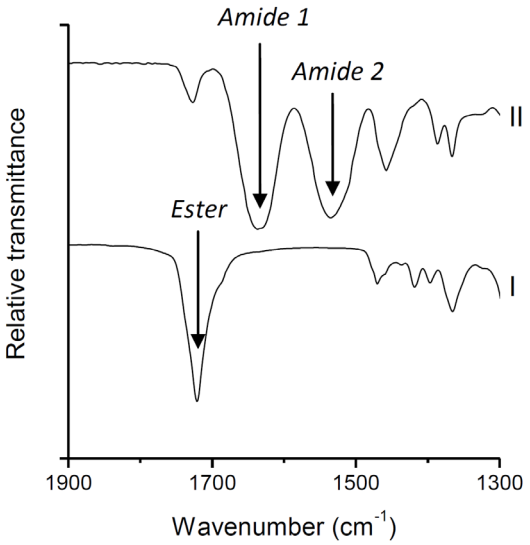

Figure 4.2. *ATR-FTIR analysis of pure (I) and PNIPAM (II) modified free-standing PCL films, respectively.*

4.2.2 Controlled cellular adhesion

Cell attachment results showed that all samples sustained cell growth. As already proven by Sui *et al.*[59], the use of high density brushes can determine a lower cell attachment compared to the PNIPAM non-modified (control) films. Fluorescent pictures of the PCL surfaces (Figure 4.3) were taken both before and after cell detachment. No significant differences can be seen on EDA-modified, initiator-modified and unmodified PCL films among the pictures taken above and below the LCST (Figure 4.3). PNIPAM modified samples presented cells attached and spread on the surface (Figure 4.3d), whereas after lowering the temperature no cells could be observed on the films (Figure 4.3h), revealing a complete detachment of the cells. This confirmed that the detachment was triggered only by the temperature change and not by swelling or any physicochemical modification of

the PCL films. The significantly lower amount of cells adhering on the PNIPAM modified samples was related to the thickness of the brush layer. It is suggested in literature that cells can not adhere on PNIPAM beyond a critical range, even at 37°C.[57, 63-64] However, recently Sui et al. showed that for 200 nm high density PNIPAM brushes, MC-3T3 fibroblasts were able to adhere although the adhesion was significantly reduced compared to thinner and lower brush density layers.[65]

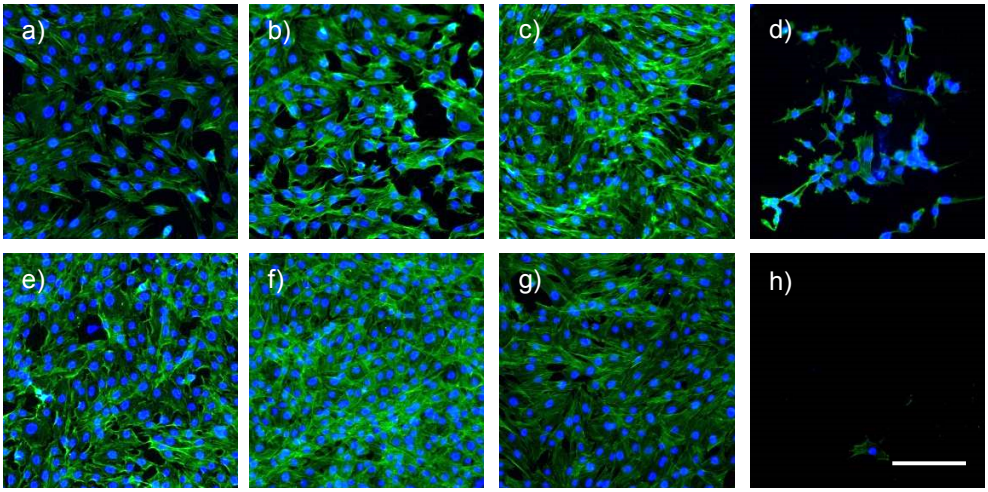

Figure 4.3. *Fluorescent images of cell attachment at 37°C (a-d) and cell detachment at 25°C (e-h) on PCL (a, e), PCL modified with EDA (b, f), PCL modified with initiator (c, g), and PCL modified with PNIPAM (d, h). Scale bar is 200 µm.*

As shown by fluorescent microscopy, cells adhered to the surface and spread on it when cultured above the LCST (37°C). When the temperature was decreased below the LCST, cells assumed a rounded shape and started to detach from the surface of the PCL films modified with PNIPAM brushes. Conversely, no changes on cell morphology and adhesion could be seen on the control surfaces, where cells maintained their spread shape. In order to harvest the cells, PCL surfaces were rinsed with cell culture media. After rinsing, the same media with suspended cells was used to re-seed the cells on a tissue culture plate (TCP). As confirmed in Figure 4.4, the amount of cells obtained from the EDA modified surface and the PCL unmodified surface was negligible compared to the amount of cells obtained from the PNIPAM modified PCL films. Cells detached as sheets from

the PNIPAM modified surfaces. After 12 hours of incubation, cells proliferated and covered the bottom of the TCP (insets in Figure 4.4). The cells harvested from the unmodified surfaces were also able to attach and proliferate, but at a much lower density than those harvested from the PNIPAM modified surfaces, These results suggest that the newly functionalized PNIPAM-PCL substrates could find potential application for different areas of tissue engineering such as autologous cartilage implantation or cell-sheet tissue engineering.[53]

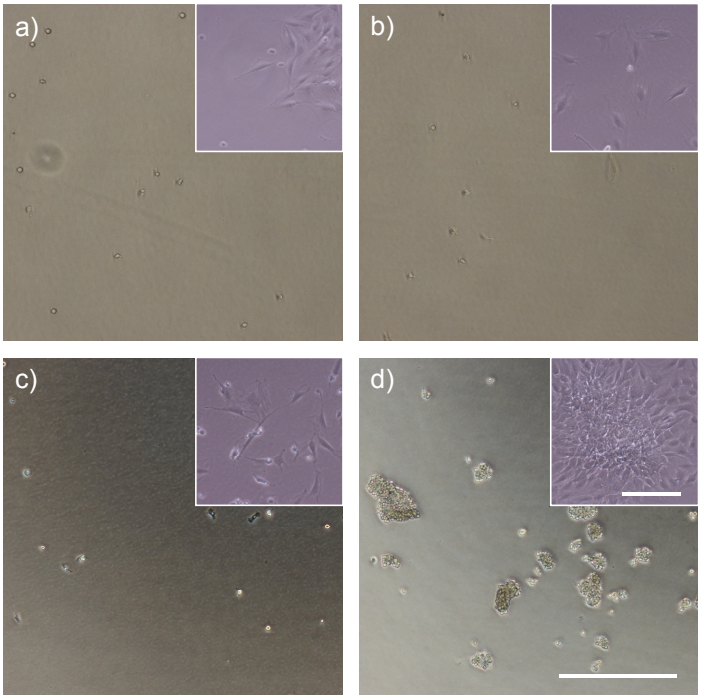

Figure 4.4. *Images of cell reseeding on TCP after cell detachment of (a) PCL, (b) PCL modified with EDA , (c) PCL modified with initiator and (d) PCL modified with PNIPAM. Scale bar is 500 µm. The insets show images after 16 hours of incubation of the detached cells. Scale bar is 200 µm.*

To show that PNIPAM was still thermoresponsive, free-standing PCL films that are modified on one side with PNIPAM were fabricated using a procedure presented by Takeoka and *et al*.[66-67] This procedure is based on the solidification of a poly(vinyl alcohol) (PVA) coating casted onto the PNIPAM covered PCL. Peeling off the solid PVA will release the PCL layer from the silicon substrate and by dissolving the PVA in water will result in a freestanding PNIPAM-PCL sheet.

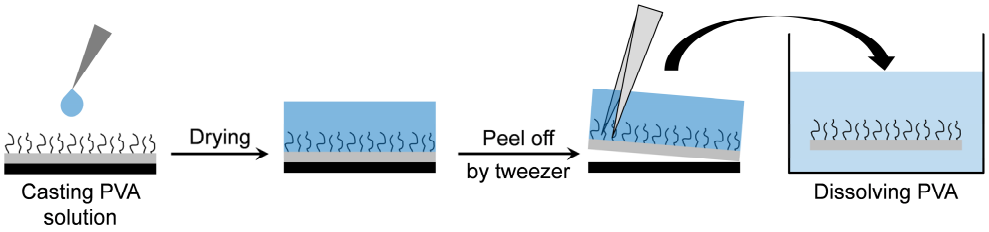

Scheme 4.2. *Procedure for the fabrication of freestanding PCL films containing a single sided PNIPAM layer.*

These sheets were subjected to a temperature shift above the LCST and showed a coiled, collapsed configuration below the LCST (Figure 4.5a) and a stretched configuration above the LCST (Figure 4.5b). This behavior can be explained by the hydrophobic nature of PCL and the hydrophobic or hydrophilic nature of PNIPAM depending on the temperature. Below the LCST, PNIPAM assumes a stretched hydrated configuration (hydrophilic state) while above the LCST, PNIPAM assumes a collapsed globular configuration (hydrophobic state). Thus, when keeping the free-standing PCL film below the LCST, the side with PNIPAM assumes the hydrophilic state, folding the hydrophobic PCL side inwards (Figure 4.5a). Subjecting the film to a temperature above the LCST, both sides of the film became hydrophobic, which leads to a stretched configuration (Figure 4.5b). As a control, an unmodified PCL film was subjected to the same temperature. This film did not show the folded configuration, indicating that the shrunk coiled state shown in Figure 4.3c and 4.3d was indeed due to the thermoresponsive character of PNIPAM. We note that coiling of a film by polymer brushes was also reported by Zou *et al* for polyvinyl chloride modified with poly(N,N-dimethylacrylamide) (PDMA).[68]

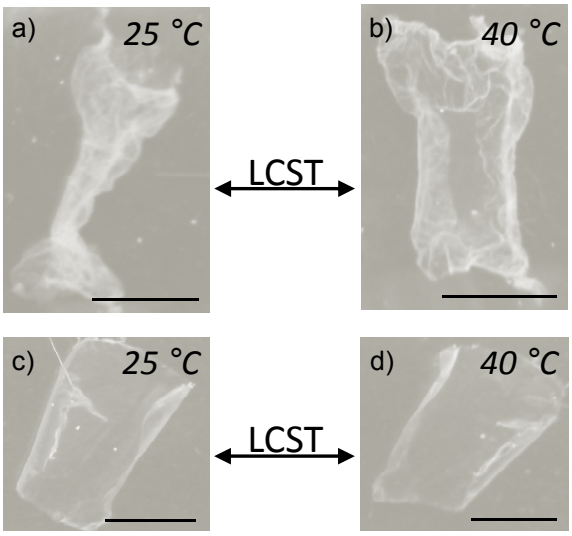

Figure 4.5. *Photographs showing the thermo-responsive effect of PNIPAM modified free-standing PCL films below (25°C) and above (40°C) the LCST (a, b) and the non-responsive non-modified free-standing PCL films (c, d). Scale bar is 5 mm.*

4.3 Conclusions

In the present work, a way to grow brushes on PCL film while maintaining the main properties of the material in terms of biocompatibility and ability of the brush to respond to temperature changes was presented. PCL was modified using aminolysis and ATRP of the thermoresponsive polymer, PNIPAM. The attachment of PNIPAM was confirmed by FTIR and AFM measurements. The thermoresponsive activity was proven by the bending and stretching behavior of unmodified and modified free-standing PCL films. Cells could attach, spread and grow on all surfaces including the PNIPAM modified surface. The possibility to detach cells after cooling the media below the LCST was assessed. Cells were released in the form of patches/sheets from the PNIPAM modified surfaces and their viability after being harvested was evaluated by their ability to grow and expand again on tissue culture plates. The possibility to harvest cells only from the PNIPAM modified samples confirmed that the detachment was triggered only by the temperature change.

4.4 Experimental section

Materials:

N-Isopropylacrylamide (NIPAM, Aldrich, 97%) was recrystallized twice from a toluene/hexane solution (50% v/v) and dried under vacuum prior to use. Copper(I) bromide (CuBr, Aldrich, 98%) was purified by stirring in glacial acetic acid, filtering, and washing with ethanol three times, followed by drying in vacuum at room temperature overnight. Hexane (ACS) and ethanol (absolute) were purchased from Merck. Methanol (absolute) and isopropanol (absolute) were purchased from Biosolve. Copper(II) bromide (Sigma-Aldrich, ≥99%), triethylamine (Sigma-Aldrich, 99,5%), *N,N,N',N",N"*- pentamethyldiethylenetriamine (PMDETA) (Acros Organics, 98%), 2-bromo-2-methylpropionyl bromide (Aldrich, 98%) and (3-aminopropyl)-trimethoxysilane (Aldrich, 97%) were used as received. All water used in the experiments was Millipore Milli-Q grade.

Formation of the PCL substrates:

For the fabrication of the supported PCL films, either glass or silicon substrates were first cleaned with Piranha solution, then rinsed extensively with water and ethanol. *Caution: Piranha solution reacts violently with many organic materials and should be handled with great care!* Thin PCL films were obtained by spin-coating PCL from a chloroform solution (5 wt%) at 2000 rpm for 1 minute.

Activation of the polymer films:

The spin coated PCL films were immersed into a 50 mL solution of 0.005 mol/L ethylenediamine (ED) in isopropanol (IPA). The reaction was allowed to proceed for 15 minutes under room temperature conditions. Samples were then rinsed with ice-cold water and subsequently soaked in an ice water bath, then dried in a stream of nitrogen and in an evacuated vacuum oven. The aminated PCL films were immersed into 20 ml of hexane and 0.6 mL of triehtylamine (TEA), to which 2 mL of 2-bromoisobutyryl bromide (BIBB) was added dropwise. The reaction mixture was gently stirred for 2 hours at 0 °C to produce the 2-bromoisobutyryl-immobilized PCL surface. The PCL substrates were then washed repeatedly with an ethanol/water (1/1, v/v) mixture and dried under a stream of nitrogen.

ATRP of PNIPAM brushes:

NIPAM (2g, 17.4 mmol) monomer and PMDETA (110µL, 0.35 mmol) were added to a water (6.26 ml) and methanol (0.7 ml) mixture. The solution was purged with nitrogen for 30 min. CuBr (24.9mg, 0.17mmol) and $CuBr_2$ (3.9mg, 0.017mmol) were added into another reaction flask and flushed with nitrogen. Monomer, ligand and catalyst were then combined and stirred for another 30 minutes to facilitate the formation of the organometallic complex. This solution was then transferred into the flasks containing the substrates covered with SAMs. The flasks were sealed with rubber septa and kept at room temperature under nitrogen. After reaching the desired reaction time of 30 minutes, the substrates were removed from the polymerization solution, exhaustively rinsed with water to remove any unreacted and not surface tethered substances and subsequently dried in a stream of nitrogen.

Preparation of the free-standing PCL films:

For the preparation of the free-standing PCL films, a 10 wt% polyvinyl alcohol (PVA) aqueous solution was cast onto the spin-coated PCL film and subsequently dried in vacuum. Then, the PCL and PVA bilayer was peeled off from the solid substrate and immersed into Milli-Q water to dissolve PVA.

AFM measurements:

A Dimension D3100 AFM equipped with a hybrid scanner and a NanoScope IVa controller (Digital Instruments, Veeco-Bruker, Santa Barbara, CA) was operated in tapping mode using commercially available silicon cantilevers (PointProbe® Plus silicon probes, PPP-NCH, Nanosensors, Neuchatel, Switzerland) to obtain the surface morphology of the pure and modified PCL substrates.

Static contact angle measurements:

An optical contact angle device equipped with an electronic syringe unit (OCA15, Dataphysics, Germany) connected to a charge-coupled device (CCD) video camera was used for static water contact angle measurements. The sessile drop technique was used to determine the change in wettability of the modified PCL films. A drop was deposited onto the PCL surfaces by the syringe, after which the drop contour was fitted by the Young-Laplace method.

Attenuated Total Reflectance FTIR spectroscopy:

ATR-FTIR measurements were performed on an Alpha-P FTIR (Bruker Optics, Germany) fitted with the Platinum ATR QuickSnap^{TM} sampling module. The spectra were analysed using Opus 6.5 spectroscopy software (Bruker Optics, Germany).

Cell culture and cell image analysis:

A murine osteoblastic cell line MC3T3 was cultured at 37°C in a humidified atmosphere of 5% carbon dioxide, using as culture medium *α*-MEM supplemented with 10 v/v % FBS, 2 mM L-Glutamine, 1 mM sodium pyruvate, 100 U/mL of penicillin and 100 µg/mL of streptomycine. The cells were seeded at a density of 20,000 cells/cm^2 on PCL substrates modified with PNIPAM brushes. Cell attachment and detachment on the PNIPAM modified surfaces was assessed above or below LCST by light microscopy connected with a digital camera (Nikon Eclipse TE 300). Cells were detached by lowering the temperature for 1.5 hrs at 25 °C. The surface was gently rinsed with culture medium and the detached cells collected and re-seeded on tissue culture poly(styrene) for 3 days to confirm their viability. The images of the surfaces taken after detachment were used to confirm that all the cells were removed from the samples. Substrates were washed twice with PBS and fixed with a 3.7 v/v % formaldehyde solution in PBS for 10 minutes at room temperature. Next, the samples were washed two or more times with PBS. Cell membrane was permeabilized by treating the samples with 0.1 v/v % Triton X-100 solution in PBS. Specimens were washed again with PBS and cell nuclei stained with DAPI diluted 1:100 in a 1 v/v % bovine serum albumin solution in PBS for 10 minutes. Cell cytoskeleton was stained with a phalloidin-rhodamine solution diluted 1:200 in PBS for 20 minutes at room temperature. Pictures were taken using a Nikon fluorescent microscope Eclipse E600.

4.5 References

1 Wang, J. S.; Matyjaszewski, K., *Macromolecules* **1995,** *28,* 7901-7910.

2 Matyjaszewski, K.; Patten, T. E.; Xia, J. H., *Journal of the American Chemical Society* **1997,** *119,* 674-680.

3 Edmondson, S.; Osborne, V. L.; Huck, W. T. S., *Chemical Society Reviews* **2004,** *33,* 14-22.

4 Barbey, R.; Lavanant, L.; Paripovic, D.; Schuwer, N.; Sugnaux, C.; Tugulu, S.; Klok, H. A., *Chemical Reviews* **2009,** *109,* 5437-5527.

5 Xu, F. J.; Neoh, K. G.; Kang, E. T., *Progress in Polymer Science* **2009,** *34,* 719-761.

6 Braunecker, W. A.; Matyjaszewski, K., *Progress in Polymer Science* **2007,** *32,* 93-146.

7 Coessens, V.; Pintauer, T.; Matyjaszewski, K., *Progress in Polymer Science* **2001,** *26,* 337-377.

8 Matyjaszewski, K.; Xia, J. H., *Chemical Reviews* **2001,** *101,* 2921-2990.

9 Matyjaszewski, K.; Miller, P. J.; Shukla, N.; Immaraporn, B.; Gelman, A.; Luokala, B. B.; Siclovan, T. M.; Kickelbick, G.; Vallant, T.; Hoffmann, H.; Pakula, T., *Macromolecules* **1999,** *32,* 8716-8724.

10 Börner, H. G.; Beers, K.; Matyjaszewski, K.; Sheiko, S. S.; Möller, M., *Macromolecules* **2001,** *34,* 4375-4383.

11 Pyun, J.; Kowalewski, T.; Matyjaszewski, K., *Macromolecular Rapid Communications* **2003,** *24,* 1043-1059.

12 Sheiko, S. S.; Sumerlin, B. S.; Matyjaszewski, K., *Progress in Polymer Science* **2008,** *33,* 759-785.

13 Lee, H.-i.; Pietrasik, J.; Sheiko, S. S.; Matyjaszewski, K., *Progress in Polymer Science* **2010,** *35,* 24-44.

14 Yamamoto, S.-I.; Pietrasik, J.; Matyjaszewski, K., *Journal of Polymer Science Part A: Polymer Chemistry* **2008,** *46,* 194-202.

15 Lee, S. B.; Koepsel, R. R.; Morley, S. W.; Matyjaszewski, K.; Sun, Y. J.; Russell, A. J., *Biomacromolecules* **2004,** *5,* 877-882.

16 Murata, H.; Koepsel, R. R.; Matyjaszewski, K.; Russell, A. J., *Biomaterials* **2007,** *28,* 4870-4879.

17 Bencherif, S. A.; Gao, H.; Srinivasan, A.; Siegwart, D. J.; Hollinger, J. O.; Washburn, N. R.; Matyjaszewski, K., *Biomacromolecules* **2009,** *10,* 1795-1803.

18 Park, S.; Cho, H. Y.; Yoon, J. A.; Kwak, Y.; Srinivasan, A.; Hollinger, J. O.; Paik, H.-j.; Matyjaszewski, K., *Biomacromolecules* **2010,** *11,* 2647-2652.

19 Siegwart, D. J.; Bencherif, S. A.; Srinivasan, A.; Hollinger, J. O.; Matyjaszewski, K., *Journal of Biomedical Materials Research Part A* **2008,** *87A,* 345-358.

20 Benetti, E. M.; Chung, H. J.; Vancso, G. J., *Macromolecular Rapid Communications* **2009,** *30,* 411-417.

21 Santonicola, M. G.; de Groot, G. W.; Memesa, M.; Meszyńska, A.; Vancso, G. J., *Langmuir* **2010,** *26,* 17513-17519.

22 Ma, H.; Hyun, J.; Stiller, P.; Chilkoti, A., *Advanced Materials* **2004,** *16,* 338-341.

23 Ma, H.; Wells, M.; Beebe, T. P.; Chilkoti, A., *Advanced Functional Materials* **2006,** *16,* 640-648.

24 Zhang, Z.; Chen, S. F.; Jiang, S. Y., *Biomacromolecules* **2006,** *7,* 3311-3315.

25 Zhang, Z.; Chen, S.; Chang, Y.; Jiang, S., *The Journal of Physical Chemistry B* **2006,** *110,* 10799-10804.

26 Yu, W. H.; Kang, E. T.; Neoh, K. G.; Zhu, S., *The Journal of Physical Chemistry B* **2003,** *107,* 10198-10205.

27 de las Heras Alarcon, C.; Farhan, T.; Osborne, V. L.; Huck, W. T. S.; Alexander, C., *Journal of Materials Chemistry* **2005,** *15,* 2089-2094.

28 Andruzzi, L.; Senaratne, W.; Hexemer, A.; Sheets, E. D.; Ilic, B.; Kramer, E. J.; Baird, B.; Ober, C. K., *Langmuir* **2005,** *21,* 2495-2504.

29 Ebara, M.; Yamato, M.; Aoyagi, T.; Kikuchi, A.; Sakai, K.; Okano, T., *Biomaterials* **2008,** *29,* 3650-3655.

30 Ebara, M.; Yamato, M.; Aoyagi, T.; Kikuchi, A.; Sakai, K.; Okano, T., *Advanced Materials* **2008,** *20,* 3034-3038.

31 Mizutani, A.; Kikuchi, A.; Yamato, M.; Kanazawa, H.; Okano, T., *Biomaterials* **2008,** *29,* 2073-2081.

32 Fan, X.; Lin, L.; Dalsin, J. L.; Messersmith, P. B., *Journal of the American Chemical Society* **2005,** *127,* 15843-15847.

33 Fan, X.; Lin, L.; Messersmith, P. B., *Biomacromolecules* **2006,** *7,* 2443-2448.

34 Zhang, F.; Shi, Z. L.; Chua, P. H.; Kang, E. T.; Neoh, K. G., *Industrial & Engineering Chemistry Research* **2007,** *46,* 9077-9086.

35 Dalsin, J. L.; Lin, L. J.; Tosatti, S.; Vörös, J.; Textor, M.; Messersmith, P. B., *Langmuir* **2005,** *21,* 640-646.

36 Raynor, J. E.; Petrie, T. A.; García, A. J.; Collard, D. M., *Advanced Materials* **2007,** *19,* 1724-1728.

37 Xu, F. J.; Wang, Z. H.; Yang, W. T., *Biomaterials* **2010,** *31,* 3139-3147.

38 Xu, F. J.; Zheng, Y. Q.; Zhen, W. J.; Yang, W. T., *Colloids and Surfaces B-Biointerfaces* **2011,** *85,* 40-47.

39 Ke, Z. J.; Dai, B. H.; Li, L.; Yan, G. P.; Zhou, D. S., *Journal of Applied Polymer Science* **2010,** *115,* 976-980.

40 Cole, M. A.; Voelcker, N. H.; Thissen, H.; Griesser, H. J., *Biomaterials* **2009,** *30,* 1827-1850.

41 Synytska, A.; Svetushkina, E.; Puretskiy, N.; Stoychev, G.; Berger, S.; Ionov, L.; Bellmann, C.; Eichhorn, K. J.; Stamm, M., *Soft Matter* **2010,** *6,* 5907-5914.

42 Wischerhoff, E.; Badi, N.; Lutz, J. F.; Laschewsky, A., *Soft Matter* **2010,** *6,* 705-713.

43 Yu, Q.; Zhang, Y. X.; Chen, H.; Zhou, F.; Wu, Z. Q.; Huang, H.; Brash, J. L., *Langmuir* **2010,** *26,* 8582-8588.

44 Schmaljohann, D.; Oswald, J.; Jorgensen, B.; Nitschke, M.; Beyerlein, D.; Werner, C., *Biomacromolecules* **2003,** *4,* 1733-1739.

45 Cooperstein, M. A.; Canavan, H. E., *Langmuir* **2009,** *26,* 7695-7707.

46 Bradley, C.; Jalili, N.; Nett, S. K.; Chu, L. Q.; Forch, R.; Gutmann, J. S.; Berger, R., *Macromolecular Chemistry and Physics* **2009,** *210,* 1339-1345.

47 Laloyaux, X.; Mathy, B.; Nysten, B.; Jonas, A. M., *Langmuir* **2010,** *26,* 838-847.

48 Sui, X. F.; Chen, Q.; Hempenius, M. A.; Vancso, G. J., *Small* **2011,** *7,* 1440-1447.

49 Mendez, S.; Andrzejewski, B. P.; Canavan, H. E.; Keller, D. J.; McCoy, J. D.; Lopez, G. P.; Curro, J. G., *Langmuir* **2009,** *25,* 10624-10632.

50 Nagase, K.; Kobayashi, J.; Okano, T., *Journal of the Royal Society Interface* **2009,** *6,* S293-S309.

51 Shimizu, H.; Ohashi, K.; Utoh, R.; Ise, K.; Gotoh, M.; Yamato, M.; Okano, T., *Biomaterials* **2009,** *30,* 5943-5949.

52 Takahashi, H.; Nakayama, M.; Yamato, M.; Okano, T., *Biomacromolecules* **2010,** *11,* 1991-1999.

53 Okano, T.; Yamada, N.; Okuhara, M.; Sakai, H.; Sakurai, Y., *Biomaterials* **1995,** *16,* 297-303.

54 Uhlig, K.; Wischerhoff, E.; Lutz, J. F.; Laschewsky, A.; Jaeger, M. S.; Lankenau, A.; Duschl, C., *Soft Matter* **2010,** *6,* 4262-4267.

55 Kumashiro, Y.; Yamato, M.; Okano, T., *Ann Biomed Eng* **2010,** *38,* 1977-1988.

56 Xu, F. J.; Zhong, S. P.; Yung, L. Y. L.; Kang, E. T.; Neoh, K. G., *Biomacromolecules* **2004,** *5,* 2392-2403.

57 Akiyama, Y.; Kikuchi, A.; Yamato, M.; Okano, T., *Langmuir* **2004,** *20,* 5506-5511.

58 Kong, B.; Choi, J. S.; Jeon, S.; Choi, I. S., *Biomaterials* **2009,** *30,* 5514-5522.

59 Sui, X.; Di Luca, A.; Klein Gunnewiek, M.; Kooij, S.; van Blitterswijk, C. A.; Moroni, L.; Hempenius, M. A.; Vancso, G. J., *Australian Journal of Chemistry* **2011,** *In press*.

60 Tugulu, S.; Klok, H.-A., *Macromol Symp* **2009,** *279,* 103-109.

61 Lavanant, L.; Pullin, B.; Hubbell, J. A.; Klok, H.-A., *Macromolecular Bioscience* **2010,** *10,* 101-108.

62 Sui, X. F.; Zapotoczny, S.; Benetti, E. M.; Schon, P.; Vancso, G. J., *Journal of Materials Chemistry* **2010,** *20,* 4981-4993.

63 Fukumori, K.; Akiyama, Y.; Kumashiro, Y.; Kobayashi, J.; Yamato, M.; Sakai, K.; Okano, T., *Macromolecular Bioscience* **2010,** *10,* 1117-1129.

64 Fukumori, K.; Akiyama, Y.; Yamato, M.; Kobayashi, J.; Sakai, K.; Okano, T., *Acta Biomaterialia* **2009,** *5,* 470-476.

65 Sui, X.; Di Luca, A.; Klein Gunnewiek, M.; Kooij, E. S.; van Blitterswijk, C. A.; Moroni, L.; Hempenius, M. A.; Vancso, G. J., *Australian Journal of Chemistry* **2011,** *64,* 1259-1266.

66 Fujie, T.; Haniuda, H.; Takeoka, S., *Journal of Materials Chemistry* **2011,** *21,* 9112-9120.

67 Fujie, T.; Park, J. Y.; Murata, A.; Estillore, N. C.; Tria, M. C. R.; Takeoka, S.; Advincula, R. C., *ACS Applied Materials & Interfaces* **2009,** *1,* 1404-1413.

68 Zou, Y. Q.; Lam, A.; Brooks, D. E.; Phani, A. S.; Kizhakkedathu, J. N., *Angew. Chem.-Int. Edit.* **2011,** *50,* 5116-5119.

Thin polymer brush decouples biomaterial's micro-/nano-topology and stem cell adhesion

This Chapter studies thin semicrystalline poly(ε-caprolactone) (PCL) films, which exhibited a variation of surface morphologies and roughness originating from different spherulitic superstructures. Such substrates were obtained by spincoating and varying the parameters of the thermal processing, i.e. crystallization conditions. Extensive cell shape analysis showed that cells attached to these polymer substrates adopted different morphologies responding to variations in spherulite density and size. In order to decouple substrate topology effects on the cells, sub-100 nm bio-adhesive polymer brush coatings of oligo(ethylene glycol) methacrylates were grafted from PCL and functionalized with fibronectin. On surfaces featuring different surface textures and sub-100 nm thick brush coatings cells showed to respond irrespective to the underlying topology. Thus, polymer brushes decouple substrate micro-/nanoscale surface topology and the adhesion of stem cells.

* This Chapter has been published in: M. Klein Gunnewiek, E.M. Benetti, A. Di Luca, C.A. van Blitterswijk, L. Moroni, G.J. Vancso; *Langmuir* **2013**, 29, 13843-13852

5.1 Introduction

Cell-biomaterial interactions have been increasingly studied in the last decade aiming to shed light on the mechanisms which govern cellular attachment and proliferation. Thus, increasing efforts have been dedicated to replicate the characteristics of natural tissues by engineering synthetic extra-cellular matrix (ECM) environments. Hereby particular attention has been paid to structural details, bulk physical properties and cytocompatibility of the synthetic substrates. Morphological and chemical structuring of surfaces have been demonstrated to influence the behavior of adhering cells, with differences depending on cell type. Similar ECM manipulations have been demonstrated to trigger a cascade of biomolecular events which eventually contribute to determining cells' fate.[1-2] In this respect, particular interest was devoted to stem cells, and specifically to human mesenchymal stem cells (hMSCs), as starting platforms for possible new tissue regeneration strategies.[3-4] These are adult cells of easy accessibility, which possess the capability to differentiate in various lineages such as neuronal[5], myotic[6] or osteoblast-like cells[7].

Different environmental parameters were recently demonstrated to control hMSCs activity, and thus stability, morphology, proliferation and differentiation. Among these, ECM elasticity,[8] micro-/nano-topology,[9-10] and availability of ligands[11] represented the main determining factors. As a general approach, all the fabrication methods aiming at directing particular stem cells' lineage specification have been centered on mimicking the corresponding natural tissue environments.[2, 12] Additionally, a direct consequence of hMSCs behavior was related to artificial ECM-driven changes in cell shape.

In particular, different biomaterials' surface roughness[13-14] and micro/nano-patterned topology[15-17] have been demonstrated to determine hMSCs adhesion and behavior. Namely, cells incubated on different patterned substrates could preferentially differentiate into neuronal, osteogenic or adipogenic lineages[18-19]. In these experiments, controlled structuring of the topology at the scaffold interface translated into a morphological response by the adhered cells, which subsequently lead to a preferential differentiation towards a defined cell tissue type.

Increasing attention has, thus, been devoted to the physico-chemical properties of cell-biomaterial interfaces, which determine the performance of the matrix i.e. cells-biomaterial adhesion and scaffold integration in the natural tissue environment. Among the engineering methods used to tune all the characteristics relevant for biomaterial surfaces, polymer grafting represents one of the most attracting and promising strategies. Densely surface-grafted polymers, also termed brushes, proved to be versatile coatings featuring tailorable chemistries, multifunctionalities and responsive behavior.[20-21] Their application as coatings allow one to tune interfacial properties, which are highly relevant for biological systems, such as swelling (directly determining bio-adhesion),[22-24] stiffness, and controlled exposure of biological cues.[25-26] Specifically, adhesive biomolecules such as arginine-glycine-aspartic acid sequences (RGD), fibronectin (FN), or collagen have been immobilized on brush films obtaining multilayered architectures which strongly enhanced the cell-substrate affinity.[27-28]

Polymer brushes have been broadly applied as surface modifiers for biomaterials. Specifically the multi-functional and morphological characteristics of densely grafted films have been exploited to design bio-passive and bio-functional films regulating the interaction between biomaterials and cells, proteins or bacteria.[20-21] In particular the highly hydrated nature of poly(ethylene glycol) (PEGs)-based brushes (or analogues)[29-31] provided biopassivity to organic and inorganic surfaces.[32-34] On the contrary, high density of functions on bio-adhesive brushes allowed an enhanced surface-loading of ECM proteins during cell culturing thus triggering biological adhesion.[26-27, 33]

This Chapter particularly focuses on the decoupling effect by cell-adhesive brushes between different surface topologies and hMSCs adhesion. To this aim, surface-initiated atom transfer radical polymerization (SI-ATRP)[21, 35] of oligo(ethylene glycol) (OEG) methacrylates[34, 36-37] was employed to generate functionalizable sub-100 nm brush layers which, following FN immobilization, were finally applied as study platforms for the adhesion of hMSCs. Poly(ε-caprolactone) (PCL) films were used as substrates for brush growth. This thermoplastic biodegradable polymer has been extensively used for the fabrication of scaffolds as supports for cells culturing, due to its excellent biocompatibility.[38-40] In particular, PCL is attractive due to its long term degradation, good solubility in different

solvents and high permeability to drugs.[41] In order to produce different surface topologies on PCL surfaces, spin-coated films were subjected to different thermal treatments from melts, resulting in alternatively fast and slow crystallization. Thus, tuning of the assembly kinetics of polymer chains into lamellar structures determined the density and size of PCL spherulites, which in-turn influenced the substrate micro-/nano-topologies. This method represented an effective and costless strategy to introduce different topologies with diverse orders of periodicities and pattern types (Figure 5.1a-c).

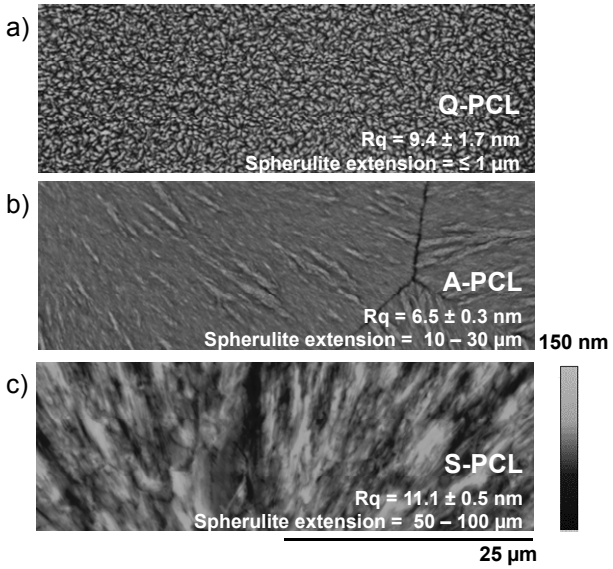

Figure 5.1. *Preparation of PCL surfaces by different thermal processing to obtain Q-PCL (a), A-PCL (b) and S-PCL (c).*

These different PCL films were treated with FN and subsequently incubated with hMSCs to investigate the effect of different topologic parameters on cell adhesion. Alternatively, they were used as precursor surfaces for the fabrication of sub-100 nm POEGMA cell-adhesive brushes (Scheme 5.1).

The interfacial effect of uniform brush coatings on different semicrystalline topologies was finally studied by assessing the morphological response of adhered hMSCs. An in-depth focus was furthermore given to the capability of POEGMA brushes to efficiently tune cell adhesion irrespective to the underlying substrate

characteristics (roughness and surface morphology). Brush coatings for scaffolds and tissue engineering supports would additionally confer function and tunable surface properties to these biomaterials, thus enabling their more specific application.

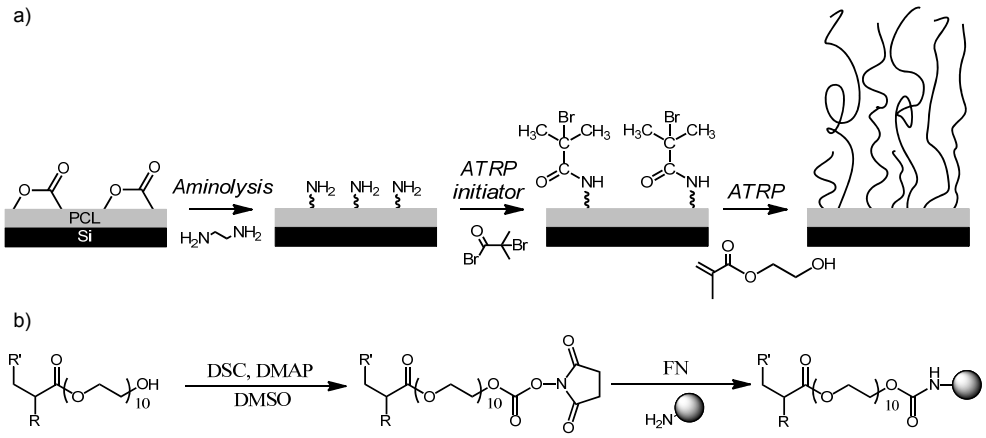

Scheme 5.1. *(a) Reaction scheme for the modification of PCL films using aminolysis and surface-initiated-ATRP of OEGMA to produce surface tethered POEGMA brushes and (b) the subsequent bioactivation with fibronectin (FN).*

5.2 Results and discussion

5.2.1 Topology induced cell adhesion

Three different semi-crystalline topologies were obtained on 100 nm thick spin-coated PCL films by first annealing the films at 75°C and subsequently applying different cooling rates, namely (1) quenching of crystallization by dipping the samples in liquid N_2, (3) fast cooling at room temperature and (2) slow cooling at 0.5 °C/min. These different thermal treatments determined PCL crystallization and, consequently, the topology of the exposed interfaces, as can be seen in the atomic force microscopy (AFM) micrographs reported in Figures 5.1a-c. Quenched PCL films showed sub-micron sized spherulitic structures (up to 1 μm) (Figure 5.1a, samples labeled as Q-PCL) uniformly and densely covering the whole film. On the contrary, slower cooling rates triggered the formation of larger spherulites ranging from sub-50 μm (Figure 5.1b, samples labeled as A-PCL) to several hundred μm

(Figure 5.1c, samples labeled as S-PCL). In the two last cases, lamellar aggregates expand from the center of nucleation to the edges of the spherulites. This coarsens film topology with radial aggregates displaying typical thickness of 50-100 nm and depth of 5-10 nm (Figure 5.1c). A-PCL topologies presented denser coverages of sub-50 μm, thus smaller features compared to typical hMSCs projected areas (Figure 5.1), while S-PCL samples displayed much larger spherulites presenting uniform lamellar expansions. These spanned over several hundreds of μm and, thus, function as homogeneously patterned areas for several adhering cells. All the so-formed PCL films were subsequently functionalized by FN through physical adsorption of the protein in order to favor the adhesion of hMSCs. It is noteworthy to mention that all the obtained topologies showed similar values of roughness (Rq= 11.1±0.5, 6.5±0.3 and 9.4±1.7 nm for Q-, A- and S-PCL, respectively) as measured with AFM (sampling areas = 20 x 20 μm^2, n = 12). In addition, in all the series of different PCL samples the surface concentration of FN was kept constant as measured by XPS (Figure 5.2. and data interpretation reported in the experimental section). Namely, 20 ± 5 and 40 ± 5 ng/cm^2 for the pure PCL and the PCL with POEGMA brush samples.

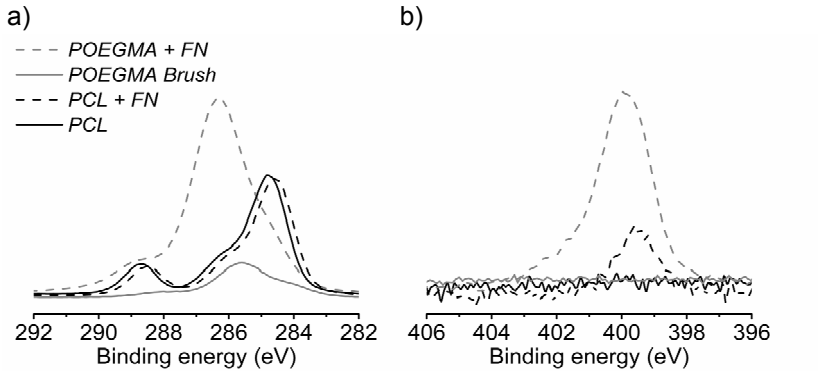

Figure 5.2. *XPS spectra for carbon (C1s) (a) and nitrogen (N1s) (b) on both the pure PCL films and on the PCL films containing POEGMA brushes, either with or without fibronectin.*

The morphology of hMSCs following 4 hours of incubation on the different PCL topologies was evaluated by optical (OM) and immunofluorescent microscopies concentrating on the effect of film micro-/nano-structure i.e. spherulites organization and size. Generally, hMSCs morphology responded to

differences in semicrystalline topologies of PCL. This can be seen in Figures 5.3 and 5.4. hMSCs adhering on sub-micron Q-PCL and small spherulites typical of A-PCL showed branching and irregular shapes (Figure 5.3a and 5.3b), also confirmed by immunofluorescence imaging (Figure 5.4).

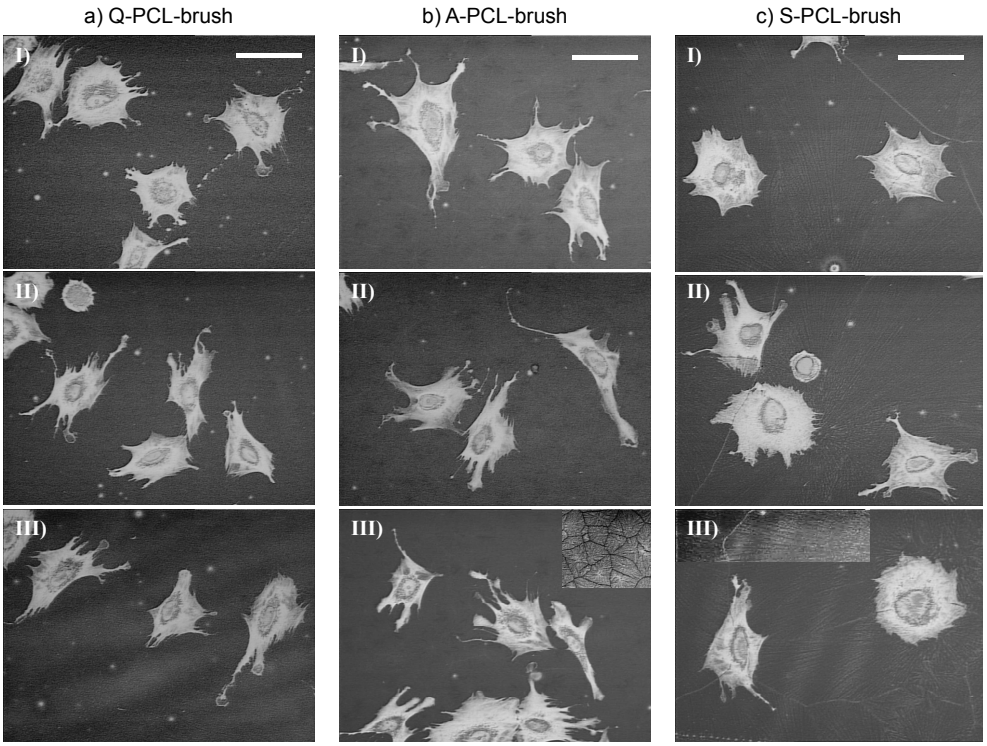

Figure 5.3. *HMSC's adhering on Q-PCL (a), A-PCL (b) and S-PCL structures (c). Three representative images are reported for each set of samples (I, II and III). The insets in III (b) and III (c) are highly contrasted OM areas on the corresponding samples and highlight the PCL topologies at the surface. The scale bars for all the OM micrographs are 50 μm.*

On the contrary hMSCs incubated on large spherulitic organizations (S-PCL) displayed more regular and symmetric shapes with limited branching (Figures 5.3c and 5.4c). Evaluation of cell parameters calculated from OM and immunofluorescence images corroborated the qualitative analysis of hMSCs morphology upon adhesion on the different PCL topologies. In Figure 5.5 average values of cells area, perimeter (P) and roundness (RN) are reported for all the PCL samples studied. hMSCs projected areas increased with the size of the spherulitic

patterns (P<0.05 between Q-/A-PCL and S-PCL). Simultaneously, both P and RN decremented for cells adhering on S-PCL compared to Q- and A-PCL samples (P<0.05).

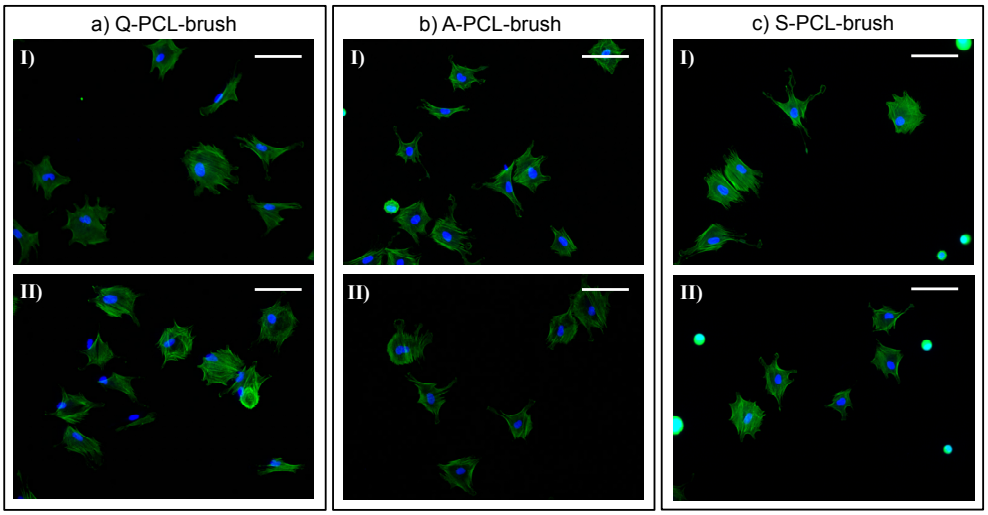

Figure 5.4. *Immunofluorescence images of hMSCs adhered on a) Q-PCL, b) A-PCL and c) S-PCL topologies following 4 hours of incubation. Two representative images are reported for each set of samples (I and II). The scale bars for all the fluorescent pictures are 100 μm.*

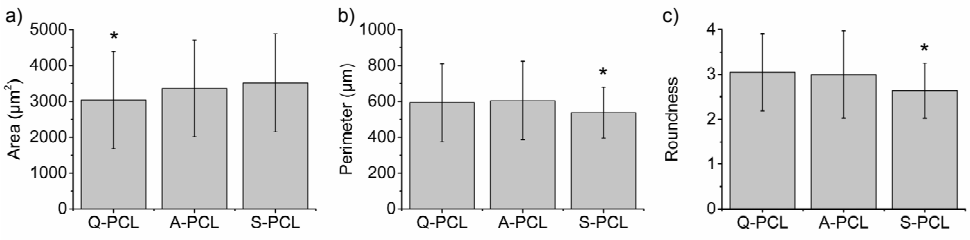

Figure 5.5. *Projected area a), perimeter b) and roundness values c) of cell adhering on PCL with different topologies (Q-PCL, A-PCL and S-PCL). * denotes statistical significant differences between the assigned and the non-assigned topologies (p < 0.05) (n = 100 cells).*

In summary, dense assemblies of sub-50 μm spherulites (shown in Q- and A-PCL) induced cells to adapt to irregular and disperse features presenting lamellar aggregates which expand in all directions and across variable surface radii. On these samples hMSCs' projection covered several spherulites and cells

were thus shown to respond to these disconnected features by an irregular spreading and a more pronounced branching.

Conversely, when incubated on extended lamellar patterns developing over hundreds of μm, cells adopted more symmetrical and regular shapes with larger projected areas (Figure 5.3 and 5.4). In these cases the increase of symmetry and regularity by cells' morphology were also recorded as a decrease in the average values of P and RN (Figure 5.5).

The roles played by surface roughness and pattern type on the adhesion and the behavior of hMSCs have been studied during the last decade.[5, 42-44] Namely, different patterns induced specific cell orientation and stretching by contact guidance, which in some cases also affected their differentiation.[5, 42] In addition, different roughness on inorganic and polymeric supports was shown to affect the density of adhering hMSCs.[45-46] In this context, the simple processing method proposed here represents an effective and low-cost strategy to introduce different topologies with diverse orders of periodicities and different resolutions (from nano- to micro-scale) on semicrystalline supports (Figure 5.1a-c). A simple control over the thermal processing conditions, often eluded during biomaterial preparations, turned into tuning over surface features and hMSCs adhesion.

5.2.2 Decoupling effect by POEGMA coatings

Having established the dependence of hMSCs morphology on substrate features (type and extension), the activity by a thin brush coating on cell-topology interactions is subsequently investigated. In order to accomplish this, the different PCL supports were coated with a sub-100 nm POEGMA brush by PCL chemical activation, following SI-ATRP.[24, 27]

All POEGMA brushes grafted from PCL samples present thickness values between 60 and 70 nm and a constant swelling ratio of around 1.6. The average grafting density of 0.34 chains/nm^2 was estimated using the swelling ratio and applying the following equation:

$$\sigma = \rho_0 \, h_{dry} \, N_A / (N \, M_0) \qquad (5.1)$$

Here ρ_0 is the estimated POEGMA layer density (1.40 g/cm^3),[47] N_A is Avogadro's number, M_0 is the monomer molecular weight (526 g/mol) and N is the degree of polymerization estimated according to:

$$N = [0.227] (h_{swollen})^{3/2} / (h_{dry})^{1/2} \qquad (5.2)$$

where 0.227 is a constant related to the excluded volume parameter and the Kuhn length of a monomer unit.[47] The brush coating formed thus uniformly, covering all the different PCL topological features as shown in Figure 5.6.

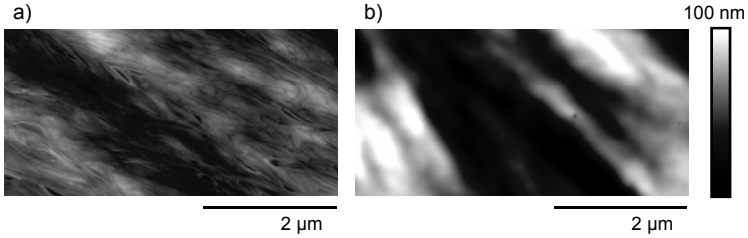

Figure 5.6. *High resolution AFM images on S-PCL (a) and S-PCL with a POEGMA supporting layer (b).*

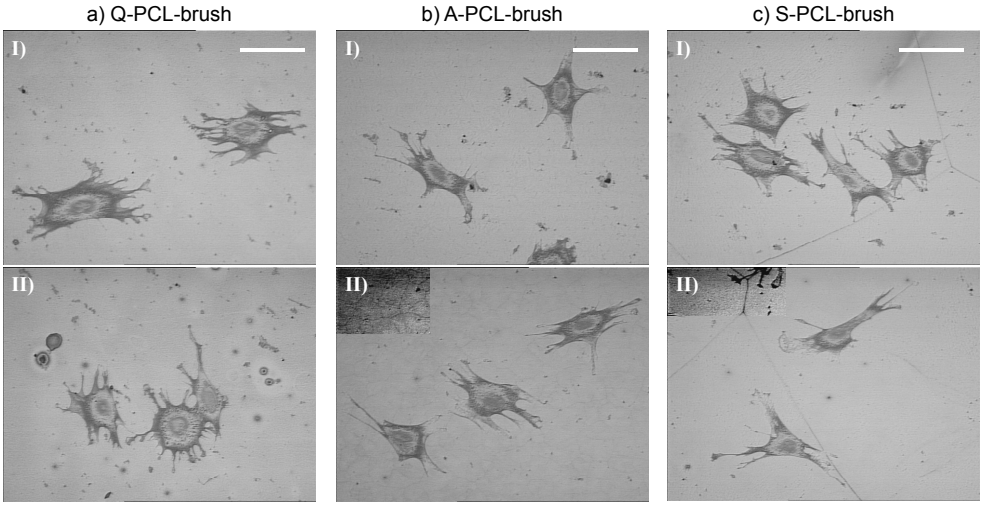

Figure 5.7. *Optical images of cells adhering on Q-PCL (a), A-PCL (b) and S-PCL (c) with the supporting POEGMA brush. Two representative images are reported for each set of samples (I and II). The insets in II (b) and II (c) are highly contrasted OM areas on the corresponding samples and highlight the brush-coated PCL topologies at the surface. The scale bars for all the OM micrographs are 50 µm.*

POEGMA-brushes were later on “bio-activated” with FN. In POEGMA-coated PCL surfaces the protein concentration was found to be around 40 ng/cm^2 if compared to the “pure” PCL surfaces (20 ± 5 ng/cm^2 for all the different PCL topologies studied). This was due to multiple binding by POEGMA side-chains along the brush structure.[25] After 4h seeding, hMSCs morphology on brush-coated PCL topologies (named as Q-PCL-, A-PCL- and S-PCL-brush in the case of coated Q-PCL, A-PCL and S-PCL topologies, respectively) was investigated by both OM and immunofluorescence imaging (Figure 5.7 and 5.8).

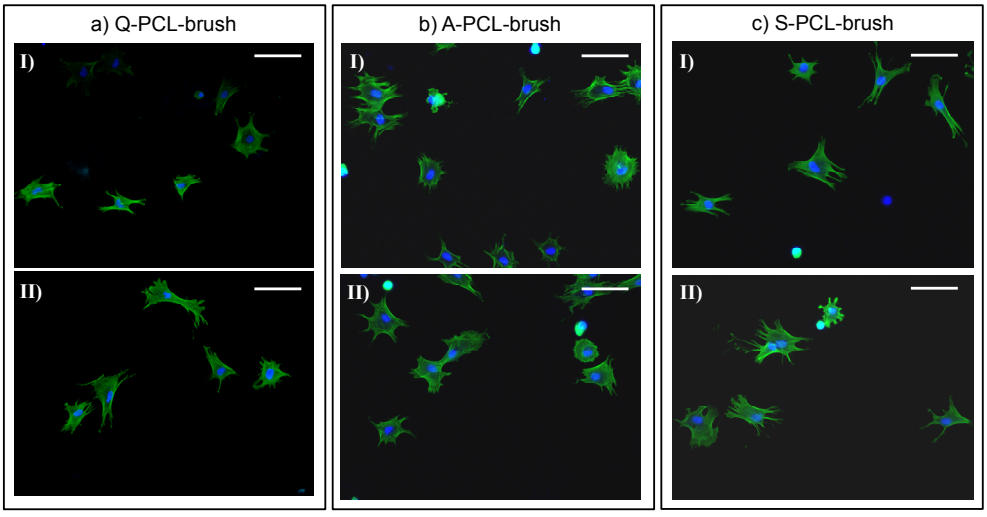

Figure 5.8. *Immunofluorescence images of hMSCs adhered on a) Q-PCL-, b) A-PCL- and c) S-PCL-brush films following 4 hours of incubation. Two representative images are reported for each set of samples (I and II).The scale bars for all the fluorescent pictures are 100 μm.*

The same cell shape parameters were subsequently calculated from these micrographs and compared to cells adhered on the corresponding uncoated PCL samples (Figure 5.9).

As shown in Figure 5.7 and 5.8, hMSCs cultured on all PCL-brush surfaces showed very similar morphologies despite the underlying PCL topology. Specifically, cells were characterized by a stellate shape, a higher degree of branching and smaller projected areas if compared to cells adhered on the starting PCL samples.

Despite the higher surface concentration of FN found on the POEGMA brush, the average number of adhered cells did not increase substantially compared to uncoated PCL morphologies. Thus, given the sampling depth of XPS (around 10 nm, performed on dry POEGMA brush), one can assume that the higher concentration of FN refers also to proteins within the swollen brush and not accessible to cells. The surface density of cell-ligands was found determining cell adhesion and spreading.[48-49] In addition, it has been reported how cell adhesion on ligand-functionalized brushes was dominated by the composition of the outer polymer brush interface.[25]

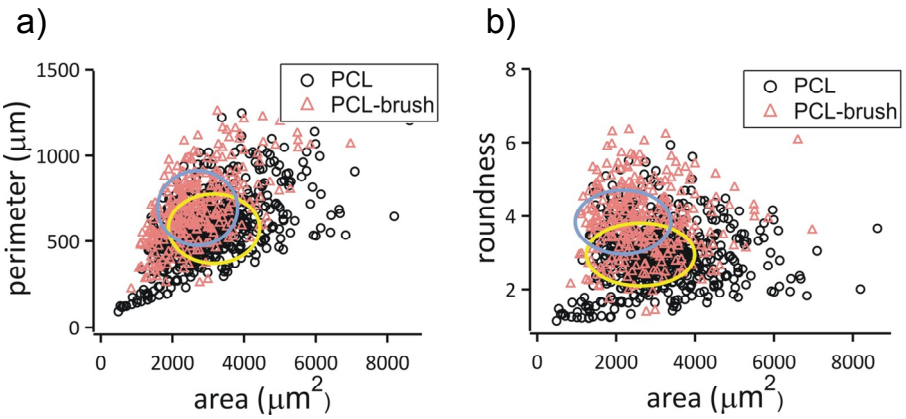

Figure 5.9. *Perimeter a) and roundness b) plotted versus the projected area of each individual cell adhering either on a pure PCL (**O**) or on the PCL-POEGMA system (**Δ**).*

Hence, assuming a comparable interfacial FN concentration between PCL and POEGMA-coated PCL, proteins exposition at the interface[50-51] together with the different physico-chemical properties of the substrates are the determining factors for the different hMSCs adhesion.

In order to shed light on cell spreading mechanism onto PCL-brush in comparison to PCL uncoated films, for each individual cell the P and RN values were plotted versus projected area.[52] In Figure 5.9, the distributions of P and RN values (Figure 5.9a and 5.9b, respectively) for all the cells analyzed on bare PCL (black circle markers) and on the corresponding PCL-brush films (pink triangle markers) are reported. These were highlighted as colored ellipses centered on the average values and presenting semi-axes equal to the calculated standard

deviations of each parameter. Thus, the difference in cell behavior between the two series of substrates could be also visualized as a degree of overlying ellipses on each graph.

The behavior of adhered hMSCs was markedly influenced by the physico-chemical nature of the polymeric supports used. The dispersion of data points reported in Figure 5.9a for cells attaching on brush-coated surfaces concentrated at higher P values with increasing areas, if compared to bare PCL samples. A similar trend was observed in the case of RN values in Figure 5.9b, where cell behavior upon spreading (towards larger areas) was characterized by RN concentrated at higher values when the substrates presented POEGMA brushes at interfaces. Thus, on PCL-brush surfaces cells generally protruded by branching and spread independently from the underlying PCL topology. On the contrary, on bare PCL hMSCs responded to the different semicrystalline features alternatively branching on small and diffused aggregates or covering larger areas and uniformly spreading on extended spherulitic organizations. The behavior of hMSCs on these surfaces was thus found substrate topology-dependent. The presence of a very thin, sub-100 nm POEGMA brush establishes the physical and chemical characteristics of the PCL interface. The interplay of amplified water content,[22-24] control exposure of protein cues,[26, 48] and film compliance,[8, 53-54] peculiar to a dense and uniform brush coating, dominates the biological response at the brush-medium interface. Hence, for all the PCL-brush samples the behavior of hMSCs was demonstrated as substrate topology-independent. From this result, it can be concluded that even a very thin polymer brush significantly influences cell behavior irrespective of the underlying support characteristics in such a way that it decouples substrate nano-/micro-topology and cell response. This is particularly interesting for stem cells, as the brush-modified substrates can be proposed as a universal system to culture cells in a standardized manner without influencing their differentiation state.

The influence of a polymer brush architecture on cell adhesion has been recently investigated by us and others.[25-26] In these reports, protein ligands exposure and anchoring by densely grafted polymer spacers were found to affect the adhesion and morphology of different cell types. In this context, the present study clarifies the fundamental activity of biomaterial-tethered brushes, which

interpose flexible attachment sites for cells capable of re-organize in response to cell adhesion.[25]

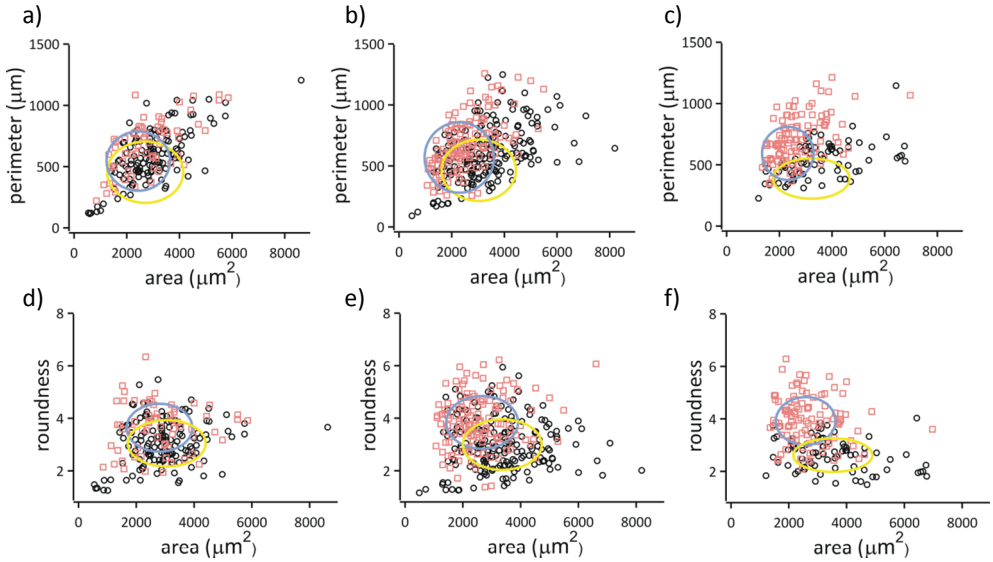

Figure 5.10. *Perimeter (a,b,c) and roundness (d,e,f) plotted versus the projected area of each individual cell adhering either on a pure PCL (***O***) or on the PCL-POEGMA system (□). Q-PCL (a,d), A-PCL (b,e) and S-PCL (c,f).*

POEGMA brush decoupling effect was further clarified by analyzing the behavior of hMSCs on each PCL topology before and after brush coating (Figure 5.10). Also in this case, the dispersions of P and RN values were recorded for each cell adhering on the three different types of PCL surfaces as a function of the corresponding cell projected area. As it can be noticed moving from Figure 5.10a to 5.10c, i.e. following the increase of spherulite extension from Q- to S-PCL, both P and RN distributions increasingly dissociated between uncoated and coated PCL films. Hence, POEGMA brush decoupling activity was demonstrated to become more pronounced with increasing pattern extension. In conclusion, on platforms presenting topologies ranging from sub-micron aggregates to several hundred µm-extended lamellar organizations, the morphology of hMSCs was “normalized” by a dense and thin brush coating. This representation of polymer brush activity justifies their application and function as biomaterial surface-modifiers. Dense assemblies of bio-activated brushes applied to synthetic ECMs are capable of tuning the

performance of the matrix by their peculiar physical properties. The exquisite combination of swelling, compliance and flexibility by tethered chains determines their function, i.e. the exposure and reception of cell cues and decoupling of substrate morphology towards cell adhesion. Particularly in the cases where contact guidance[5-7, 55-57] and roughness effects[58-60] are driving the behavior of adhering cells, brush adlayers are capable of tuning the properties of biomaterial surfaces.

5.3 Conclusions

This Chapter describes the effects on adult bone marrow-derived mesenchymal stem cell adhesion by semicrystalline topologies of PCL supports and thin polymer brush films grafted on such substrates. Micro-/nano-topologies induced by simple thermal processing are shown to alter the behavior of hMSCs upon attachment and spreading. Cells adopt different morphologies responding to spherulite density and size. Following the coarsening and the extension of the lamellar organizations hMSCs spread more uniformly, covering increasing areas. On the contrary on sub-μm and densely dispersed semicrystalline features cells branch and adopt more irregular shapes. On these differently patterned surfaces dense and sub-100 nm thick POEGMA brush coatings are capable of determining the response of cells, irrespective to the underlying topology. Thus, polymer brushes decouple substrate micro-/nano-topology and the adhesion of stem cells. Brush film compliance, chain flexibility and controlled ligand exposure simultaneously act to determine the interfacial phenomena between biological medium and the biomaterial. These results emphasize the role of thin brushes as ECM-cell mediating layers, to decouple cells-topology interactions and to effectively mask any contact guidance or roughness effect. Due to their intrinsic robustness, high density and tunable configuration, polymer brushes have been demonstrated as effective components for the design of next-generation artificial ECM for homogenous stem cell preparations.

5.4 Experimental section

Materials:

Oligo(ethylene glycol) methacrylate (OEGMA, Aldrich, Mn = 526 g/mol) was purified from hydrochinone inhibitors by passing it through a basic alumina column using dichloromethane (DCM, Biosolve) as an eluent. Afterwards DCM was removed under vacuum. Copper(I) chloride (CuCl, Aldrich, 98%) was purified by stirring in glacial acetic acid, filtering, and washing with ethanol three times, followed by drying in vacuum at room temperature overnight. Copper(II) bromide (Sigma-Aldrich, ≥99%), methanol (Biosolve, absolute), isopropanol (iPA, Biosolve), ethylenediamine (EDA, Sigma-Aldrich, ≥99%), dry hexane (Acros, Extra Dry over Molecular Sieve, 97%), N,N-Dimethylformamide (DMF) (Acros, Extra Dry over Molecular Sieve, 99,8%), pyridine (Sigma-Aldrich, anhydrous, 99,8%), 2,2'-bipyridil (BiPy) (Sigma-Aldrich, ≥99%), 2-bromoisobutyryl bromide (BIBB) (Aldrich, 98%), Ethylenediaminetetraacetic acid disodium salt dihydrate (EDTA) (Sigma, 99%), 4-dimethylaminopyridine (DMAP) (Sigma-Aldrich, ≥99%), N,N´-disuccinimidyl carbonate (Sigma-Aldrich, 98%), triethylamine (Sigma-Aldrich, ≥99%), and FN (Invitrogen) were used as received. All water used in the experiments was Millipore Milli-Q grade. Basic cell culture media was prepared by adding to a α-MEM cell medium (Invitrogen), 10 v/v% of Fetal Bovine Serum (FBS), 2 mM of L-Glutamine, 100 U/mL of penicillin, 100 µg/mL of streptomycine, and 0.2 mM of ascorbic acid. All the mentioned components were obtained from Invitrogen. Furthermore, Invitrogen provided phosphate buffered saline (PBS), bovine serum albumin (BSA), trypsin, 4',6-diamidino-2-phenylindole (DAPI), fluorescein isothiocyanate (FITC). Formalin (neutral buffered, 10%) and triton x-100 were both purchased from Sigma-Aldrich.

Activation of the polymer films:

Silicon or glass substrates were first cleaned with Piranha solution, then rinsed extensively with water and ethanol. Caution: Piranha solution reacts violently with many organic materials and should be handled with great care! PCL films were spin coated (2000 rpm for 1 minute) onto the cleaned substrates from a chloroform solution (1 wt%). Subsequently, the PCL films were annealed at 70 °C for 1 hour

and cooled down by either quenching the films in liquid nitrogen (Q-PCL), removing the films from the oven and cooling to ambient temperature (A-PCL), or by slow cooling at 0.5 °C/min (S-PCL). The differently treated PCL films were subsequently immersed into a solution of 5 mM ethylenediamine (EDA) in isopropanol (iPA). The reaction was allowed to proceed for 10 minutes under room temperature conditions. Samples were then rinsed with ice-cold water and subsequently rinsed with water at room temperature, then dried in a stream of nitrogen. (2) The aminated PCL films were immersed into 10 ml of dry hexane and 100 µL of dry pyridine, to which 100 µL of 2-bromoisobutyryl bromide (BIBB) was added dropwise. The reaction mixture was gently stirred for 1 hours at room temperature to produce the 2-bromoisobutyryl-immobilized PCL surface (the PCL-Br surface). The PCL-Br substrate was then washed repeatedly with a methanol/water (1/1, v/v) mixture and dried under a stream of nitrogen.

Atom transfer radical polymerization (ATRP) of OEGMA brushes:
Purified OEGMA monomer (5 g, 9.5 mmol) and 2,2'bipyridine (81.7 mg, 0.52 mmol) were added to a water (5ml) and methanol (1,26ml) mixture. The solution was purged with nitrogen for 30 min. CuCl (18.75 mg, 0.19 mmol) and $CuBr_2$ (2 mg, 0.009 mmol) were added into another reaction flask and also flushed with nitrogen. Monomer, ligand and catalyst were then combined and stirred for another 30 minutes to facilitate the formation of the organometallic complex. This solution was then transferred into the flasks containing the activated PCL substrates. The flasks were sealed with rubber septa and kept at room temperature under nitrogen. After reaching the desired reaction time of 60 minutes, the substrates were removed from the polymerization solution, exhaustively rinsed with water to remove any unreacted and not surface tethered substances and subsequently dried in a stream of nitrogen. Afterwards the samples were washed with a 0.1M EDTA solution overnight to extract the copper from the polymer brushes.

Fibronectin functionalization:
The samples were placed in a dry DMSO solution containing 100 mM of DSC and DMAP. Subsequently the samples were incubated in a 0,1 mM FN solution overnight in order to covalently couple the FN to the polymer brush. On the

contrary, pure PCL substrates were incubated in a 0,01 mM FN solution overnight to ensure a final surface concentration of FN comparable to the brush-coated corresponding samples.

XPS: A Quantera SXM scanning XPS microprobe (Physical Electronics, Chanhassen, MN, USA) using a Al Kα, monochromatic X-ray at 1486.6 eV was used to measure the atomic composition of the surfaces of POEGMA brushes with or without functionalization with FN. The surface coverage of FN (σ_{FN}) was calculated according to:

$$\sigma_{FN} = \rho\, h\, r_{N/C,\, sample} / r_{N/C,\, FN} \qquad (5.3)$$

where ρ is the density (1 g/cm^3), h the sampling depth of XPS (7.5 nm) and r is the nitrogen to carbon ratio measured for our samples and for pure FN (0.270)[61].

Cell culture and cell image analysis:

Human mesenchymal stem cells were cultured at 37°C in a humidified atmosphere of 5% carbon dioxide, using as culture medium α-MEM supplemented with 10 v/v % FBS, 2 mM L-Glutamine, 1 mM sodium pyruvate, 100 U/mL of penicillin and 100 µg/mL of streptomycin. The cells were seeded at a density of 2,000 cells/cm^2 on PCL substrates, unmodified and modified with POEGMA brushes. After 4 hours, the substrates were washed twice with PBS and fixed with a 3.7 v/v % formaldehyde solution in PBS for 10 minutes at room temperature. Next, the samples were washed two or more times with PBS containing 1 w/v % bovine serum albumin (BSA). Cell membrane was permeabilized by treating the samples with 0.1 v/v % Triton X-100 solution in PBS-BSA after which the specimens were washed again with PBS-BSA. Cell nuclei were stained with DAPI diluted 1:100 and cell cytoskeleton was stained with a phalloidin-rhodamine FITC solution diluted 1:50 in a PBS-BSA for 30 minutes at room temperature. Pictures were taken using a Nikon fluorescent microscope Eclipse E600. In order to use the samples for optical imaging, the substrates were dehydrated by submerging the samples into a solution for 10 minutes containing an increasing amount of ethanol. Optical imaging was performed on a BX60 optical microscope (Olympus, Tokyo, Japan). For determining the cell shape parameters area and perimeter, Cell^D

software (Olympus Soft Imaging Solutions, Münster, Germany) was used. The Roundness (RN) was subsequently calculated using:[62]

$$RN = Perimeter / (4\pi \times Area)^{1/2} \quad (5.4)$$

To test the statistical significance of the difference in the cell shape parameters, a one-way ANOVA test followed by a Tukey's post-hoc test was performed. Statistical significance was set at a p value of 0.05.

AFM Imaging:

A Dimension D3100 AFM equipped with a hybrid scanner and a NanoScope IVa controller (Digital Instruments, Veeco-Bruker, Santa Barbara, CA) was operated in tapping mode using commercially available silicon cantilevers (PointProbe® Plus silicon probes, PPP-NCH, Nanosensors, Neuchatel, Switzerland) to obtain the surface morphology of the PCL substrates.

Ellipsometry:

The optical experiments were performed using a Woollam variable-angle spectroscopic ellipsometer system. Measurements were performed as a function of photon energy in the range 1.0–4.5 eV with a step size of 0.1 eV; this corresponds to a wavelength range of 275–1240 nm. Ellipsometry measurements on the collapsed POEGMA layers were performed at angles of incidence of θ = 65°, 70° and 75°. Measurements in water were performed in a liquid cell containing two windows at a fixed angle of incidence of θ = 63°. A third window enabled alignment of the sample at normal incidence as well as allowing visual inspection of the sample during in situ experiments. The ellipsometry spectra, i.e. Ψ and Δ as a function of wavelength, were analyzed using *CompleteEASE* (Woollam), using bulk dielectric functions for silicon, silicon dioxide, and water.

5.5 References

1 Daley, W. P.; Peters, S. B.; Larsen, M., *Journal of Cell Science* **2008,** *121,* 255-264.

2 Guilak, F.; Cohen, D. M.; Estes, B. T.; Gimble, J. M.; Liedtke, W.; Chen, C. S., *Cell Stem Cell* **2009,** *5,* 17-26.

3 Chamberlain, G.; Fox, J.; Ashton, B.; Middleton, J., *Stem Cells* **2007,** *25,* 2739-2749.

4 Bianco, P.; Robey, P. G.; Simmons, P. J., *Cell Stem Cell* **2008,** *2,* 313-319.

5 Yim, E. K. F.; Pang, S. W.; Leong, K. W., *Experimental Cell Research* **2007,** *313,* 1820-1829.

6 Pittenger, M. F.; Mackay, A. M.; Beck, S. C.; Jaiswal, R. K.; Douglas, R.; Mosca, J. D.; Moorman, M. A.; Simonetti, D. W.; Craig, S.; Marshak, D. R., *Science* **1999,** *284,* 143-147.

7 McBeath, R.; Pirone, D. M.; Nelson, C. M.; Bhadriraju, K.; Chen, C. S., *Developmental Cell* **2004,** *6,* 483-495.

8 Engler, A. J.; Sen, S.; Sweeney, H. L.; Discher, D. E., *Cell* **2006,** *126,* 677-689.

9 Dalby, M. J.; Gadegaard, N.; Tare, R.; Andar, A.; Riehle, M. O.; Herzyk, P.; Wilkinson, C. D. W.; Oreffo, R. O. C., *Nature Materials* **2007,** *6,* 997-1003.

10 McMurray, R. J.; Gadegaard, N.; Tsimbouri, P. M.; Burgess, K. V.; McNamara, L. E.; Tare, R.; Murawski, K.; Kingham, E.; Oreffo, R. O. C.; Dalby, M. J., *Nature Materials* **2011,** *10,* 637-644.

11 Trappmann, B.; Gautrot, J. E.; Connelly, J. T.; Strange, D. G. T.; Li, Y.; Oyen, M. L.; Stuart, M. A. C.; Boehm, H.; Li, B.; Vogel, V.; Spatz, J. P.; Watt, F. M.; Huck, W. T. S., *Nature Materials* **2012,** *11,* 642-649.

12 Shih, Y.-R. V.; Tseng, K.-F.; Lai, H.-Y.; Lin, C.-H.; Lee, O. K., *Journal of Bone and Mineral Research* **2011,** *26,* 730-738.

13 Gittens, R. A.; McLachlan, T.; Olivares-Navarrete, R.; Cai, Y.; Berner, S.; Tannenbaum, R.; Schwartz, Z.; Sandhage, K. H.; Boyan, B. D., *Biomaterials* **2011,** *32,* 3395-3403.

14 Nandakumar, A.; Birgani, Z. T.; Santos, D.; Mentink, A.; Auffermann, N.; van der Werf, K.; Bennink, M.; Moroni, L.; van Blitterswijk, C.; Habibovic, P., *Biofabrication* **2013,** *5*.

15 Unadkat, H. V.; Hulsman, M.; Cornelissen, K.; Papenburg, B. J.; Truckenmüller, R. K.; Carpenter, A. E.; Wessling, M.; Post, G. F.; Uetz, M.; Reinders, M. J. T.; Stamatialis, D.; van Blitterswijk, C. A.; de Boer, J., *Proceedings of the National Academy of Sciences* **2011,** *108,* 16565-16570.

16 Biggs, M. J. P.; Richards, R. G.; McFarlane, S.; Wilkinson, C. D. W.; Oreffo, R. O. C.; Dalby, M. J., *Journal of the Royal Society Interface* **2008,** *5,* 1231-1242.

17 Dalby, M. J.; Riehle, M. O.; Johnstone, H.; Affrossman, S.; Curtis, A. S. G., *Biomaterials* **2002,** *23,* 2945-2954.

18 Song, W.; Lu, H. X.; Kawazoe, N.; Chen, G. P., *Langmuir* **2011,** *27,* 6155-6162.

19 Kilian, K. A.; Bugarija, B.; Lahn, B. T.; Mrksich, M., *Proceedings of the National Academy of Sciences* **2010,** *107,* 4872-4877.

20 Ayres, N., *Polymer Chemistry* **2010,** *1,* 769-777.

21 Barbey, R.; Lavanant, L.; Paripovic, D.; Schuwer, N.; Sugnaux, C.; Tugulu, S.; Klok, H. A., *Chemical Reviews* **2009,** *109,* 5437-5527.

22 Cooperstein, M. A.; Canavan, H. E., *Langmuir* **2010,** *26,* 7695-7707.

23 Hu, Z. B.; Cai, T.; Chi, C. L., *Soft Matter* **2010,** *6,* 2115-2123.

24 Klein Gunnewiek, M.; Di Luca, A.; Sui, X.; van Blitterswijk, C. A.; Moroni, L.; Vancso, G. J., *Israel Journal of Chemistry* **2012,** *52,* 339-346.

25 Navarro, M.; Benetti, E. M.; Zapotoczny, S.; Planell, J. A.; Vancso, G. J., *Langmuir* **2008,** *24,* 10996-11002.

26 Tugulu, S.; Silacci, P.; Stergiopulos, N.; Klok, H.-A., *Biomaterials* **2007,** *28,* 2536-2546.

27 Xu, F. J.; Wang, Z. H.; Yang, W. T., *Biomaterials* **2010,** *31,* 3139-3147.

28 Xu, F. J.; Zheng, Y. Q.; Zhen, W. J.; Yang, W. T., *Colloids and Surfaces B-Biointerfaces* **2011,** *85,* 40-47.

29 Konradi, R.; Acikgoz, C.; Textor, M., *Macromolecular Rapid Communications* **2012,** *33,* 1663-1676.

30 Jiang, S.; Cao, Z., *Advanced Materials* **2010,** *22,* 920-932.

31 Liu, Q. S.; Singh, A.; Lalani, R.; Liu, L. Y., *Biomacromolecules* **2012,** *13,* 1086-1092.

32 Raynor, J. E.; Petrie, T. A.; García, A. J.; Collard, D. M., *Advanced Materials* **2007,** *19,* 1724-1728.

33 Xu, F. J.; Liu, L. Y.; Yang, W. T.; Kang, E. T.; Neoh, K. G., *Biomacromolecules* **2009,** *10,* 1665-1674.

34 Tugulu, S.; Klok, H.-A., *Macromolecular Symposia* **2009,** *279,* 103-109.

35 Edmondson, S.; Osborne, V. L.; Huck, W. T. S., *Chemical Society Reviews* **2004,** *33,* 14-22.

36 Ma, H.; Hyun, J.; Stiller, P.; Chilkoti, A., *Advanced Materials* **2004,** *16,* 338-341.

37 Brown, A. A.; Khan, N. S.; Steinbock, L.; Huck, W. T. S., *European Polymer Journal* **2005,** *41,* 1757-1765.

38 Le, D. M.; Kulangara, K.; Adler, A. F.; Leong, K. W.; Ashby, V. S., *Advanced Materials* **2011,** *23,* 3278-3283.

39 Lendlein, A.; Schmidt, A. M.; Schroeter, M.; Langer, R., *Journal of Polymer Science Part a-Polymer Chemistry* **2005,** *43,* 1369-1381.

40 Ping, P.; Wang, W. S.; Chen, X. S.; Jing, X. B., *Biomacromolecules* **2005,** *6,* 587-592.

41 Woodruff, M. A.; Hutmacher, D. W., *Progress in Polymer Science* **2010,** *35,* 1217-1256.

42 Guvendiren, M.; Burdick, J. A., *Biomaterials* **2010,** *31,* 6511-6518.

43 Watari, S.; Hayashi, K.; Wood, J. A.; Russell, P.; Nealey, P. F.; Murphy, C. J.; Genetos, D. C., *Biomaterials* **2012,** *33,* 128-136.

44 Kulangara, K.; Yang, Y.; Yang, J.; Leong, K. W., *Biomaterials* **2012,** *33,* 4998-5003.

45 Ponsonnet, L.; Reybier, K.; Jaffrezic, N.; Comte, V.; Lagneau, C.; Lissac, M.; Martelet, C., *Materials Science and Engineering: C* **2003,** *23,* 551-560.

46 Samaroo, H. D.; Lu, J.; Webster, T. J., *International Journal of Nanomedicine* **2008,** *3,* 75-82.

47 Singh, N.; Cui, X.; Boland, T.; Husson, S. M., *Biomaterials* **2007,** *28,* 763-771.

48 Massia, S. P.; Hubbell, J. A., *The Journal of Cell Biology* **1991,** *114,* 1089-1100.

49 Cook, A. D.; Hrkach, J. S.; Gao, N. N.; Johnson, I. M.; Pajvani, U. B.; Cannizzaro, S. M.; Langer, R., *Journal of Biomedical Materials Research* **1997,** *35,* 513-523.

50 Webb, K.; Hlady, V.; Tresco, P. A., *Journal of Biomedical Materials Research* **2000,** *49,* 362-368.

51 Keselowsky, B. G.; Collard, D. M.; Garcia, A. J., *Journal of Biomedical Materials Research Part A* **2003,** *66A,* 247-259.

52 Dolatshahi-Pirouz, A.; Jensen, T. H. L.; Kolind, K.; Bünger, C.; Kassem, M.; Foss, M.; Besenbacher, F., *Colloids and Surfaces B: Biointerfaces* **2011,** *84,* 18-25.

53 Discher, D. E.; Janmey, P.; Wang, Y. L., *Science* **2005,** *310,* 1139-1143.

54 Nam, K.; Fukaya, R.; Hashimoto, Y.; Ito, Y.; Kimura, T.; Kishida, A., *Chemistry Letters* **2010,** *39,* 1164-1165.

55 Loesberg, W. A.; te Riet, J.; van Delft, F. C. M. J. M.; Schön, P.; Figdor, C. G.; Speller, S.; van Loon, J. J. W. A.; Walboomers, X. F.; Jansen, J. A., *Biomaterials* **2007,** *28,* 3944-3951.

56 van Delft, F. C. M. J. M.; van den Heuvel, F. C.; Loesberg, W. A.; te Riet, J.; Schön, P.; Figdor, C. G.; Speller, S.; van Loon, J. J. W. A.; Walboomers, X. F.; Jansen, J. A., *Microelectronic Engineering* **2008,** *85,* 1362-1366.

57 Wieringa, P.; Tonazzini, I.; Micera, S.; Cecchini, M., *Nanotechnology* **2012,** *23,* 275102-275102.

58 Balloni, S.; Calvi, E. M.; Damiani, F.; Bistoni, G.; Calvitti, M.; Locci, P.; Becchetti, E.; Marinucci, L., *International Journal of Oral & Maxillofacial Implants* **2009,** *24,* 627-635.

59 Hu, X.; Park, S.-H.; Gil, E. S.; Xia, X.-X.; Weiss, A. S.; Kaplan, D. L., *Biomaterials* **2011,** *32,* 8979-8989.

60 Yu, B.-Y.; Chen, P.-Y.; Sun, Y.-M.; Lee, Y.-T.; Young, T.-H., *Journal of Biomaterials Science-Polymer Edition* **2012,** *23,* 1-26.

61 Galtayries, A.; Warocquier-Clérout, R.; Nagel, M. D.; Marcus, P., *Surface and Interface Analysis* **2006,** *38,* 186-190.

62 Andersson, A. S.; Backhed, F.; von Euler, A.; Richter-Dahlfors, A.; Sutherland, D.; Kasemo, B., *Biomaterials* **2003,** *24,* 3427-3436.

CHAPTER SIX

POEGMA systems with variable grafting density and thickness grafted from polymer substrates

This Chapter studies poly(oligo(ethylene glycol) methacrylate (POEGMA) brushes grafted from initiator-modified polycaprolactone (PCL) surfaces which presented different brush thicknesses and grafting densities. Such substrates were obtained by spincoating PCL and varying the initiator coverage or the polymerization time. Extensive cell shape analysis showed that cells attached to these POEGMA coatings adopted different morphologies responding to variations in grafting density and thickness.

Linear gradients of POEGMA brush thickness were conjugated with fibronectin (FN) to obtain cell adhesive samples featuring a graded variation in graft-ligand length at the surface. Cells adhered uniformly on the gradient and the cell shape showed to be independent of the POEGMA thickness. On the contrary, differences in FA formation and morphologies were related to a variation of both the lateral extendibility of brushes.

6.1 Introduction

The fabrication and application of synthetic extra-cellular matrices (ECMs) presenting a variation of (bio)chemical/physical properties by gradient morphologies have been increasingly investigated in tissue engineering (TE).[1-2] Biomaterials and scaffolds presenting "graded" characteristics might efficiently replicate the peculiar properties of natural ECMs. Thus, these preparations coupled to the application of stem cells could not only trigger specific cellular processes (such as adhesion[3-4], migration[5-7] and differentiation[8-10]) but it might also offer a number of simplified and easily accessible study platforms to investigate the complex behavior of cells within specific environments.

Supports which present a gradient-like variation of properties along one or more directions of their available surface (2D systems) or volume (3D scaffolds) were recently studied in the presence of cells or stem cells. The typical properties that could be easily tailored were elasticity within hydrogel supports[11-12], wettability on surfaces[13-15] and concentration of biochemical cues on both 2D and 3D systems[16-19]. Particularly substrate elasticity, a fundamental parameter governing stem cells differentiation, could be efficiently varied within supports featuring a gradient in stiffness along multiple directions[20-23]. Among the different materials which were proposed to fabricate interfaces and 3D supports with graded variations in mechanical properties, hydrogels were the most often applied. These possessed several advantageous properties such as biocompatibility and controlled biodegradability. In addition, fine tuning of physical properties such as modulus and hydration, could be easily attained by varying their crosslink density through simple polymer chemistry approaches.[23-26] These and other similar elastomeric substrates featuring tailorable physical characteristics were showed to control cell spreading and cell mobility.[7, 27-31] Additionally, cellular migration and differentiation into specific cell lineages were affected by the mechanical properties of these supports and gradients of stiffness could be used to spatially control such cellular phenomena.[32-34] Integration of all these supports with cells passes through cellular attachment and spreading on the exposed biomaterial interface. Thus the specific surface properties of the supports define the first cell-biomaterial contact which often determines the fate of cells and the subsequent performance of the

synthetic constructs. Cell adhesion mechanisms on biomaterials presenting different physico-chemical or graded properties are constantly mediated through the formation of focal adhesion complexes (FA) at the cell outer membrane.[35-36] These protein organizations originate at the ECM-integrin junctions[37] and trigger a variety of cellular phenomena including migration, proliferation and differentiation.[38-40] Specifically, different adhesion mechanisms are reflected by a variation of the morphology and functioning of FAs in the cell body.[41] As an example, through FA points the elasticity of a specific substrate is transferred to the cell interior. In the case of hydrogels presenting different mechanical properties, less contractile cells on soft hydrogels will modulate the size of FA complexes compared to rigid supports where a stronger attachment is needed.[36, 42]

Covalent grafting of functional macromolecules has represented an attractive and promising strategy to finely modulate the surface properties of biomaterials and thus to control the adhesion mechanism of cells.[43] In the previous Chapters I have already introduced how surface-initiated polymerization techniques (SIP) and, specifically, surface-initiated atom-transfer radical polymerizations (SI-ATRP) could be applied to graft a variety of polymer compositions to form polymer brush layers presenting tunable properties.[44] These densely grafted assemblies could provide multidimentional control over hydrophilicity[45], protein concentration[46-47] as well as the mechanical stiffness[48] through the formation of polymer brush gradients.[49-50] In these cases one can spatially vary the density[51] and the thickness[52] of the brush within one single substrate in order to tune physical or covalent bio-conjugation of different peptide and protein species. Thanks to the highly controlled and living character of SI-ATRP[53-55] a linear relationship between brush thickness (molecular weight/chain length) and polymerization time is obtained. This enabled the easy fabrication of surface gradients of brush thickness through a variation of the polymerization time along an initiator-covered substrate.[45, 52, 56] The grafting density could be also varied adjusting the initiator density at the surface through the formation of mixed monolayer surfaces.[16-17, 57-58]

In the present study I fabricated various poly(oligo(ethylene glycol) methacrylate (POEGMA) brushes from initiator-modified polycaprolactone (PCL) surfaces which presented different brush thicknesses and grafting densities (Scheme 6.1). Brush grafting density was controlled by varying the surface

concentration of ATRP initiator on the surface, while variation of polymerization time was used to vary brush thickness. The unspecific adhesion of human mesenchymal stem cells (hMSCs) was tested on these films highlighting the effect of the different physico-chemical properties of the brush on the morphology of adhering cells. Subsequently, linear gradients of POEGMA brush thickness on single PCL-coated substrates, followed by conjugation of fibronectin (FN), were fabricated to obtain cell adhesive samples featuring a graded variation in graft-ligand length at the surface. These last samples were also incubated with hMSCs to investigate the adhesion and spreading of cells on differently brush-supported protein ligands.

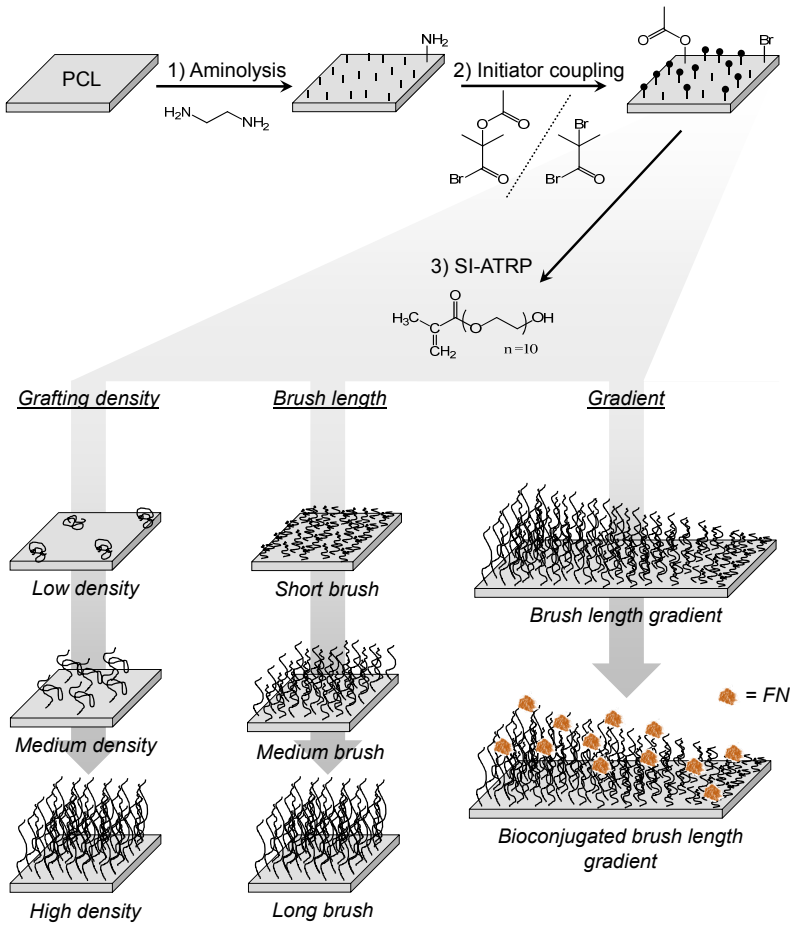

Scheme 6.1. *Schematic representation of various POEGMA architectures grafted from PCL thin films spin coated on silicon substrates.*

6.2 Results and discussion

6.2.1 Fabrication of various POEGMA brush architectures

The adhesion of human mesenchymal stem cells (hMSCs) on POEGMA brushes presenting a gradient-like variation of grafting densities and brush thickness was first investigated. POEGMA brushes were grafted from flat, spin-coated (~100 nm) PCL films using SI-ATRP. Aminolysis of the PCL surface was used to produce free amino groups that can be used to couple the ATRP initiator functions (α-bromoisobutyryl bromide, BIBB). The initiator density on the PCL surface was varied by mixing BIBB with the unreactive 1-bromocarbonyl-1-methylethyl acetate (BMA)[59] (Scheme 6.1, step 2). Subsequent SI-ATRP of OEGMA produced different POEGMA grafting densities on separate homogeneous samples. Since for a given polymerization time the molar mass of the grafted polymers (chain length) was constant irrespective of the initiator density at the surface, the increase in film thickness following an increase of coverage of BIB-functions was solely due to chain crowding and subsequent stretching at the interface.[60] As can be seen in Figure 6.1 by increasing the initiator coverage the thickness of the POEGMA layer measured by ellipsometry increased from few nanometers to more than 50 nm.

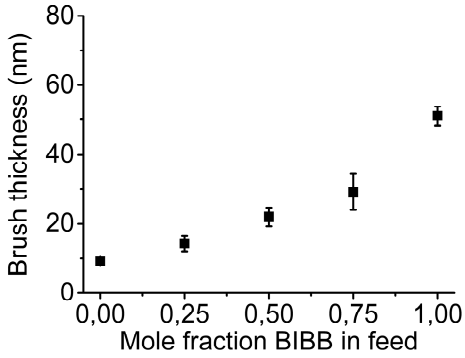

Figure 6.1. *Brush thickness of a POEGMA polymer brush layer as a function of mole fraction of BIBB in a mixture with BMA (Step 2, scheme 6.1).*

Comparison of the POEGMA films thickness values in dry and swollen conditions (in milliQ water, measured at equilibrium, see Experimental Section for details) was used to estimate the grafting density (σ), according to equation 6.1:

$$\sigma = \rho_0 \, h_{dry} \, N_A / (N \, M_0) \qquad (6.1)$$

Here ρ_0 is the estimated POEGMA layer density (1.40 g/cm^3),[61] N_A is Avogadro's number, M_0 is the monomer molecular weight (526 g/mol) and N is the degree of polymerization estimated according to:

$$N = [0.227] \, (h_{swollen})^{3/2} / (h_{dry})^{1/2} \qquad (6.2)$$

where 0.227 is a constant related to the excluded volume parameter and the Kuhn length of a monomer unit.[61] The estimated grafting density values were listed in Table 6.1 and they showed a constant increase with increasing BIBB concentration during initiator coupling at the PCL surface.

Table 6.1. *Dry and swollen thickness values, swelling ratio and the grafting density values for POEGMA layers grafted from PCL substrates using various BIBB concentrations. Dry and swollen thickness values of POEGMA grafted layers measured with ellipsometry. The swelling ratio values were calculated by dividing the swollen by the dry thickness, the grafting density values were derived from equation 6.1.*

Mole fraction on BIBB	**0,50**	**1**
Dry thickness (nm)	23 ± 1	70 ± 1
Wet thickness (nm)	168 ± 6	114 ± 4
Swelling ratio	7.4 ± 0.7	1.6 ± 0.1
Grafting density (chains/nm^2)	0.035 ± 0.005	0.341 ± 0.020

Subsequent adhesion of hMSCs on POEGMA films showed different cell morphology as a function of the specific grafting density. In the absence of initiator at the PCL surface hMSCs adhered onto bare PCL and are spread homogeneously in all direction (Figure 6.2a). However, when the grafting density of POEGMA increased, cell adhesion was hindered and hMSCs increasingly showed a rounded morphology (Figure 6.2b-c).

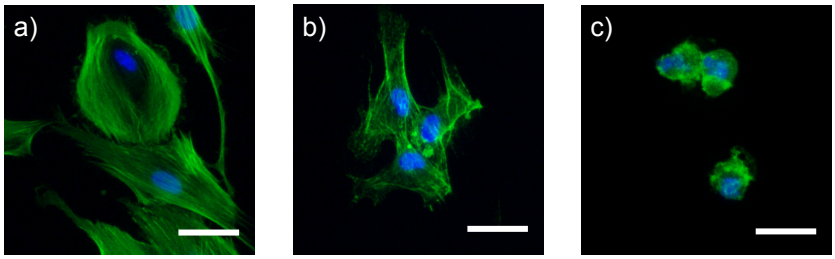

Figure 6.2. *Fluorescent micrographs of hMSCs adhering on bare PCL (a) or on an POEGMA film with 0.035 chains/nm^2 (b) and 0.341 chains/nm^2 (c).*

The decreased adhesion of cells with increasing POEGMA grafting density was also reflected by the steady variation of cell shape parameters as shown in Figure 6.2a-c. Both the cell projected area (Figure 6.3a) and the cell perimeter (Figure 6.3b) were 3 to 4 times smaller for POEGMA brushes presenting σ=0.035 ± 0.005 chain/nm^2 compared to MSCs attached onto the bare PCL. While for cells adhering on densely grafted POEGMA brushes (σ=0.341 ± 0.020), the area and perimeter showed even smaller vales, 8 to 9 times lower than the average values recorded for hMSCs on PCL (Figure 6.3a-b). The relatively high roundness values obtained for cells attached onto bare PCL were directly related to the spreading of hMSCs with irregular shapes (Figure 6.3c). As the grafting density of POEGMA chains increased, the roundness values decreased towards 1, indicating the adoption of more circular shapes. The hindering of cell adhesion due to POEGMA grafting was due to the non-biofouling behavior of the grafted polymer, which became a predominant parameter by increasing polymer grafting density at the surface.[62-63]

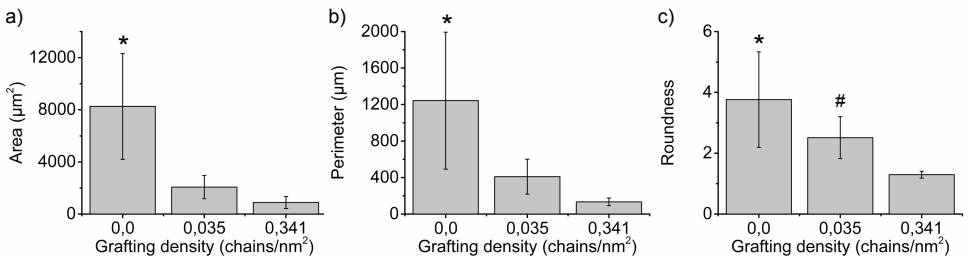

Figure 6.3. *Projected area (a), perimeter (b), and roundness values (c) of cell adhering on POEGMA brush layers with different grafting densities. * and # denotes statistical significant differences between the assigned and the non-assigned topologies (p < 0.05) (n = 20).*

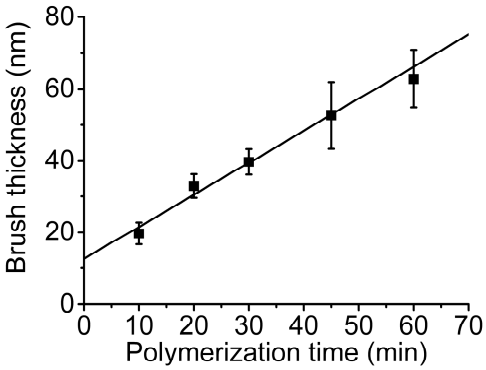

Figure 6.4. *Brush thickness of a POEGMA polymer brush layer as a function of polymerization time (Step 3, scheme 6.1).*

Due to the "living" character of SI-ATRP, POEGMA brush thickness could be well controlled by adjusting the polymerization time. Thus different samples presenting increasing POEGMA brush thicknesses (keeping constant σ) could be synthesized from initiator-modified PCL films and subsequently incubated in hMSCs to test cell adhesion. Figure 6.4 reported a linear relationship between the polymerization time and POEGMA brush thickness.

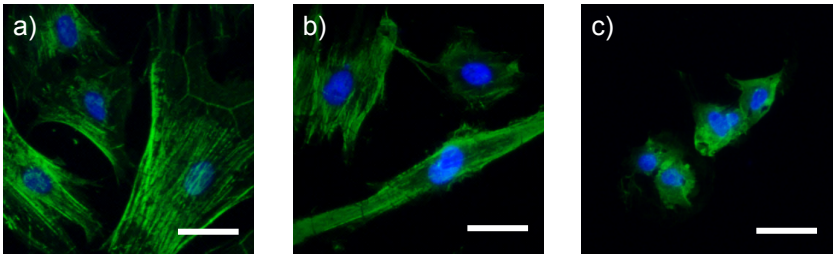

Figure 6.5. *Fluorescent micrographs of hMSCs adhering on POEGMA films with a thickness of 20 (a), 40 (b), and 60 nm (c).*

By varying the exposure of the initiator-functionalized PCL films to OEGMA SI-ATRP solution between 10 and 60 minutes, POEGMA brush thicknesses ranging from 20 to around 60 nm were obtained. Subsequent adhesion of HMSCs showed a clear influence of brush thickness on cell adhesion. Namely, HMSCs attaching on thin brushes (~20 nm) showed a spread morphology and a clear cytoskeleton (Figure 6.5a). On the contrary, increase in POEGMA brush thickness

significantly reduced cell size of adhering hMSCs which showed a more rounded morphology and a less developed cytoskeleton (Figure 6.5b-c).

The effect of POEGMA brush thickness on stem cells adhesion was also reflected in the values of cell shape parameters for the different POEGMA brushes used as platforms (Figure 6.6). Both cell projected areas (Figure 6.6a) and cell perimeters (Figure 6.6b) significantly decreased with increasing POEGMA brush thickness. In addition, roundness values (Figure 6.6c) of cells adhering on 60 nm were all around 1, reflecting an almost circular shape adopted by the adhering cells. In contrast hMSCs adhered on thinner, 20 nm thick POEGMA brushes showed roundness values comparable to the ones previously found for the same cells attached on bare PCL films. This observation indicated how cells could be affected by the characteristics of the underlying substrate when very thin brush coatings (see previous Chapter 5 for a detailed study on the decoupling effect of POEGMA brushes) are grafted and exposed at the interface. This behavior was also observed by Navarro et al., how showed that the cell-adhesive arginine-glycine-aspartic acid (RGD) motifs could be sensed by adhering cells even under a 10 nm thick poly(methacrylic acid) (PMAA) brush layer.[64]

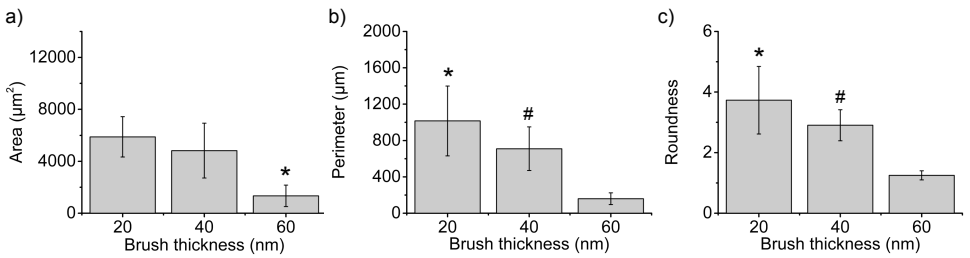

Figure 6.6. *Projected area (a), perimeter (b), and roundness values (c) of cell adhering on POEGMA brush layers with different thicknesses. * and # denotes statistical significant differences between the assigned and the non-assigned topologies ($p < 0.05$) ($n = 20$).*

To investigate the effect of a gradual variation of POEGMA brush thickness on the unspecific adhesion of hMSCs, a thickness gradient was fabricated on a single PCL support and it was subsequently incubated with hMSCS (Figure 6.7). Here the dry brush height is plotted as a function of the position on the substrate. Specifically, POEGMA brush thickness gradient

was formed by vertically placing a 10 x 20 mm initiator-functionalized PCL-coated substrate inside an argon-purged vial, while OEGMA SI-ATRP solution was slowly added via a syringe pump-controlled injector (see Scheme 6.2).

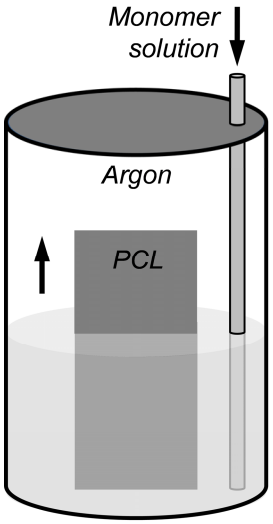

Scheme 6.2. *Schematic representation of the setup for creating surface grafted POEGMA with a gradient in brush thickness.*

As shown in Figure 6.7a the POEGMA brush thickness gradients obtained showed a linear morphology with a constant decrease of brush thickness from around 60 to 0 nm (bare PCL film exposed), varying along a distance of 20 mm on the substrate.

Following 24 hours of incubation, hMSCs adhered on the gradient brush to a different extent as a function of the POEGMA brush thickness and thus depending on the lateral position on the substrate (Figure 6.7b-h). Figure 6.7b reported the number of hMSCs adhered on the gradient POEGMA brush. A clear increase of number of cells with decreasing brush thickness could be observed. Optical micrographs of hMSCs adhering at specific positions on these substrates were reported in Figure 6.7c-h. From these micrographs, the few cells attached on 65 nm thick POEGMA brush (as indicated in Figure 6.7c) showed a rounded shape which is comparable to cells adhering on single substrates presenting a POEGMA brush with

similar thickness (Figure 6.5c). Increase of brush thickness across the samples was followed by a clear increase in number of adhered cells and cells spreading. These expanded their projected areas with decreasing POEGMA length until uniform cell coverage for samples presenting sub-20 nm thick POEGMA at the PCL interface. In these particular positions on the gradient samples (Figure 6.7g-h) hMSCs spread homogeneously in all directions following morphologies which were similar to the ones showed on homogeneous POEGMA brushes with comparable thicknesses (Figure 6.5a).

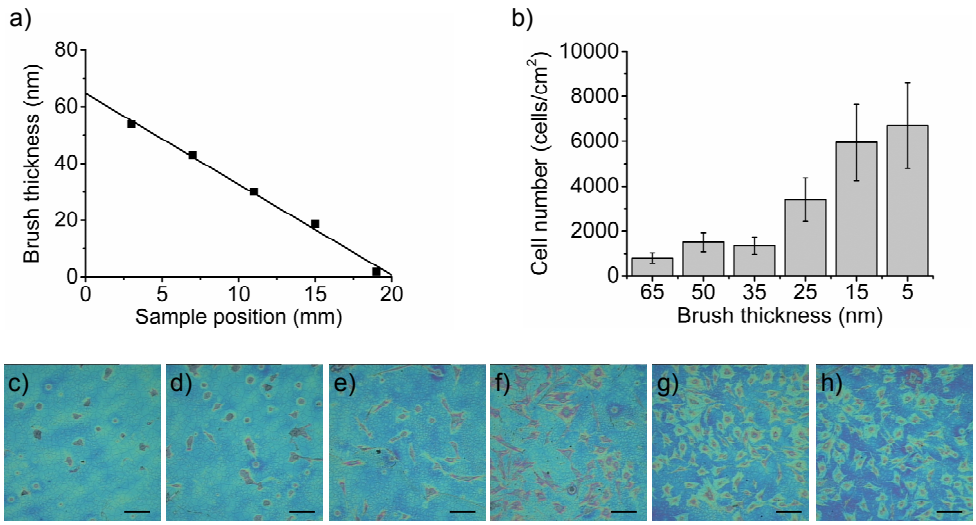

Figure 6.7. *(a) Thickness profile measured by ellipsometry of a POEGMA brush grafted by SI-ATRP from an initiator-functionalized PCL film. (b) Cell number and the (c-h) corresponding optical micrographs of hMSCs adhering on specific positions on a POEGMA brush thickness gradient: (c) 65, (d) 50, (e) 35, (f) 25, (g) 15, and (h) 5 nm POEGMA thickness. The scale bar for all the optical micrographs is equal to 200 μm.*

For all the different brush thicknesses tested, on both homogeneous and gradient samples, hMSCs adhesion was directly related to the cell-repulsive character of POEGMA brushes. This was related to the macromolecular parameters of the brush i.e. the length of the grafted chains. Increasing brush thickness and thus chain length incremented the anti-biofouling character of the film inducing a more efficient screening of protein

adhesion and subsequent cell attachment at the surface. Short chains forming a thin sub-20 nm POEGMA brush allowed the adsorption of proteins from the cell culture solution and thus triggered the formation of attaching points for the adhesion and spreading of hMSCs. On the contrary, long grafted chains within thick POEGMA brush layers quantitatively depleted protein adsorption and keeping the surface antifouling during cell culture. This phenomenon inhibited cell adhesion and induced rounding and presumably apoptosis for the few attached cells.[62-63]

6.2.2 Bioactivation of POEGMA gradient coatings

In order to fabricate cell-adhesive POEGMA brush films the side hydroxyl-terminated chains of the monomer units of POEGMA were used to immobilize fibronectin (FN) via DSC-mediated coupling (see Experimental section for details) (Scheme 6.1). This functionalization procedure was performed on POEGMA brush on PCL films presenting a gradient thickness ranging from 25 to 65 nm. Subsequent incubation in hMSCs culture allowed to investigate the influence of the polymer "support" length of the FN ligand on the adhesion and spreading of stem cells. Due to the protein repellency by POEGMA brushes, which could affect the chemisorption of FN at the "activated" side chains, the surface coverage of FN fragments was investigated by X-ray photoelectron spectroscopy (XPS) on POEGMA films presenting different thickness. Namely, XPS was performed at different positions on gradient samples and the signals originating from the N-containing protein fragments was analyzed. The N1s core level spectra were measured by XPS (Figure 6.8a) at each position on the POEGMA brush sample and they were correlated to the corresponding FN surface concentration, as reported in Figure 6.8b (see Experimental section for details). While a slight increase in FN surface concentration was recorded for the thicker POEGMA brushes, the average protein concentration was found in the range between 20-40 ng/cm2 across the whole sample. Thus, considering an average XPS sampling depth of around 7.5 nm[65] it could be concluded that the interfacial concentration of FN units did not show a marked variation on "activated" POEGMA brush supports presenting thickness values ranging from 25 to 65 nm.

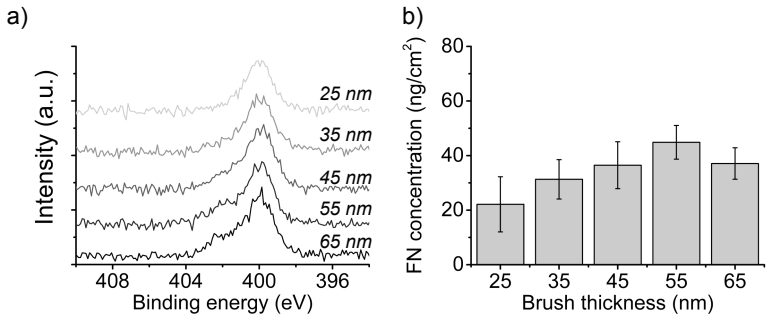

Figure 6.8. *(a) Averaged (n=4) N1s core level XPS spectra and (b) the corresponding FN concentration measured at different brush lengths on a POEGMA gradient brush layer.*

Lateral force microscopy (LFM) was additionally employed to qualitatively measure the lateral bending of POEGMA-FN brush conjugates featuring different brush thicknesses i.e. different lengths of chain supporting FN ligands (recorded on different positions on the gradient samples). The "mobility" of RGD ligands on the surface was reported to affect the adhesion of cells, specifically influencing the concentration and the morphology of focal adhesion complexes at the cell membrane.[66] In order to modulate ligand mobility and exposure at the interface several physico-chemical characteristics of polymeric "spacers" binding FN or RGD units from flat surfaces can be effectively varied. These include steric hindrance by the polymeric graft, swelling and molar mass (chain length), some of which were recently reported to show a relevant role in the mechanism of cell attachment.[67-68]

In the present study, the length of the grafted POEGMA chains binding FN units was varied by controlling the ATRP process along the substrate. Lateral bending of POEGMA brushes presenting different lengths in the hydrated state could be qualitatively measured by sliding laterally a colloidal probe and recording the corresponding friction force loops.[69] The static friction force due to adhesion of the silica colloid onto the POEGMA brush interface coupled to the hydration and the compliancy of the swollen brush caused an initial tilting of the friction loop Figure 6.9 and Figure 6.10a. Steady sliding could be attained just when the static friction force could be overcome by the spring force of the bent brush underlayer (X_s in Figure

6.10a). As an example, in Figure 6.10a a friction loop recorded on 65 nm thick POEGMA-FN brush was reported. Initial tilting of the loop at the scanning direction reversal points was observed until steady-state sliding contact between the counter surface of the silica colloid and the top surface of the brush occurred. The lateral piezo displacement corresponding to the tilted section of the loop (T in Figure 6.10a) could be related to the maximum extension of the swollen brush.[69] Thus, thicker polymeric grafts in the swollen state originated a longer tilted section in the experimental friction loop compared to thinner brushes. In Figure 6.10b the single trace loops for 25, 45 and 65 nm thick POEGMA-FN brushes were reported, highlighting the lateral scanning direction with an arrow overlapping each trace. The increment of POEGMA-FN brush thickness reflected an increase in the length of the tilted loop section before the occurrence of steady sliding after 60, 180 and 240 nm, for 25, 45 and 65 nm thick brush, respectively (highlighted with points A, B and C in Figure 6.10b).

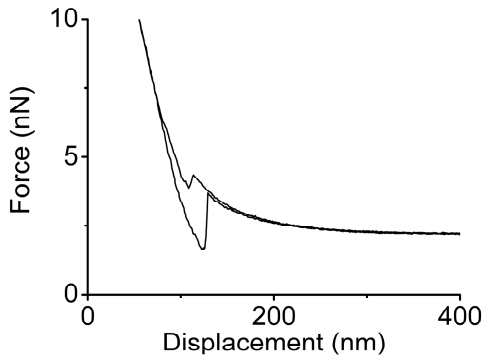

Figure 6.9. *A representative force-displacement curve measured on a 65nm thick POEGMA brush.*

Hence, despite the nearly constant surface concentration of FN units, a variation of thickness of the swollen POEGMA brush support produced polymer-ligand conjugates that can experience a different maximum lateral extension. Considering the lateral pressure exerted by adhering cells during surface attachment and spreading, which was estimated as 5.5 nN/μm^2 per

FA,[70] differences in lateral chain bending along the gradient would certainly affect the mechanism of cell adhesion.

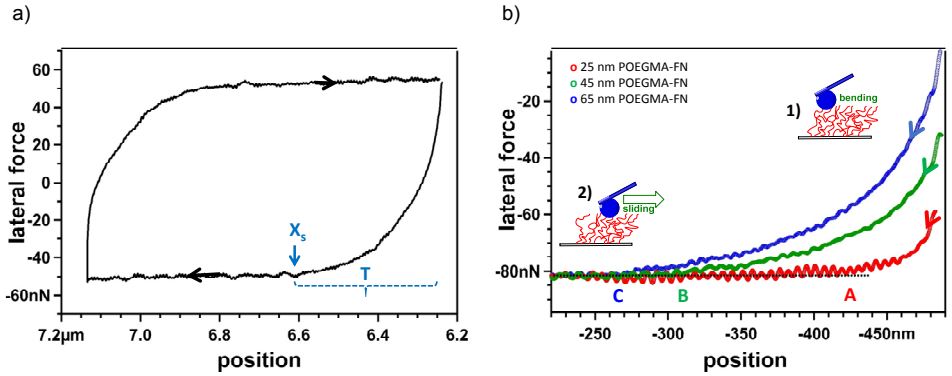

Figure 6.10. *AFM analysis of the POEGMA brush layers. (A) A representative friction loop recorded on a 65nm thick POEGMA brush. T indicates the lateral piezo displacement corresponding to the brush tilting section of the loop and X_s correspond to the position from were sliding occurs. (B) The single trace loops for 25 nm, 45 nm and 65nm thick POEGMA brushes were reported.*

In order to test the adhesion of hMSCs on POEGMA-FN brushes presenting different thicknesses, the gradient samples were incubated in cell cultures for 24 hours and subsequently studied by optical and immunofluorescence microscopies (see Experimental Section for details). Figure 6.11 reported optical micrographs of hMSCs adhering at different positions on gradient POEGMA-FN brush grafted from PCL. HMSCs morphology did not show a significant influence of the brush thickness. This was further proven by analyzing the cell projected areas, perimeters, and roundness values on brush-FN films with different average thicknesses (Figure 6.12a-c). In addition, also the number of cells did not show a remarkable difference as a function of the underlying POEGMA-FN brush thickness (Figure 6.12d). This observation confirmed the almost constant interfacial concentration of FN across the sample, as the number of cells adhering on flat surfaces was found dependent on the ligand surface coverage.[47, 68, 71-72]

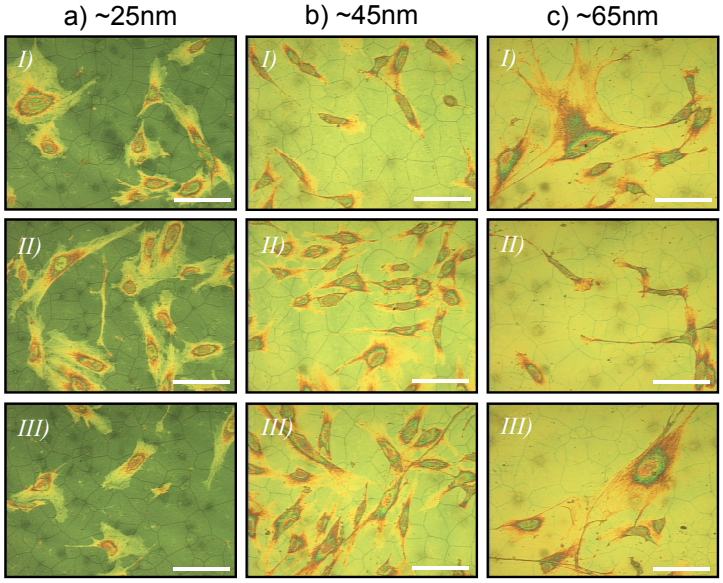

Figure 6.11. *Optical micrographs taken at different positions on a single sample containing a POEGMA gradient. Brush height of 25 nm (a), 45 nm (b), and 65nm (c). Scale bar is 200 µm.*

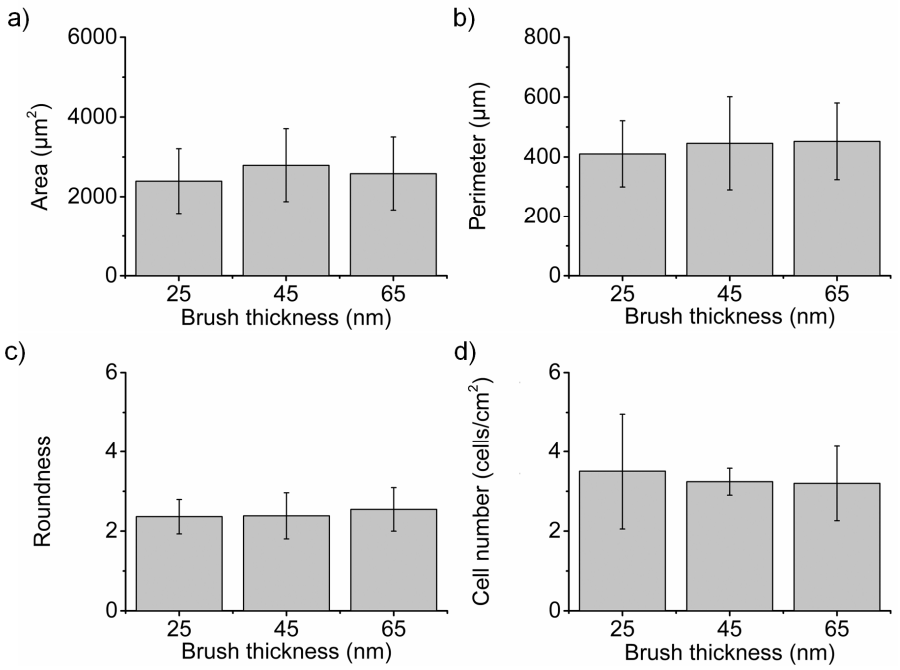

Figure 6.12. *Projected areas (a), perimeters (b), roundness values (c) and cell number (d) for hMSCs adhering on POEGMA-FN brushes presenting different thicknesses (25 nm, 45 nm, 65 nm).*

6.2.3 Cell adhesion mechanism

Immunofluorescence microscopy allowed the investigation of focal adhesion (FA) formation upon cell attachment on POEGMA-FN brushes with different thicknesses. Recently, Bermudez and coworkers proved that cells can sense ligand mobility and substrate lateral contractibility producing FA complexes presenting different areas and morphologies.[66] In general, the presence of clear FAs was recorded for cells adhering on all the different POEGMA-FN brush thicknesses studied. This indicated that the peptide ligand density presented on the different brushes was sufficient to offer strong contact points. In addition, the micrographs reported in Figure 6.11 showed that on the thinner POEGMA-FN layers, FA points could be found spreading over the whole cell membrane (Figure 6.13a). However, with increasing brush thickness, the FA points around the cell nuclei progressively disappeared while clear complexes were increasingly concentrated at the periphery of the spread membrane (Figure 6.13b-c). A similar behavior was observed by Klok et al. for 20nm POEGMA-RGD brush coatings with different EG side chain lengths.[67] In this last work, polymer brush-RGD layers presenting the shortest side chains, i.e. poly(2-hydroxyethyl methacrylate) (PHEMA), induced FA formation by vein endothelial cells (HUVECs) primarily at the periphery of the cell membranes. In contrast, HUVECs adhering on brushes with side chains made of longer monomer units, with 6 and 10 OEGs, showed FA formation concentrated towards the cell nuclei. This phenomenon was related to the higher flexibility by polymer graft-ligand conjugates presenting shorter side chains (as PHEMA) compared to the more rigid, laterally hindered POEGMAs.

In the present study brush-ligand conjugates presenting different lengths showed also different maximal lateral extension, as previously demonstrated by the LFM analysis on POEGMA-FN brushes with different thicknesses. Different extendibility of the ligands at the brush interface thus showed to induce diverse FA concentrations across membrane of adhering HMSCs. Namely, shorter POEGMA-FN brushes presenting a limited lateral mobility induced a uniform coverage of FA over the cell membrane. In

contrast, longer POEGMA-FN brush conjugates, more capable of being laterally extended, favored the formation of FA complexes towards the periphery of the cells, presumably along their spreading directions.

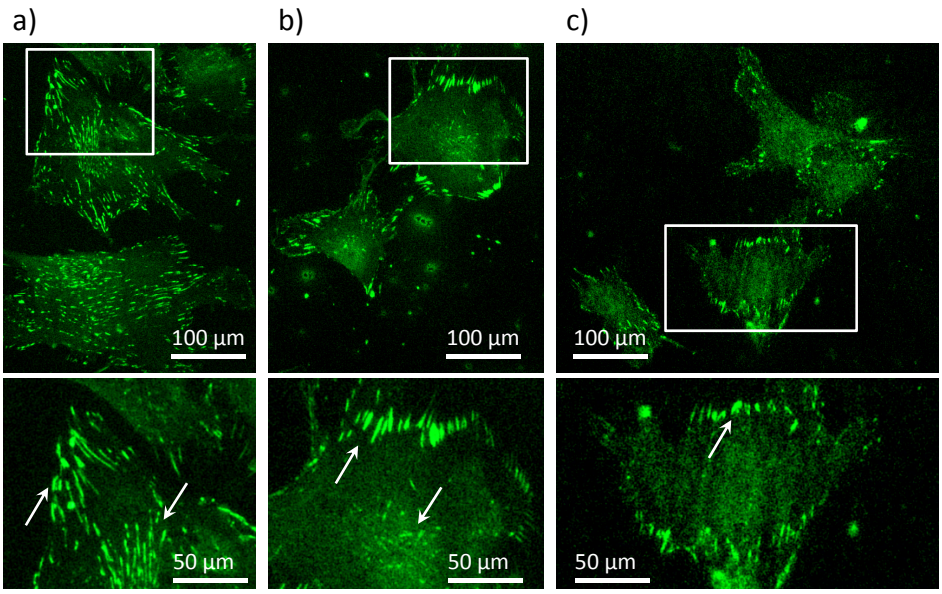

Figure 6.13. *Immunofluorescent micrographs of hMSCs visualizing the vinculin-associated FA points. PCL substrates covered by 25 nm (A), 45 nm (B) and 65 nm (C) POEGMA brushes.*

Besides the position of FA points, also their morphology showed to change depending on the brush length. In the fluorescent micrographs in Figure 6.12 it could be observed that FAs showed a larger and more elongated morphology when hMSCs adhered on shorter, 25 nm thick POEGMA-FN brushes. This observation was also confirmed by measuring the average FA areas and aspect ratios for the different samples studied (Figure 6.14a and 6.14b, respectively). FA areas decreased almost linearly with increasing brush length, while the aspect ratios reached a plateau value of around 2.7 for brush thickness above 45 nm. A similar morphological change of FA was already observed by Pelham et al.[27] who showed that elongated FA points were preferentially formed on more rigid substrates, while on more compliant supports a dot-like morphology was preferentially formed. In a similar manner, the dependence of FA shape on brush

thickness which was found in the present study could be presumably due to the different "effective" stiffness experienced by HMSCs on POEGMA-FN-coated PCL films presenting different thicknesses of interfacial brush layer. Namely, thinner brush films will not screen efficiently the stiffness of the underlying PCL substrate (which has a typical modulus of 400 MPa[73] inducing the formation of elongated FAs. On the contrary, thicker POEGMA-FN brushes more effectively hindered the PCL support exposing a more compliant brush at the interface. This effect by thick POEGMA-FN brushes triggered the formation of smaller and more circular FA complexes.

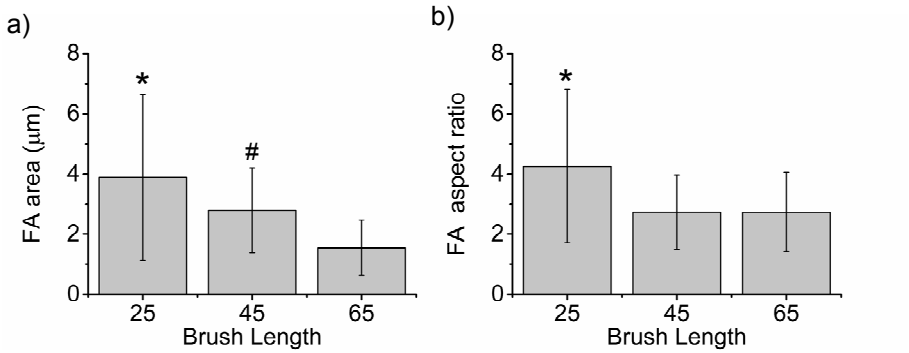

Figure 6.14. *Characterization of FA in cells on different POEGMA brush lengths. (a) Average FA area and (b) average FA aspect ratio. * and # denotes statistical significant differences between the assigned and the non-assigned topologies ($p < 0.05$) ($n = 50$).*

6.3 Conclusions

In this Chapter the effect on the adhesion of adult bone marrow-derived hMSCs of the grafting density and the brush thickness by POEGMA brushes grafted on PCL substrates was studied. Unfunctionalized POEGMA brushes with low thicknesses (sub-20 nm) or low densities (0.035 chains/nm^2) were shown to allow hMSCs adhesion, while thicker (60 nm) or dense (0.341 chains/nm^2) layers showed cell-repulsive properties due to the efficient resistance by dense and long grafts against protein adsorption.

POEGMA brushes functionalized with FN units were subsequently fabricated presenting a gradient in brush thickness. Despite the different grafted-chain lengths

across the gradient samples, the chemisorption of FN ligands was found nearly uniform on the whole brush platforms. Hence, irrespective of the brush-FN thickness, hMSCs adhered uniformly on the gradient and showed a similar morphology on both thin and thick brush supports. In contrast, differences in FA formation and morphologies were related to a variation of both the lateral extendibility of brushes and the screening of the underlying PCL substrate as a function of brush thickness. Longer chain-FN conjugates organized in thicker brush films originated peripheral FA concentrations which presented a dot-like morphology due to the compliancy of brush interface. Shorter brush-FN films presenting limited lateral-chain bending induced a uniform spreading of FAs across the cell membrane, which additionally adopted elongated shapes due to the ineffective screening of the stiff, underlying PCL surface.

The results summarized in this Chapter thus highlighted how substrate coverage and chain flexibility by an hydrated brush could be effectively tuned by SI-ATRP. This tailored platforms in combination with FN- conjugation triggered the adhesion of hMSCs, which showed a brush structure-dependent adhesion mechanism. The controlled grafting of similar brush layers on scaffolds for tissue engineering is thus envisioned as an effective strategy not only to modulate the adhesion of stem cells but also to control their further differentiation and the integration of the support within the synthetic extra-cellular matrix.

6.4 Experimental section

Materials:

Oligo(ethylene glycol) methacrylate (OEGMA, Aldrich, Mn = 526 g/mol) was purified from hydrochinone inhibitors by passing it through a basic alumina column using dichloromethane (DCM, Biosolve) as an eluent. Afterwards DCM was removed under vacuum. Copper(I) chloride (CuCl, Aldrich, 98%) was purified by stirring in glacial acetic acid, filtering, and washing with ethanol three times, followed by drying in vacuum at room temperature overnight. Poly(ε-caprolactone) (PCL, Mn = 45 kDa) was obtained from Sigma. Copper(II) bromide (Sigma-Aldrich, ≥99%), methanol (Biosolve, absolute), isopropanol (iPA, Biosolve), ethylenediamine (EDA, Sigma-Aldrich, ≥99%), dry hexane (Acros, Extra Dry over

Molecular Sieve, 97%), N,N-Dimethylformamide (DMF, Acros, Extra Dry over Molecular Sieve, 99,8%), pyridine (Sigma-Aldrich, anhydrous, 99,8%), 2,2'-bipyridil (BiPy, Sigma-Aldrich, ≥99%), 2-bromoisobutyryl xbromide (BIBB, Aldrich, 98%), 1-Bromocarbonyl-1-methylethyl acetate (BMA), Ethylenediaminetetraacetic acid disodium salt dihydrate (EDTA, Sigma, 99%), 4-dimethylaminopyridine (DMAP, Sigma-Aldrich, ≥99%), N,N´-disuccinimidyl carbonate (DSC, Sigma-Aldrich, 98%), triethylamine (Sigma-Aldrich, ≥99%), and fibronectin (Invitrogen) were used as received. All water used in the experiments was Millipore Milli-Q grade. The human mesenchymal stem cells (hMSCs) were used for the cell culture and were obtained from Donor 249 from the hospital. Basic cell culture media was prepared by adding to a α-MEM cell medium (Invitrogen), 10 v/v% of Fetal Bovine Serum (FBS), 2 mM of L-Glutamine, 100 U/mL of penicillin, 100 µg/mL of streptomycin, and 0.2 mM of ascorbic acid. All the mentioned components were obtained from Invitrogen. Furthermore, Invitrogen provided phosphate buffered saline (PBS), bovine serum albumin (BSA), trypsin, 4',6-diamidino-2- phenylindole (DAPI), rhodamine phalloidin. Monoclonal Anti-Vinculin−FITC antibody was purchased from Sigma-Aldrich.

Activation of the polymer films:

PCL films were spin coated (2000 rpm for 1 minute) onto cleaned silicon substrates from a chloroform solution (1 wt%). The spin coated PCL films were subsequently immersed into a solution of 5 mM ethylenediamine (EDA) in isopropanol (iPA). The reaction was allowed to proceed for 10 minutes under room temperature conditions. Samples were then rinsed with ice-cold water and subsequently rinsed with water at room temperature, then dried in a stream of nitrogen. The aminated PCL films were immersed into 10 ml of dry hexane and 100 µL of dry pyridine, to which 2-bromoisobutyryl bromide (BIBB) and 1-Bromocarbonyl-1-methylethyl acetate (BMA) in a predetermined ratio were added dropwise. The reaction mixture was gently stirred for 1 hours at room temperature to produce the 2-bromoisobutyryl-immobilized PCL surface (the PCL-Br surface). The PCL-Br substrate was then washed repeatedly with a methanol/water (1/1, v/v) mixture and dried under a stream of nitrogen.

Atom transfer radical polymerization of OEGMA:

Purified OEGMA monomer (5 g, 9.5 mmol) and 2,2'bipyridine (81.7 mg, 0.52 mmol) were added to a water (5ml) and methanol (1,26ml) mixture. The solution was purged with nitrogen for 30 min. CuCl (18.75 mg, 0.19 mmol) and CuBr2 (2 mg, 0.009 mmol) were added into another reaction flask and also flushed with nitrogen. Monomer, ligand and catalyst were then combined and stirred for another 30 minutes to facilitate the formation of the organometallic complex. This solution was then transferred into the flasks containing the activated PCL substrates. The flasks were sealed with rubber septa and kept at room temperature under nitrogen. After reaching the desired reaction time of 60 minutes, the substrates were removed from the polymerization solution, exhaustively rinsed with water to remove any unreacted and not surface tethered substances and subsequently dried in a stream of nitrogen. Afterwards the samples were washed with a 0.1M EDTA solution overnight to extract the copper from the polymer brushes.

Functionalization of OEGMA brushes with fibronectin (FN):

First the POEGMA layer was activated by placing the samples in a dry DMF solution containing 0.2 mM of DSC and DMAP. Subsequently the samples were incubated in a 0.1 mM FN solution overnight in order to covalently couple the FN to the polymer brush.

Ellipsometry:

Thickness measurements were performed using a variable angle spectroscopic ellipsometer (VASE) (J.A. Woollam Co., Lincoln, NE, USA) in the range from 1 to 4.5 eV with a step size of 0.1eV; this corresponds to a wavelength range of 275–1240 nm. The measurements were performed at three different incident angles, namely 65°, 70° and 75°. Measurements in water were performed in a liquid cell containing two windows at a fixed angle of incidence of $\theta = 63°$. A third window enabled alignment of the sample at normal incidence as well as allowing visual inspection of the sample during in situ experiments. The dry thickness of the gradient samples was measured at equal distant positions (5 mm) along the sample. The ellipsometry spectra, i.e. Ψ and Δ as a function of wavelength, were analyzed using the software package *CompleteEASE* (Woollam), employing the tabulated dielectric functions for both silicon and silicon oxide as the substrate. A

standard Cauchy model was employed to analyze the thickness of the spincoated PCL, and the total thickness of the collapsed POEGMA brush layer and PCL. Subtracting the PCL layer thickness before polymerization, from the total thickness after polymerization resulted in the POEGMA thickness. The swollen thickness was modeled using a graded Cauchy model for the POEGMA layer on top of a fitted PCL layer.

XPS:

A Quantera SXM scanning XPS microprobe (Physical Electronics, Chanhassen, MN, USA) using a Al Kα, monochromatic X-ray at 1486.6 eV was used to measure the atomic composition of the surfaces of POEGMA brushes with or without functionalization with FN. The surface coverage of FN (σ_{FN}) was calculated according to:

$$\sigma_{FN} = \rho\, h\, r_{N/C,\, sample} / r_{N/C,\, FN} \qquad (6.3)$$

where ρ is the density (1 g/cm^3), h the sampling depth of XPS (7.5 nm)[65] and r is the nitrogen to carbon ratio measured for our samples and for pure FN (0.270)[74].

Cell culture and cell imaging:

Human mesenchymal stem cells were cultured at 37°C in a humidified atmosphere of 5% carbon dioxide, using as culture medium α-MEM supplemented with 10 v/v % FBS, 2 mM L-Glutamine, 1 mM sodium pyruvate, 100 U/mL of penicillin and 100 µg/mL of streptomycin. The cells were seeded at a density of 2,000 cells/cm2 on PCL substrates, unmodified and modified with POEGMA brushes. After 4 hours, the substrates were washed twice with PBS and fixed with a 3.7 v/v % formaldehyde solution in PBS for 10 minutes at room temperature. Next, the samples were washed two or more times with PBS containing 1 w/v % bovine serum albumin (BSA). Cell membrane was permeabilized by treating the samples with 0.1 v/v % Triton X-100 solution in PBS-BSA after which the specimens were washed again with PBS-BSA. The FA points were stained overnight at 0°C using a monoclonal Anti-Vinculin−FITC antibody diluted 1:400 in a PBS-BSA solution. Cell nuclei were stained with DAPI diluted 1:100 and cell cytoskeleton was stained with

a phalloidin-rhodamine diluted 1:50 in a PBS-BSA solution for 30 minutes at room temperature. Micrographs were taken using a Nikon fluorescent microscope Eclipse E600. In order to use the samples for optical and AFM imaging, the substrates were dehydrated by submerging the samples into a solution for 10 minutes containing an increasing amount of ethanol. Optical imaging was performed on a BX60 optical microscope (Olympus, Tokyo, Japan). For determining the cell shape parameters area and perimeter, Cell^D software (Olympus Soft Imaging Solutions, Münster, Germany) was used. The Roundness (RN) was subsequently calculated using:

$$RN = \text{Perimeter}/(4\pi \times \text{Area})^{0.5} \qquad (6.4)$$

The FA shape parameters area and aspect ratio were determined using ImageJ software version 1.47v (National Institutes of Health, USA).

Atomic force microscopy:

Colloidal Probe Microscopy (CPM): Normal-force and friction measurements between a silica microsphere and POEGMA-FN brush films were carried out in Milli-Q water using an AFM (MFP3D, Asylum Research, Santa Barbara, USA) equipped with a liquid cell. The normal spring constant of the Au-coated tipless cantilever (NSC-12, Mikromash, Estonia) was measured by the thermal-noise method[75] and the torsional spring constant was measured according to Sader's method.[76] Both normal and torsional spring constants of the cantilever were measured before attaching the colloidal microsphere. A silica microparticle (EKA chemicals AB, Kromasil R) was glued with UV-curable glue (Norland optical adhesive 63) to the end of the tipless cantilever by means of a home-built micromanipulator, to be further used for colloidal probe microscopy.[77]

6.5 References

1 Mikos, A. G.; Herring, S. W.; Ochareon, P.; Elisseeff, J.; Lu, H. H.; Kandel, R.; Schoen, F. J.; Toner, M.; Mooney, D.; Atala, A.; Van Dyke, M. E.; Kaplan, D.; Vunjak-Novakovic, G., *Tissue Engineering* **2006,** *12,* 3307-3339.

2 Lutolf, M. P.; Hubbell, J. A., *Nat Biotech* **2005,** *23,* 47-55.

3 Burdick, J. A.; Khademhosseini, A.; Langer, R., *Langmuir* **2004,** *20,* 5153-5156.

4 He, J.; Du, Y.; Villa-Uribe, J. L.; Hwang, C.; Li, D.; Khademhosseini, A., *Advanced Functional Materials* **2010,** *20,* 131-137.

5 DeLong, S. A.; Moon, J. J.; West, J. L., *Biomaterials* **2005,** *26,* 3227-3234.

6 DeLong, S. A.; Gobin, A. S.; West, J. L., *Journal of Controlled Release* **2005,** *109,* 139-148.

7 Kyburz, K. A.; Anseth, K. S., *Acta Biomaterialia* **2013,** *9,* 6381-6392.

8 Du, F.; Wang, H.; Zhao, W.; Li, D.; Kong, D.; Yang, J.; Zhang, Y., *Biomaterials* **2012,** *33,* 762-770.

9 Min, H. K.; Oh, S. H.; Lee, J. M.; Im, G. I.; Lee, J. H., *Acta Biomaterialia* **2014,** *10,* 1272-1279.

10 Kim, T.; Oh, S.; Kwon, E.; Lee, J.; Lee, J., *Macromol. Res.* **2013,** *21,* 878-885.

11 Trappmann, B.; Gautrot, J. E.; Connelly, J. T.; Strange, D. G. T.; Li, Y.; Oyen, M. L.; Cohen Stuart, M. A.; Boehm, H.; Li, B.; Vogel, V.; Spatz, J. P.; Watt, F. M.; Huck, W. T. S., *Nat Mater* **2012,** *11,* 642-649.

12 Engler, A. J.; Sen, S.; Sweeney, H. L.; Discher, D. E., *Cell* **2006,** *126,* 677-689.

13 Finlay, J. A.; Callow, M. E.; Ista, L. K.; Lopez, G. P.; Callow, J. A., *Integrative and Comparative Biology* **2002,** *42,* 1116-1122.

14 Lee, J. H.; Khang, G.; Lee, J. W.; Lee, H. B., *Journal of Colloid and Interface Science* **1998,** *205,* 323-330.

15 Lee, J. H.; Lee, J. W.; Khang, G.; Lee, H. B., *Biomaterials* **1997,** *18,* 351-358.

16 Bhat, R. R.; Chaney, B. N.; Rowley, J.; Liebmann-Vinson, A.; Genzer, J., *Advanced Materials* **2005,** *17,* 2802-2807.

17 Bhat, R. R.; Tomlinson, M. R.; Genzer, J., *Journal of Polymer Science Part B-Polymer Physics* **2005,** *43,* 3384-3394.

18 Smith, J. T.; Elkin, J. T.; Reichert, W. M., *Experimental Cell Research* **2006,** *312,* 2424-2432.

19 Smith, J. T.; Tomfohr, J. K.; Wells, M. C.; Beebe Jr, T. P.; Kepler, T. B.; Reichert, W. M., *Langmuir* **2004,** *20,* 8279-8286.

20 Tse, J. R.; Engler, A. J., *PLoS ONE* **2011,** *6,* 1-9.

21 Vincent, L. G.; Choi, Y. S.; Alonso-Latorre, B.; del Álamo, J. C.; Engler, A. J., *Biotechnology Journal* **2013,** *8,* 472-484.

22 Isenberg, B. C.; DiMilla, P. A.; Walker, M.; Kim, S.; Wong, J. Y., *Biophysical Journal* **2009,** *97,* 1313-1322.

23 Marklein, R. A.; Burdick, J. A., *Soft Matter* **2010,** *6,* 136-143.

24 Zaari, N.; Rajagopalan, P.; Kim, S. K.; Engler, A. J.; Wong, J. Y., *Advanced Materials* **2004,** *16,* 2133-2137.

25 Carr, L. R.; Krause, J. E.; Ella-Menye, J. R.; Jiang, S., *Biomaterials* **2011,** *32,* 8456-8461.

26 Piraino, F.; Camci-Unal, G.; Hancock, M. J.; Rasponi, M.; Khademhosseini, A., *Lab on a Chip - Miniaturisation for Chemistry and Biology* **2012,** *12,* 659-661.

27 Pelham, R. J.; Wang, Y.-l., *Proceedings of the National Academy of Sciences of the United States of America* **1997,** *94,* 13661-13665.

28 Wang, H. B.; Dembo, M.; Wang, Y. L., *American Journal of Physiology - Cell Physiology* **2000,** *279,* C1345-C1350.

29 Engler, A.; Bacakova, L.; Newman, C.; Hategan, A.; Griffin, M.; Discher, D., *Biophysical Journal* **2004,** *86,* 617-628.

30 Thomas, T. W.; DiMilla, P. A., *Med. Biol. Eng. Comput.* **2000,** *38,* 360-370.

31 Genes, N. G.; Rowley, J. A.; Mooney, D. J.; Bonassar, L. J., *Archives of Biochemistry and Biophysics* **2004,** *422,* 161-167.

32 Lo, C. M.; Wang, H. B.; Dembo, M.; Wang, Y. L., *Biophysical Journal* **2000,** *79,* 144-152.

33 Wong, J. Y.; Velasco, A.; Rajagopalan, P.; Pham, Q., *Langmuir* **2003,** *19,* 1908-1913.

34 Gray, D. S.; Tien, J.; Chen, C. S., *Journal of Biomedical Materials Research - Part A* **2003,** *66,* 605-614.

35 Geiger, B.; Spatz, J. P.; Bershadsky, A. D., *Nature Reviews Molecular Cell Biology* **2009,** *10,* 21-33.

36 Prager-Khoutorsky, M.; Lichtenstein, A.; Krishnan, R.; Rajendran, K.; Mayo, A.; Kam, Z.; Geiger, B.; Bershadsky, A. D., *Nat Cell Biol* **2011,** *13,* 1457-1465.

37 Mitra, S. K.; Hanson, D. A.; Schlaepfer, D. D., *Nat Rev Mol Cell Biol* **2005,** *6,* 56-68.

38 Fraley, S. I.; Feng, Y.; Krishnamurthy, R.; Kim, D. H.; Celedon, A.; Longmore, G. D.; Wirtz, D., *Nature Cell Biology* **2010,** *12,* 598-604.

39 Cukierman, E.; Pankov, R.; Yamada, K. M., *Current Opinion in Cell Biology* **2002,** *14,* 633-640.

40 Wozniak, M. A.; Modzelewska, K.; Kwong, L.; Keely, P. J., *Biochimica et Biophysica Acta (BBA) - Molecular Cell Research* **2004,** *1692,* 103-119.

41 Discher, D. E.; Janmey, P.; Wang, Y. L., *Science* **2005,** *310,* 1139-1143.

42 Goffin, J. M.; Pittet, P.; Csucs, G.; Lussi, J. W.; Meister, J.-J.; Hinz, B., *The Journal of Cell Biology* **2006,** *172,* 259-268.

43 Raynor, J. E.; Capadona, J. R.; Collard, D. M.; Petrie, T. A.; Garcia, A. J., *Biointerphases* **2009,** *4,* FA3-FA16.

44 Milner, S. T., *Science* **1991,** *251,* 905-914.

45 Ren, T.; Mao, Z.; Guo, J.; Gao, C., *Langmuir* **2013,** *29,* 6386-6395.

46 Mei, Y.; Elliott, J. T.; Smith, J. R.; Langenbach, K. J.; Wu, T.; Xu, C.; Beers, K. L.; Amis, E. J.; Henderson, L., *Journal of Biomedical Materials Research Part A* **2006,** *79A,* 974-988.

47 Mei, Y.; Wu, T.; Xu, C.; Langenbach, K. J.; Elliott, J. T.; Vogt, B. D.; Beers, K. L.; Amis, E. J.; Washburn, N. R., *Langmuir* **2005,** *21,* 12309-12314.

48 Sui, X.; Chen, Q.; Hempenius, M. A.; Vancso, G. J., *Small* **2011,** *7,* 1440-1447.

49 Genzer, J., *Annual Review of Materials Research* **2012,** *42,* 435-468.

50 Morgenthaler, S.; Zink, C.; Spencer, N. D., *Soft Matter* **2008,** *4,* 419-434.

51 Wu, T.; Efimenko, K.; Vlček, P.; Šubr, V.; Genzer, J., *Macromolecules* **2003,** *36,* 2448-2453.

52 Tomlinson, M. R.; Genzer, J., *Macromolecules* **2003,** *36,* 3449-3451.

53 Matyjaszewski, K.; Xia, J. H., *Chemical Reviews* **2001,** *101,* 2921-2990.

54 Barbey, R.; Lavanant, L.; Paripovic, D.; Schuwer, N.; Sugnaux, C.; Tugulu, S.; Klok, H. A., *Chemical Reviews* **2009,** *109,* 5437-5527.

55 Edmondson, S.; Osborne, V. L.; Huck, W. T. S., *Chemical Society Reviews* **2004,** *33,* 14-22.

56 Li, L.; Zhu, Y.; Li, B.; Gao, C., *Langmuir* **2008,** *24,* 13632-13639.

57 Wu, T.; Gong, P.; Szleifer, I.; Vlček, P.; Šubr, V.; Genzer, J., *Macromolecules* **2007,** *40,* 8756-8764.

58 Ren, T.; Yu, S.; Mao, Z.; Moya, S. E.; Han, L.; Gao, C., *Biomacromolecules* **2014,** *15,* 2256-2264.

59 Sui, X.; Di Luca, A.; Klein Gunnewiek, M.; Kooij, E. S.; van Blitterswijk, C. A.; Moroni, L.; Hempenius, M. A.; Vancso, G. J., *Australian Journal of Chemistry* **2011,** *64,* 1259-1266.

60 Wu, T.; Efimenko, K.; Genzer, J., *Journal of the American Chemical Society* **2002,** *124,* 9394-9395.

61 Singh, N.; Cui, X.; Boland, T.; Husson, S. M., *Biomaterials* **2007,** *28,* 763-771.

62 Ma, H.; Hyun, J.; Stiller, P.; Chilkoti, A., *Advanced Materials* **2004,** *16,* 338-341.

63 Chen, S.; Li, L.; Zhao, C.; Zheng, J., *Polymer* **2010,** *51,* 5283-5293.

64 Navarro, M.; Benetti, E. M.; Zapotoczny, S.; Planell, J. A.; Vancso, G. J., *Langmuir* **2008,** *24,* 10996-11002.

65 Tan, K. L.; Woon, L. L.; Wong, H. K.; Kang, E. T.; Neoh, K. G., *Macromolecules* **1993,** *26,* 2832-2836.

66 Kourouklis, A. P.; Lerum, R. V.; Bermudez, H., *Biomaterials* **2014,** *35,* 4827-4834.

67 Tugulu, S.; Silacci, P.; Stergiopulos, N.; Klok, H.-A., *Biomaterials* **2007,** *28,* 2536-2546.

68 Pei, J.; Hall, H.; Spencer, N. D., *Biomaterials* **2011,** *32,* 8968-8978.

69 Li, A.; Ramakrishna, S. N.; Schwarz, T.; Benetti, E. M.; Spencer, N. D., *ACS Applied Materials & Interfaces* **2013,** *5,* 4913-4920.

70 Balaban, N. Q.; Schwarz, U. S.; Riveline, D.; Goichberg, P.; Tzur, G.; Sabanay, I.; Mahalu, D.; Safran, S.; Bershadsky, A.; Addadi, L.; Geiger, B., *Nat Cell Biol* **2001,** *3,* 466-472.

71 Cavalcanti-Adam, E. A.; Micoulet, A.; Blümmel, J.; Auernheimer, J.; Kessler, H.; Spatz, J. P., *European Journal of Cell Biology* **2006,** *85,* 219-224.

72 Arnold, M.; Cavalcanti-Adam, E. A.; Glass, R.; Blümmel, J.; Eck, W.; Kantlehner, M.; Kessler, H.; Spatz, J. P., *ChemPhysChem* **2004,** *5,* 383-388.

73 Engelberg, I.; Kohn, J., *Biomaterials* **1991,** *12,* 292-304.

74 Galtayries, A.; Warocquier-Clérout, R.; Nagel, M. D.; Marcus, P., *Surface and Interface Analysis* **2006,** *38,* 186-190.

75 Butt, H. J.; Jaschke, M., *Nanotechnology* **1995,** *6,* 1-7.

76 Green, C. P.; Lioe, H.; Cleveland, J. P.; Proksch, R.; Mulvaney, P.; Sader, J. E., *Review of Scientific Instruments* **2004,** *75,* 1988-1996.

77 Ducker, W. A.; Senden, T. J.; Pashley, R. M., *Nature* **1991,** *353,* 239-241.

Creeping proteins in microporous structures: Polymer brush-assisted fabrication of 3D gradients

In this Chapter, the fabrication of functional scaffolds for the controlled manipulation of stem cells is presented. These synthetic ECMs feature 3D gradients of proteins within microporous, biodegradable TE supports and they are obtained by a combination of controlled fabrication, SI-ATRP and protein coupling via solution wetting. The 3D regularly layered supports are manufactured by rapid prototyping of poly-ε-caprolactone (PCL). Subsequently, a uniform coating of the scaffold surface with "grafted-from", poly(oligo(ethylene glycol) methacrylate (POEGMA) brushes is used for the covalent immobilization of different protein species. A 3D gradient fabrication process makes use of surface energy and capillary forces provided by the POEGMA coating, while applying proteins from their solutions inside the pores. Gradients of brush-supported fibronectin thus obtained permit the controlled immobilization of human mesenchymal stem cells (hMSCs) in spatially determined cultures. Additionally, the application of growth factors coupled to POEGMA-coated PCL scaffolds proved as an effective strategy to induce hMSCs differentiation within these 3D environments.

* This Chapter has been published in: M. Klein Gunnewiek, A. Di Luca, H.Z. Bollemaat, C.A. van Blitterswijk, G.J. Vancso, L. Moroni, E.M Benetti; *Advanced Healthcare Materials* **2015**, Accepted

7.1 Introduction

Recent research in tissue engineering and regenerative medicine is increasingly revolving around effective fabrication techniques to create functional scaffolds for cell manipulations. Specifically, 3D supports presenting temporal and spatial control over the exposure of protein cues are desirable as they would allow spatial control over cell behavior.[1-2] To achieve this objective, a number of methods have been proposed to create synthetic extra-cellular matrices (ECMs) with gradient-like chemical compositions, thus mimicking the continuous variation characteristic of natural ECM.

The production of biomolecular gradients on 2D supports was proven as an effective approach to spatially adjust cell adhesion, migration and proliferation on planar substrates.[3-7] Following the development of increasingly sophisticated 3D synthetic ECMs, diverse methodologies for the fabrication of protein gradients in 3D environments have been also proposed. These biomaterials are obtained by employing hydrogel-supports[8-11] and electrospun fibers[12-13] but they commonly require complicated multi-steps preparations without achieving spatial control of the biomolecules.

The simple exposure of 3D supports to different protein solutions with variable composition[14-15] consented the production of biomaterials showing a continuous variation of protein coverage but just along one main scaffold axis. Following such preparations, electrospun fibers with varying composition could be deposited on a movable stage while changing feed, in order to create (bio)chemical gradients along the horizontal or the vertical direction.

Protein gradients were alternatively fabricated within photo-crosslinked hydrogels by gradually or locally exposing different parts of the matrix to light[8-9], followed by bio-conjugation. Analogous mono-axial hydrogel-supported gradients were also successfully produced by electrochemically-controlled enzymatic polymerization[16].

Higher control over the compositional changes characterizing synthetic ECMs was accomplished via layer-by-layer[10] or “gradient maker”-assisted[17-19] fabrications. In these processes hydrogels presenting gradient compositions along their deposition/building direction were formed.[10, 20]

The above-mentioned methods yielding gradient compositions necessitated multiple processing steps and/or time-consuming chemical treatments. These drawbacks would render them unsuitable for clinical use where fast and low-cost manipulations to reproduce and directly apply scaffolds on patients are needed. In addition, these techniques supported the formation of mono- or bi-directional gradients, while the development of concentration changes in 3D still remained a challenge.

Synthetic supports which mimicked the multi-axial compositional gradients, characteristic of natural ECM *in vivo*, would be needed to reproduce the compositional diversity of tissue environments within simplified and easily accessible matrices. These supports could be applied not only as scaffolds for the regeneration of complex tissues, but also as 3D architectures for studying cells and bacteria adhesion and migration[9, 12, 16] in 3D environments.

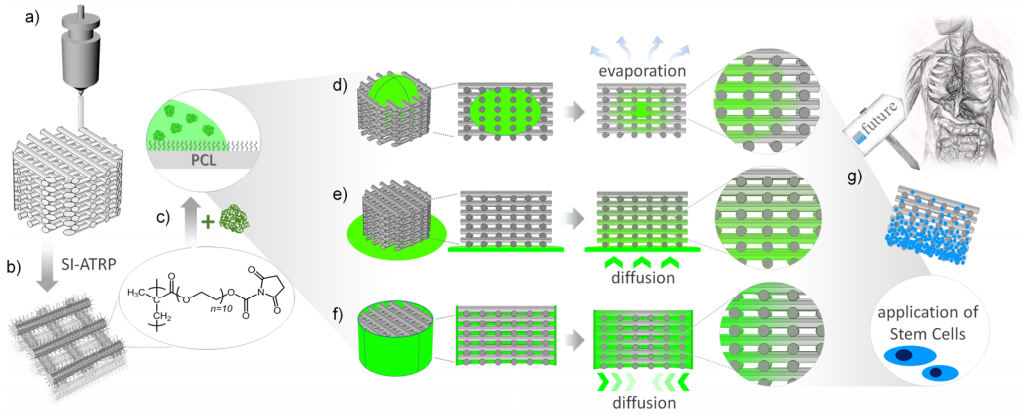

Scheme 7.1. *POEGMA-brush-assisted fabrication of 3D protein gradients within PCL scaffolds and application as platforms for stem cells immobilization. (a) fabrication of PCL microporous scaffolds by rapid prototyping; (b) SI-ATRP of OEGMA from the PCL fibers network and subsequent activation of hydroxyl side chains to form NHS esters; (c) conjugation of proteins at the brush interface by controlled diffusion of solutions within the 3D scaffolds. This last step is especially highlighted in (d), (e) and (f). Incorporation of microdroplets of protein solutions and subsequent solvent evaporation generated radial concentration gradients on brushes (d). Controlled diffusion from a soaked paper reservoir allowed the formation of axial protein concentration gradients (e). Wrapped reservoirs enabled protein diffusion from the lateral walls of the scaffolds and the consequent fabrication of radial protein gradient (f) developing oppositely to (d). The protein-functionalized scaffolds were finally applied for the spatially controlled immobilization of hMSCs (g).*

Triggered by this challenge, a novel fabrication strategy will be introduced which features a practical and affordable construction of 3D ECMs that display multi-directional variations of (bio)chemical environments. Specifically, rapid prototyping (RP)[21-23] was coupled to surface modification strategies based on surface-initiated polymerizations (SIP)[24-25] in order to fabricate microporous and highly-functional 3D architectures which could be subsequently locally decorated with different types of biomolecules.

7.2 Results and discussion

7.2.1 Fabrication of 3D protein gradients

PCL scaffolds characterized by a regularly layered network of microfibers (Scheme 7.1a) were modified by surface-initiated atom transfer radical polymerization (SI-ATRP) of POEGMA (Scheme 7.1b). The so-formed, sub-100 nm POEGMA brushes uniformly covered the scaffold surface and allowed protein coupling at the exposed hydroxyl functions of the grafted polymer[26-27] (Scheme 7.1c). In addition, the biopassive character of POEGMA brushes[28-30] assured robust covalent linkage of cues avoiding any further unspecific contamination of the matrix by physisorption of other biomolecules or bacteria attachment. The formation of protein gradients by surface conjugation was accomplished exploiting the physico-chemical properties of the hydrophilic brush in combination with the microporous structure of the PCL scaffolds. Uniform coverage of PCL by hydrophilic POEGMA brush caused a marked increase in wettability of the support (water contact angle (CA) varied from 73° to 45 ± 3° as shown in Table 7.1).

Table 7.1. Contact angle values for pure and POEGMA-modified PCL spin-coated films on silicon wafers.

	Average contact angle [°]
PCL	73 ± 3
ATRP initiator modified PCL	64 ± 3
POEGMA modified PCL	45 ± 3

This phenomenon reflected a substantial increase of surface energy within the 3D scaffold.[31-32] Hence, the interplay between high surface energy-driven wetting by the POEGMA brush and capillary forces within the microporous supports promoted the diffusion of aqueous solutions into the matrix (as highlighted in Scheme 7.1d and in the light microscope images shown in Figure 7.1).

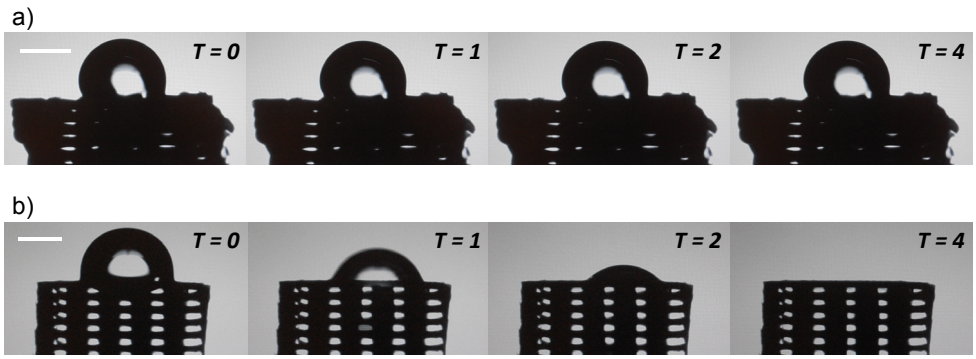

Figure 7.1. *Snapshots taken at 1 and 2 seconds intervals of 4 µl water drops placed on top of pure PCL (a) and POEGMA modified scaffolds (b). Scale bar is 1 mm.*

This simple process was exploited to incorporate protein solutions into the scaffolds and consequently couple proteins at the pre-activated brush (via NHS chemistry[33] as described in the Experimental Section). Diffusion of protein solution micro-droplets (Scheme 7.1d) and subsequent concentration of the solutions towards the inner core of the structure finally induced a radial variation of protein surface concentration (Figure 7.2). Alternatively, protein solutions could be made to diffuse from soaked paper sheets used as solution reservoir put into close contact with the scaffolds (Scheme 7.1e and Figure 7.3). In both cases, simple process parameters like microdroplets volume and diffusion time from external reservoirs allowed spatial 3D control over the concentration of the coupled proteins.

Figure 7.2a and 7.2c shows radial 3D gradients of fluorescently labeled bovine serum (BSA) attached to PCL-POEGMA scaffolds by incorporation of protein solution microdroplets and subsequent bio-conjugation. Having calculated through Equation 1 the inner volume of each scaffold as 25 µl, different volumes of microdroplets were applied in order to prepare radial gradients, yielding gradient protein coverages. Fluorescent microscopy of the cross-sectioned 3D structures

revealed the protein surface concentration profiles within the scaffolds. As shown in Figure 7.2a-b, gradient formation from 2 µl protein solutions produced a radial gradient with a high concentration of proteins in the inner core and a steady decrease of coverage after around 250 µm from the center of the scaffolds. Increase of the microdroplet volume to 10 µl produced a more uniform protein coverage through the supports with just the outer walls remaining unfunctionalized (Figure 7.2c-d). Although the volume used for these depositions was less than half of the total inner volume of the 3D scaffolds, fast diffusion of protein solutions along the hydrophilic brush-coated fibers most likely smoothened the profile of the protein gradient across the 3D structures.

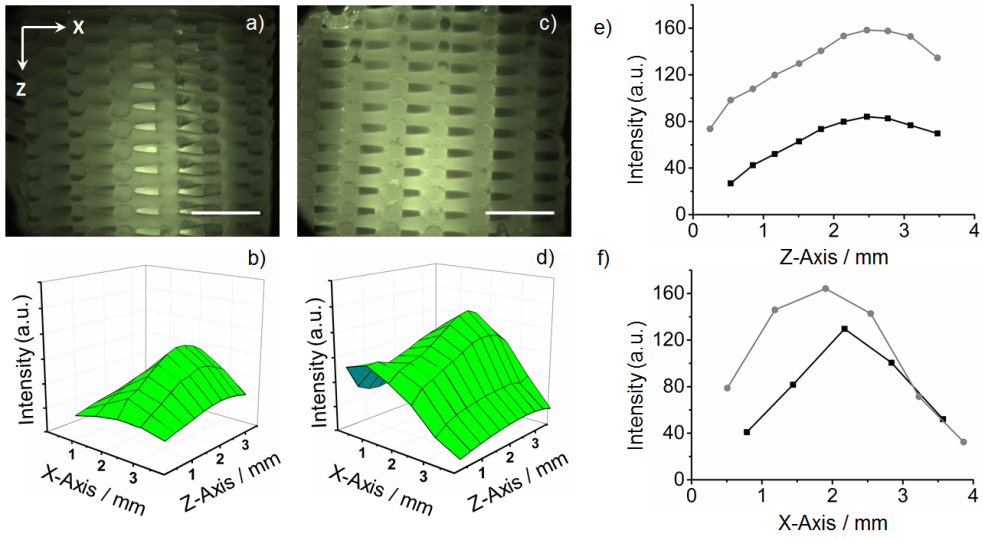

Figure 7.2. *Fluorescent micrographs (a,c) and the corresponding 3D intensity profile (b,d) of the vertical cross-section of PCL-POEGMA scaffolds functionalized with BSA-FITC using 2 µl (a,b), and 10 µl (c,d) microdroplets. Intensity profiles along the z-axis (e) and the x-axis (f) of the scaffold: ■) 2 µl, and ●) 10 µl. Scale bar is 1 mm.*

Brush-supported protein gradients developing axially along the 3D scaffold (from one external side towards the center) were obtained by applying a porous paper sheet as solution reservoir and allowing the protein medium diffuse by capillary forces (Scheme 7.1e, Figure 7.3). Slow wetting of brush-coated fibers

enabled the adjustment of the protein gradient profile as a function of the diffusion time (and thus bio-conjugation time at the POEGMA brush surface).

The fluorescent images in Figure 7.3 showed different axial gradient profiles obtained by varying the diffusion/bio-conjugation time. Both 3D and the 2D intensity plots reconstructed from the fluorescence micrographs showed that, after 30 minutes of diffusion, proteins were mainly immobilized within 700 μm from the base of the scaffold (Figure 7.3a-b). Following longer diffusion time, protein solutions covered larger volumes inside the scaffolds, homogenizing the protein coverage. After 60 minutes of diffusion (Figures 7.3c-d) proteins covered almost 1/3 of the distance across the scaffold main axis (Z axis in Figure 7.3g), keeping a rather uniform surface concentration along the X axis (Figure 7.4). After 120 minutes of diffusion the protein solutions completely wetted the inner structure of the scaffolds and consequently created a nearly linear gradient of protein coverage on the fibers (Figure 7.3e-f).

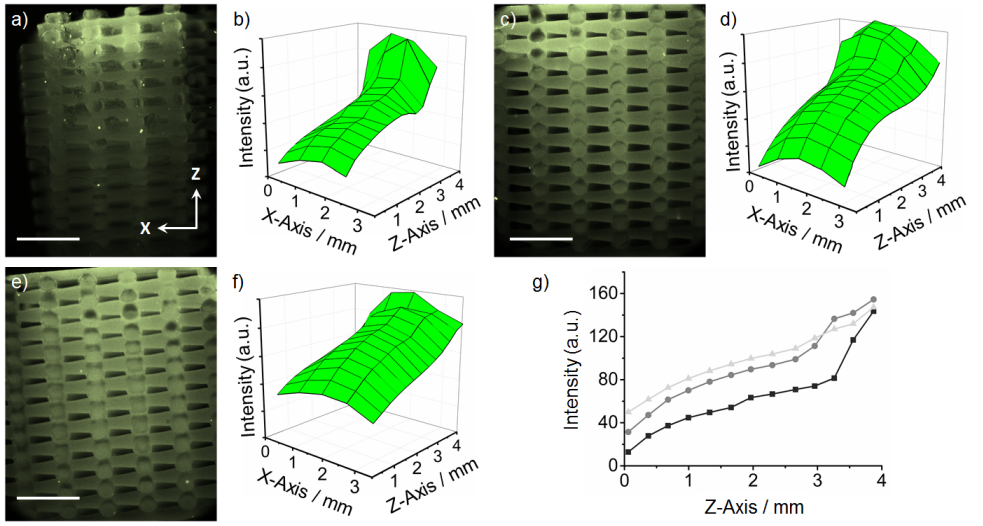

Figure 7.3. *Fluorescent micrographs (a,c,e) and the corresponding 3D intensity profiles (b,d,f) from the vertical cross-section of PCL-POEGMA scaffolds functionalized with BSA-FITC after 30 min (a,b), 60 min (c,d), and 120 min (e,f) of diffusion/functionalization times. Intensity profiles along the y-axis of the scaffolds (g) following: ■) 30 min., ●) 60 min., and ▲) 120 min of diffusion/functionalization times. Scale bar is 1 mm.*

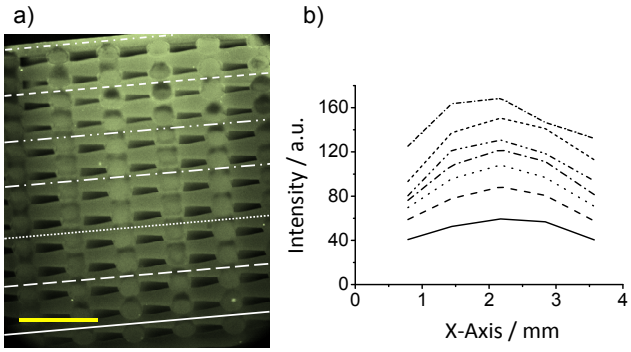

Figure 7.4. *(a) Fluorescent micrograph and (b) the corresponding 2D intensity profile along the x-axis at different positions along the z-axis from the vertical cross-section of a PCL-POEGMA scaffold functionalized with BSA-FITC. Scale bar is 1 mm.*

7.2.2 Multiple-protein gradients

The procedures used for the fabrication of single protein gradients were combined to produce double gradients of different protein species. After the formation of either a radial or an axial 3D distribution of proteins the scaffolds were not entirely covered by protein solutions. Consequently, unfunctionalized POEGMA brushes were still available for bio-conjugation on the unwetted areas within the 3D structure. Hence, a second protein solution could be additionally applied to produce a surface concentration gradient which developed in the opposite direction to the pre-existing one (as schematized in Scheme 7.1d-f). These “double” protein distributions are referred to as 3D radial and axial double gradients. In order to ease their analysis by fluorescent microscopy, two solutions of differently labeled BSA (FITC and Texas Red, named as protein A and B, respectively) were applied as representative of two different protein species. As shown in Figure 7.5a-d, a 3D radial double gradient of two different proteins was produced first incorporating a microdroplet of protein A solution within the POEGMA-PCL scaffold and subsequently wrapping around its outer surface a paper reservoir soaked with protein B. Alternatively, in order to fabricate a 3D axial double gradient of protein A and B, two different protein media were allowed to diffuse from two reservoirs placed in contact with each opposite “face” of the scaffold (Figure 7.5e-h).

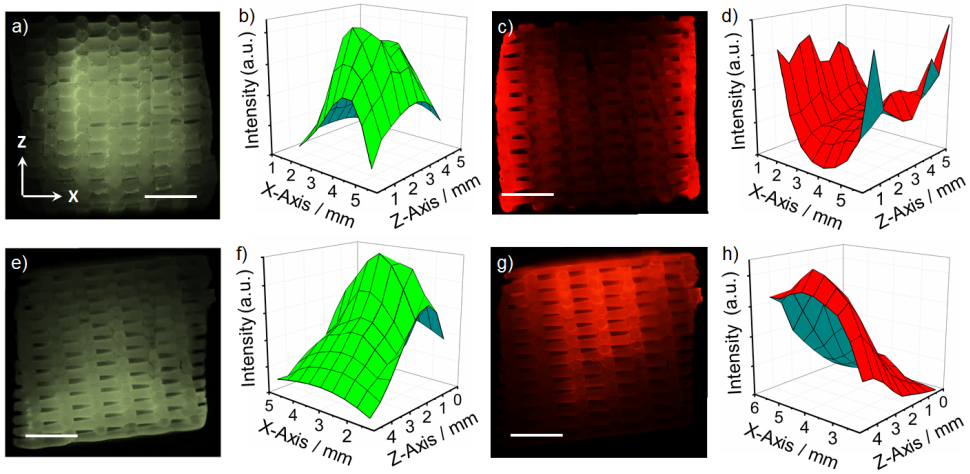

Figure 7.5. Double 3D gradients of proteins within POEGMA brush-coated microporous scaffolds. Fluorescent micrographs (a,c,e,g) and the corresponding intensity plots (b,d,f,h) of PCL-POEGMA scaffolds functionalized with BSA. Double gradients in BSA concentrations were fabricated both in the radial and axial directions; (a,b) inside-to-outside and (c,d) outside-to-inside; (e,f) bottom-to-top and (g,h) top-to-bottom. Scale bar is 1 mm.

As shown in Figures 7.5a and 7.5c and in the corresponding 3D intensity reconstructions from a typical functionalized scaffold, radial double gradients displayed continuous and interconnected variations of concentrations of proteins A and B. The radial double gradients typically presented a high concentration of protein A in the core of the scaffold, which decreased beyond around 1.5 mm towards the outer part of the scaffold (Figure 7.5b). Protein B concentrations, on the contrary, developed from the outer walls of the scaffold and showed high surface concentration within around 1 mm towards the interior of the support (Figure 7.5d). Axial double gradients (Figures 7.5e-h) showed a uniform and interconnected variation of the two proteins concentration across the main scaffold axis (Z axis in Figures 7.5f and 7.5h). In these cases, a well-pronounced concentration distribution of the two protein species along opposite directions was clearly showed.

7.2.3 3D gradients for controlled manipulation of stem cells

To prove the applicability of the proposed fabrications for cell manipulations both radial and axial 3D gradients were fabricated using fibronectin (FN) as a biological cue known to promote cell adhesion. Also in this case, brush coatings based on NHS-activated POEGMA were used as platforms for bio-conjugation and the successful linkage of FN was subsequently proven by X-ray photoelectron spectroscopy (XPS) as shown in the Chapter 5 (Figure 5.2). Following the controlled diffusion of FN solutions, functionalized scaffolds presenting a radial and an axial concentration gradient were subsequently incubated with hMSCs during 1 day. The adhered cells were subsequently stained using methylene blue and the scaffolds were sectioned along the appropriate axis in order to visualize their interior.

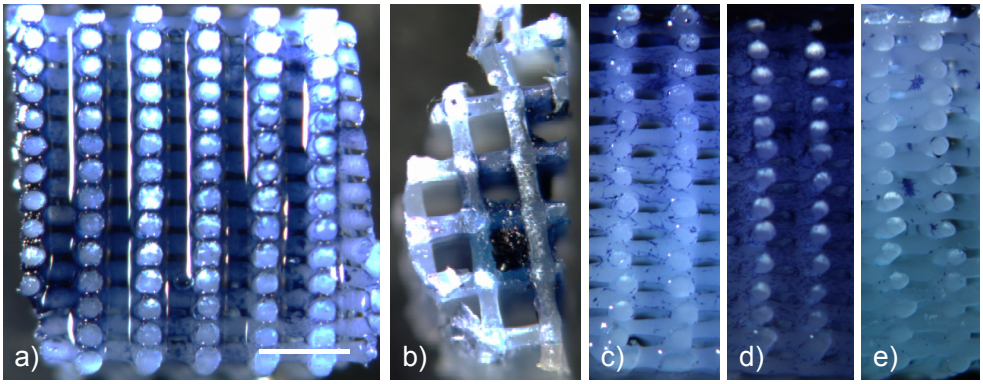

Figure 7.6. Optical images of methylene blue stained hMSCs adhering on PCL-POEGMA scaffolds. Optical images of methylene blue stained hMSCs adhering on PCL-POEGMA scaffolds. Radial gradient in FN concentration showing the vertical (a) and horizontal (b) cross-section; an axial gradient in FN concentration (c) a POEGMA coating fully covered by FN (d) and a bare POEGMA coating (e). Scale bar is 1 mm.

3D scaffolds presenting a radial gradient of FN from the core to the outer volume of the scaffolds showed higher number of cells in the interior of the structure, while at its periphery only few cells could be visualized (Figures 7.6a and 7.6b). In a similar way, axial gradients of brush-supported FN induced hMSCs adhesion mainly on one side of the scaffold, according to FN distribution and

following the gradient morphology (Figure 7.6c). Scaffolds completely functionalized with FN and “bare” POEGMA-coated supports were also seeded with hMSCs and were used as controls (Figures 7.6d and 7.6e). As shown in Figure 7.6d, the cells completely covered the uniformly functionalized scaffolds without showing any preferred area to settle. In comparison, brush-coated scaffold without fibronectin showed no cells due to the bio-passive nature of unfunctionalized POEGMA (Figure 7.6e).

The next goal was to obtain cell differentiation by functionalizing POEGMA-PCL 3D scaffolds with different growth factors (GFs), namely, bone morphogenic protein (BMP-2) and transforming growth factor (TGF- β3). To test if GFs were still active when covalently bound to the scaffold surface hMSCs were incubated on BMP-2-functionalized POEGMA-coated scaffolds. Cell differentiation was subsequently determined by measuring the alkaline phosphatase (ALP) levels following 10 days of culture. The results were reported in Figure 7.7. It can be seen that the ALP activity on BMP-2-functionalized POEGMA-PCL increased 4 times in comparison to ”bare” PCL supports, indicating that BMP-2-functionalized POEGMA-coated scaffolds efficiently stimulated hMSCs osteogenesis. As control experiment, cells did not adhere on unmodified POEGMA brushes and therefore no ALP activity was detected.

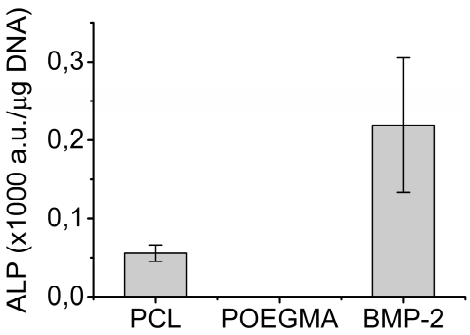

Figure 7.7. ALP activity of adhering hMSCS normalized by the total amount of DNA, measured on bare PCL scaffolds, scaffolds modified with POEGMA brushes, and scaffolds with BMP-2-functionalized POEGMA brush.

Reverse transcription polymerase chain reaction (RT-PCR) analysis was performed to investigate the expression of chondrogenic and osteogenic markers at the gene level between bare PCL scaffolds and GFs-functionalized POEGMA-PCL (Figure 7.8). BMP-2-modified POEGMA-PCL supports showed a 2 fold increase in RUNX2 expression and a 2.5 fold increase in osteocalcin (OCN) expression when compared to bare PCL (Figure 7.8a). For TGF-β3-modified POEGMA-PCL, the expression of SOX9 only increased 1.5 times in comparison to bare PCL supports. However, the ACAN expression showed a 4 times increase on TGF-β3-modified POEGMA-PCL scaffolds (Figure 7.8b). All these results proved that bio-conjugation on POEGMA-coated PCL scaffolds successfully induced differentiation of hMSCs towards different tissue types. The combination of GFs coupling on POEGMA brushes and the fabrication of 3D protein gradients within the same supports will potentially trigger the formation of regenerated interfaces between different tissue types.

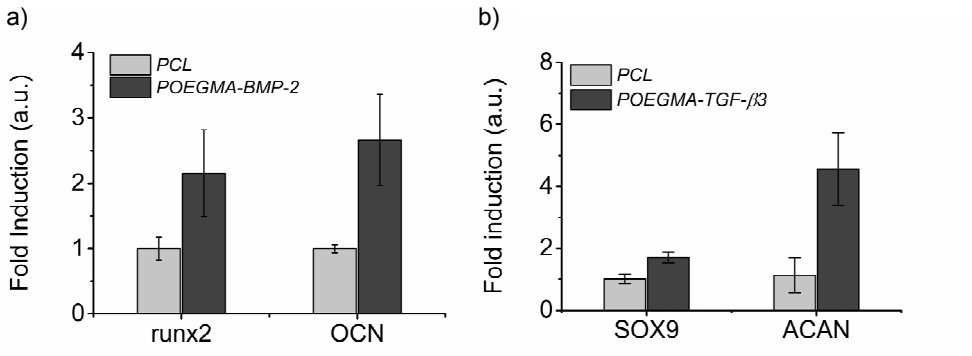

Figure 7.8. RT-PCR analysis after 10 days of hMSCs culture on POEGMA-PCL scaffolds functionalized with (a) BMP-2 and (b) TGF-β3. The osteogenic markers, runx2 and osteocalcin (OCN), were analyzed for BMP-2-functionalized scaffolds and the chondrogenic markers, Sox9 and Aggrecan (ACAN), for TGF-β3-functionalized scaffolds. The results were normalized against the response on bare PCL scaffolds.

7.3 Conclusions

All these results confirmed that the fabrication method proposed in this work represents a highly efficient strategy not only to create 3D protein gradients with designer morphologies, but also to spatially control cell adhesion within 3D scaffolds.

The use of hydrophilic and highly functional brush layers coupled to a structured support with controlled microporosity triggered diffusion and covalent immobilization of proteins from solutions. These processes could be easily manipulated by varying parameters as solution volumes and diffusion time within the 3D structures. This enabled the fabrication of 3D axial and radial protein gradients with tunable coverages.

PCL-POEGMA scaffolds with 3D protein gradients have the potential to be easily reproduced also in clinics since they do not require any inert environment or complicated chemistry. Brush-coated scaffolds could be simply incubated with the required proteins and directly applied to patients in or without the presence of cell preparations. The versatility of this technique would support the combination of multiple cues[34-38] that could eventually trigger cell adhesion, migration or differentiation, in a single 3D porous structure. The above-mentioned features made the method presented here a practical and affordable strategy to synthetically mimic natural ECMs and their 3D multidirectional diversity.

Finally, the application of GFs coupled to POEGMA-coated PCL scaffolds proved as an effective strategy to induce hMSCs differentiation within 3D environments. The envisioned application of multidirectional gradients of brush-supported GFs will have the potential to regenerate complex interfaces between different tissue types, such as bone and cartilage.

7.4 Experimental section

Materials:

Oligo(ethylene glycol) methacrylate (OEGMA, Aldrich, Mn = 526 g/mol) was purified from hydrochinone inhibitors by passing it through a basic alumina column using dichloromethane (DCM, Biosolve) as eluent. Afterwards DCM was removed under vacuum. Copper(I) chloride (CuCl, Aldrich, 98 %) was purified by stirring in glacial acetic acid, filtering, and washing with ethanol three times, followed by drying in vacuum at room temperature overnight. Poly(ε-caprolactone) (PCL, Mn = 45 kDa) was obtained from Sigma. Copper(II) bromide (Sigma-Aldrich, ≥99 %), methanol (Biosolve, absolute), isopropanol (iPA, Biosolve), ethylenediamine (EDA, Sigma-Aldrich, ≥99 %), dry hexane (Acros, Extra Dry over Molecular Sieve, 97 %), Dimethyl sulfoxide (DMSO, Acros, Extra Dry over Molecular Sieve, 99,7 %), pyridine (Sigma-Aldrich, anhydrous, 99,8 %), 2,2'-bipyridil (BiPy, Sigma-Aldrich, ≥99 %), 2-bromoisobutyryl bromide (BIBB, Aldrich, 98 %), Ethylenediaminetetraacetic acid disodium salt dihydrate (EDTA, Sigma, 99 %), 4-dimethylaminopyridine (DMAP, Sigma-Aldrich, ≥99 %), N,N´-disuccinimidyl carbonate (DSC, Sigma-Aldrich, 98 %), phosphate buffered saline (PBS) (Invitrogen) and triethylamine (Sigma-Aldrich, ≥99 %) were used as received. For brush surface modification fluorescein labeled bovine serum albumin (BSA), Texas Red labeled BSA and fibronectin (FN) were used as obtain from Invitrogen and diluted to the appropriate concentration. All water used in the experiments was Millipore Milli-Q grade. Colony-picked human mesenchymal stem cells hMSCs (male, age 22) were retrieved from the Institute of Regenerative Medicine (Temple, Texas). For cell culture Basic cell culture media was prepared by adding to a α-MEM cell medium (Invitrogen) 10 v/v % of Fetal Bovine Serum (FBS), 2 mM of L-Glutamine, 100 U/mL of penicillin, 100 µg/mL of streptomycin, and 0.2 mM of ascorbic acid. All these components were obtained from Invitrogen.

Scaffold fabrication:

3D microporous PCL scaffolds were fabricated using a rapid prototyping technique (Envisiontec GmbH, Germany). The PCL granulate was loaded into a metal syringe wrapped with a heating jacket. The copolymer was heated to 100 °C for about 45 min until it had reached the molten phase and could be dispensed through the extruder. A nitrogen pressure of 5 bar was applied on top of the metal cartridge to facilitate polymer strand extrusion from a Luer Lock stainless steel needle. A rectangle block model of 4 mm in height and 20 mm x 20 mm in area was plotted layer-by-layer and the architecture (0-90) was controlled by the Bioplotter CAD/CAM software. The layered fibers within the scaffolds were assembled in a woodpile structure having the following characteristic parameters: diameter (d_1) = 250 µm, spacing (d_2) = 650 µm, layer thickness (d_3) = 150 µm. From these values the theoretical porosity (~50%) of the scaffold was calculated, according to:

$$P = 1 - \frac{V_{Scaffold}}{V_{Cube}} = 1 - \frac{\pi}{4} \times \frac{d_1^2}{d_2 \times d_3} \qquad (7.1)$$

The 3D scaffolds used for the fabrication of the brush-supported protein gradients were cut from the rectangle block in order to obtain cylindrical shapes with a height and a diameter of 4 mm.

Activation of the polymer structures:

3D scaffolds were activated through immersion in a 5 mM isopropanol solution of ethylenediamine (EDA). The reaction was allowed to proceed for 10 minutes at room temperature. Scaffolds were then rinsed with ice-cold water and finally dried in a stream of nitrogen. The aminated PCL scaffolds were immersed into 20 ml of dry hexane and 20 µL of dry pyridine, to which 20 µL of 2-bromoisobutyryl bromide (BIBB) was added dropwise. The reaction mixture was gently stirred for 1 hour at room temperature to produce the 2-bromoisobutyrate-PCL surface (PCL-Br). PCL-Br scaffolds were later-on washed repeatedly with an ethanol/water (1/1, v/v) mixture and finally dried under a stream of nitrogen.

Atom transfer radical polymerization of OEGMA:

Purified OEGMA monomer (5 g, 9.5 mmol) and 2,2'bipyridine (81.7 mg, 0.52 mmol) were added to a water (5 ml) and methanol (1,26 ml) mixture. The solution was purged with argon for 30 minutes. CuCl (18.75 mg, 0.19 mmol) and $CuBr_2$ (2 mg, 0.009 mmol) were added into another reaction flask and also flushed with argon. Monomer, ligand and catalyst were then combined and stirred for other 30 minutes to facilitate the formation of the organometallic complex. This solution was then transferred into the flasks containing PCL-Br structures. The flasks were sealed with rubber septa and kept at room temperature under argon. Following 10 minutes of reaction time the substrates were removed from the polymerization solution, exhaustively rinsed with water to remove any unreacted compound and finally dried under a stream of nitrogen. From the detailed kinetics studies presented in Chapter 6 of SI-ATRP from PCL substrates, the average thickness of POEGMA brushes following 10 minutes of polymerization resulted as 15 nm. Before any further manipulation, PCL-POEGMA scaffolds were incubated in a 0.1 M aqueous EDTA solution overnight to remove any copper trace. In order to test the successful uniform grafting of POEGMA, functionalized scaffolds were finally placed in water containing vials (Figure S7). Pure PCL scaffolds floated due to their hydrophobic nature, while PCL-POEGMA scaffolds sank to the bottom of the vials.

Functionalization of PCL-POEGMA scaffolds:

POEGMA brushes on PCL scaffolds were activated by placing them in a dry DMSO solution containing 200 mM of DSC and DMAP. Later on, the samples were incubated in a protein solution containing either 0,4 μM fluorescently labeled BSA or 0,1 μM FN. To fabricate a radial gradient in protein concentration from the core to the outer surface of the 3D scaffolds, microdroplets of either 2 or 10 μL of PBS protein solutions were placed on the scaffold and let diffuse inside their core. After 10 minutes the scaffolds were extensively rinsed with milli-q water, blow-dried with a stream of N_2, cut over their mid-section and finally imaged with a fluorescent microscope. Reversed radial gradients from the outer surface of the scaffolds to the core were fabricated using microporous paper sheets soaked in PBS protein solutions as reservoirs. Soaked paper sheets were wrapped around the scaffolds and kept into close contact in order to let the protein solutions diffuse within the

scaffolds interior. Following 3 minutes of incubation the scaffolds were extensively rinsed with milli-q water, blow-dried with a stream of N_2, cut over their mid-section and finally imaged with a fluorescent microscope. Protein gradients along the axial direction of the scaffolds were fabricated by placing the DSC-activated PCL-POEGMA scaffolds on top of a micro porous paper sheet previously soaked with protein solutions. The contact between the scaffold's outer surface and the paper reservoir was assured by placing a weight of 7.5 g on top of the scaffolds. Following different diffusion times (30, 60 and 120 minutes) the scaffolds were extensively rinsed with milli-q water, blow-dried with a stream of N_2, cut over their mid-section and finally imaged with a fluorescent microscope.

Fluorescent microscopy:

Fluorescent micrographs of the scaffolds functionalized with labeled BSA species were recorded using a Nikon Eclipse E600. Fluorescein-labelled BSA was visualized using a filter with an excitation and emission wavelength of 475 nm and 530 nm, respectively. For Texas Red-labelled BSA, a filter with an excitation and emission wavelength of 559 nm and 630 nm, respectively, was used. Unmodified PCL scaffolds were used to set the exposure time and the gain values, such that the auto-fluorescence of the bare polymer was suppressed. Fluorescent pictures were taken from the vertical cross-section by cutting the scaffolds true the center along the z-axis. An assumption is made that the functionalization of the POEGMA layer is homogeneous and that the scaffold can be turned freely around the z-axis.

Cell culture and cell staining:

Human Mesenchymal Stem Cells (hMSCs) were cultured at 37 °C in a humidified atmosphere of 5 % carbon dioxide, using as culture medium α-MEM supplemented with 10 v/v % FBS, 2 mM L-Glutamine, 0.2 mM L-ascorbic acid 2-phosphate magnesium salt, 100 U/mL of penicillin and 10 µg/mL of streptomycin. The cells were seeded at a density of 500,000 cells in 40 µL per scaffold and after 4 hours, cell culture media was added. The scaffolds were kept in an incubator for one day. After the required culturing time, the cells were fixed with a 3.7 v/v % formaldehyde solution in PBS. Subsequently the cells were stained using a 1 % methylene blue solution in water and visualized using an optical microscope.

ALP activity:

To evaluate hMSCs differentiation toward the osteogenic lineage, ALP content was measured using a CDP star kit (Roche, Woerden, The Netherlands). For this purpose, 10 µL of sample was added to a well of a white 96-well plate and 40 µL of substrate (Disodium 2-chloro-5-(4-methoxyspiro {1,2-dioxetane-3,2'-(5'-chloro)tricycle[3.3.1.1^{3,7}] decan}-4-yl)-1-phenyl phosphate) was added. After 15 minutes incubation, luminescence was read using a spectrophotometer LS50B (Perkin Elmer). ALP activity was corrected for DNA content.

Gene expression:

For gene expression analysis the scaffolds were taken from the media, washed twice with PBS, cut into small pieces and placed in an Eppendorf containing 750 µL of TRIzol® (Invitrogen) and stored at -80ºC. In the case of partition analysis the gradient scaffolds were cut in order to separate the gradient zones and the 3 samples were located in the same vial prior the addition of the TRIzol®, in order to ensure the collection of enough RNA. RNA isolation was performed by using a Bioke RNA II nucleospin RNA isolation kit (Makerey-Nagel). 150 µL of $CHCl_3$ were added and the vials were vigorously mixed, followed by a centrifugation at 12000 g for 15 minutes at 4 ºC. The aqueous phase was transferred into a new tube and an equal amount of 70% ethanol was added. The mixture was transferred into a filter columns from the kit and the extraction was carried on by following the manufacturer's protocol. RNA concentration and purity was evaluated via an ND1000 spectrophotometer (Nanodrop Technologies, USA); cDNA was synthetized using iScript™ (BIO-RAD) according to manufacturer's protocol. Quantitative polymerase chain reaction (qPCR) was performed on the obtained cDNA by using the iQ SYBR®Gree Sipermix (BIO-RAD) and the primers listed in Table 7.2. PCR reaction was carried out on the MyiQ2 Two-Color Real-Time PCR Detection System (BIO-RAD) under the following conditions, the cDNa was denatured for 10 minutes at 95 ºC, followed by 45 cycles, consisting of 15 seconds at 95ºC, 15 seconds at 60ºC and 15 seconds at 72ºC. A melting curve was generated from each reaction to test the presence of primer dimers and a specific product. The cycle threshold (Ct) was calculated by the Bio-Rad iQ5 optical system software, in which the threshold was set in the lower log-linear region of the

fluorescent signal. Ct values were normalized by the B2M housekeeping gene and ΔCt ((average of Ct control)-Ct value). Results were expressed as fold induction in mRNA expression normalized to the gene expression of the non-functionalized scaffolds (PCL).

Table 7.2. Forward and reverse primers used for the analyses of specific genes.

Gene	Forward primer	Reverse primer
RUNX2	TGGTTACTGTCATGGCGGGTA	TCTCAGATCGTTGAACCTTGCTA
Osteocalcin	TGAGAGCCCTCACACTCCTC	CGCCTGGGTCTCTTCACTAC
Aggrecan	AGGCAGCGTGATCCTTACC	GGCCTCTCCAGTCTCATTCTC
SOX9	TGGGCAAGCTCTGGAGACTTC	ATCCGGGTGGTCCTTCTTGTG

7.5 References

1 Lutolf, M. P.; Hubbell, J. A., *Nat Biotech* **2005,** *23,* 47-55.

2 Genzer, J., *Annual Review of Materials Research* **2012,** *42,* 435-468.

3 Plummer, S. T.; Wang, Q.; Bohn, P. W.; Stockton, R.; Schwartz, M. A., *Langmuir* **2003,** *19,* 7528-7536.

4 Bhat, R. R.; Chaney, B. N.; Rowley, J.; Liebmann-Vinson, A.; Genzer, J., *Advanced Materials* **2005,** *17,* 2802-2807.

5 Bhat, R. R.; Tomlinson, M. R.; Genzer, J., *Journal of Polymer Science Part B-Polymer Physics* **2005,** *43,* 3384-3394.

6 Li, L.; Wu, J.; Gao, C., *Colloids and Surfaces B-Biointerfaces* **2011,** *85,* 12-18.

7 Burdick, J. A.; Khademhosseini, A.; Langer, R., *Langmuir* **2004,** *20,* 5153-5156.

8 Polizzotti, B. D.; Fairbanks, B. D.; Anseth, K. S., *Biomacromolecules* **2008,** *9,* 1084-1087.

9 Wylie, R. G.; Ahsan, S.; Aizawa, Y.; Maxwell, K. L.; Morshead, C. M.; Shoichet, M. S., *Nat Mater* **2011,** *10,* 799-806.

10 Sala, A.; Hanseler, P.; Ranga, A.; Lutolf, M. P.; Vörös, J.; Ehrbar, M.; Weber, F. E., *Integrative Biology* **2011,** *3,* 1102-1111.

11 Mosiewicz, K. A.; Kolb, L.; van der Vlies, A. J.; Martino, M. M.; Lienemann, P. S.; Hubbell, J. A.; Ehrbar, M.; Lutolf, M. P., *Nat Mater* **2013,** *12,* 1072-1078.

12 Shi, J.; Wang, L.; Zhang, F.; Li, H.; Lei, L.; Liu, L.; Chen, Y., *ACS Applied Materials & Interfaces* **2010,** *2,* 1025-1030.

13 Zou, B.; Liu, Y.; Luo, X.; Chen, F.; Guo, X.; Li, X., *Acta Biomaterialia* **2012,** *8,* 1576-1585.

14 Handarmin; Tan, G.; Sundaray, B.; Marcy, G.; Goh, E.; Chew, S., *Drug Deliv. and Transl. Res.* **2011,** *1,* 147-160.

15 Zhang, X.; Gao, X.; Jiang, L.; Qin, J., *Langmuir* **2012,** *28,* 10026-10032.

16 Milleret, V.; Simona, B. R.; Lienemann, P. S.; Vörös, J.; Ehrbar, M., *Advanced Healthcare Materials* **2014,** *3,* 508-514.

17 DeLong, S. A.; Gobin, A. S.; West, J. L., *Journal of Controlled Release* **2005,** *109,* 139-148.

18 DeLong, S. A.; Moon, J. J.; West, J. L., *Biomaterials* **2005,** *26,* 3227-3234.

19 Guarnieri, D.; De Capua, A.; Ventre, M.; Borzacchiello, A.; Pedone, C.; Marasco, D.; Ruvo, M.; Netti, P. A., *Acta Biomaterialia* **2010,** *6,* 2532-2539.

20 Wang, X.; Wenk, E.; Zhang, X.; Meinel, L.; Vunjak-Novakovic, G.; Kaplan, D. L., *Journal of Controlled Release* **2009,** *134,* 81-90.

21 Hutmacher, D. W., *Journal of Biomaterials Science-Polymer Edition* **2001,** *12,* 107-124.

22 Yang, S. F.; Leong, K. F.; Du, Z. H.; Chua, C. K., *Tissue Engineering* **2002,** *8,* 1-11.

23 Yeong, W.-Y.; Chua, C.-K.; Leong, K.-F.; Chandrasekaran, M., *Trends in Biotechnology* **2004,** *22,* 643-652.

24 Edmondson, S.; Osborne, V. L.; Huck, W. T. S., *Chemical Society Reviews* **2004,** *33,* 14-22.

25 Barbey, R.; Lavanant, L.; Paripovic, D.; Schuwer, N.; Sugnaux, C.; Tugulu, S.; Klok, H. A., *Chemical Reviews* **2009,** *109,* 5437-5527.

26 Tugulu, S.; Arnold, A.; Sielaff, I.; Johnsson, K.; Klok, H.-A., *Biomacromolecules* **2005,** *6,* 1602-1607.

27 Tugulu, S.; Silacci, P.; Stergiopulos, N.; Klok, H.-A., *Biomaterials* **2007,** *28,* 2536-2546.

28 Ma, H.; Hyun, J.; Zhang, Z.; Beebe, T. P.; Chilkoti, A., *Advanced Functional Materials* **2005,** *15,* 529-540.

29 Raynor, J. E.; Petrie, T. A.; García, A. J.; Collard, D. M., *Advanced Materials* **2007,** *19,* 1724-1728.

30 Moroni, L.; Klein Gunnewiek, M.; Benetti, E. M., *Acta Biomaterialia* **2014,** *10,* 2367-2378.

31 Kobayashi, M.; Terayama, Y.; Yamaguchi, H.; Terada, M.; Murakami, D.; Ishihara, K.; Takahara, A., *Langmuir* **2012,** *28,* 7212-7222.

32 Marletta, G.; Ciapetti, G.; Satriano, C.; Perut, F.; Salerno, M.; Baldini, N., *Biomaterials* **2007,** *28,* 1132-1140.

33 Diamanti, S.; Arifuzzaman, S.; Elsen, A.; Genzer, J.; Vaia, R. A., *Polymer* **2008,** *49,* 3770-3779.

34 Chiang, E. N.; Dong, R.; Ober, C. K.; Baird, B. A., *Langmuir* **2011,** *27,* 7016-7023.

35 Navarro, M.; Benetti, E. M.; Zapotoczny, S.; Planell, J. A.; Vancso, G. J., *Langmuir* **2008,** *24,* 10996-11002.

36 Yuan, S.; Xiong, G.; Wang, X.; Zhang, S.; Choong, C., *Journal of Materials Chemistry* **2012,** *22,* 13039-13049.

37 Yuan, S.; Xiong, G.; Roguin, A.; Choong, C., *Biointerphases* **2012,** *7,* 1-12.

38 Ren, T.; Mao, Z.; Guo, J.; Gao, C., *Langmuir* **2013,** *29,* 6386-6395.

Outlook

This Thesis described the fabrication and application of bio-active polymer brush layers “grafted-from” polyester-based 2D and 3D supports. Brush coatings were used to spatially control the adhesion and differentiation of human Mesenchymal Stem Cells (hMSCs). In this Chapter, possible future strategies in the application of brush coatings for cell manipulations, inspired by this work, will be summarized.

In addition to the reported brush compositions, alternative chemistries could be investigated as functionalizable coatings for tissue engineering (TE) supports. The previous Chapters aimed on studying cellular behavior on poly(oligo(ethylene glycol) methacrylate) (POEGMA) brushes. However, other systems could improve bio-conjugation and enhance the effect of the immobilized biological cues. As an example, poly(2-hydroxyethyl methacrylate) (PHEMA) could represent a potential candidate for the synthesis of brush-coated scaffolds. This polymer presents an anti-biofouling character in the brush form which is comparable to POEGMA. In addition, the surface concentration of functionalizable side-chain functions is significantly larger than in the case of POEGMA brush coatings.[1] The grafting density of the POEGMA brush layers discussed in the previous Chapters was around 0.35 chains/nm^2 while for a PHEMA brush analogue a grafting density of around 0.7 chains/nm^2 could be expected.[2] This 2 time increase in density is related to the longer side chains in POEGMA brushes in comparison to PHEMA. The composition of POEGMA and PHEMA is very similar and all the proposed methods could be easily transferred between the two. Thus, without altering the synthetic procedures and by just changing the brush composition, the concentration of covalently bound protein on the surface could be increased 2 times, when assuming similar protein coupling efficiencies.

Throughout the Thesis, cell adhesion and differentiation studies were performed using either fibronectin (FN) or growth factors (GFs) (like bone morphogenetic protein, BMP-2, or transforming growth factor, TGF-β3). However, a combination of cell adhesive and a cell differentiating protein was not tested.

Although GFs showed to be active when covalently attached to a surface, additional immobilization of FN might enhance the differentiation of hMSCs due to the increase in surface adhering cells[3-4]. This could also improve the formation of active GFs gradients. Brush-supported gradients of GFs on 3D scaffolds were not achieved due to a significantly lower cell adhesion compared to homogeneously covered supports. Increasing the concentration of the GF solution and including cell adhesive proteins could further ease the preparation of 3D gradients.

The 3D porous structures reported in Chapter 7 were fabricated via rapid prototyping. However, also other porous structures could be applied as solid supports in order to control the capillary force and the protein coupling efficiency. For example, smaller pores would increase the capillary pressure, increasing the wetting rate within the 3D supports. Although a wide range of fiber diameters and pore sizes can be obtained using various techniques (e.g. electrospinning), ranging from tens of nanometers to hundreds of microns,[5] not all porous scaffolds are usable. As the pore diameter becomes smaller, the polymer brush dynamics will be significantly altered in comparison to a planar surface.[6] The amount of chain ends will decreases while the monomer density of the swollen brush layer will increase in the direction of the pore center.[7] This will negatively influence the protein coupling efficiency of the brush layer. For decreasing fiber diameter, however, the opposite trend will be observed.[8] In this Thesis, the scaffolds used had the following characteristic parameters: diameter = 250 µm, spacing = 650 µm, layer thickness = 150 µm. Taking into consideration the above-mentioned polymer dynamics both the diameter of the fibers[8] and the pores[7] of these scaffolds are significantly large and every part of the structure can thus be considered as a planar surface.

Additionally, the capillary action inside the 3D porous scaffolds can be controlled by varying the wetting ability of a polymer brush layer. In the last months of this PhD project, both POEGMA and poly(methacrylic acid) (PMAA) coatings were grafted from the surface of porous constructs and the flow of water containing a fluorescent dye was monitored through the 3D structure using a fluorescent microscope. Both the static contact angle and the interfacial energy of PMAA (31°, 66.6 mN/M)[9] with air is slightly higher compared to that of POEGMA (44°, 61.2 mN/m)[9] and therefore a faster wetting of the PMAA coating was expected. The chemical composition between the two brush layers (PMAA and POEGMA)

significantly differs. Therefore, to systematically investigate the effect of surface energy on the capillary action it would be of interest to have a surface with tunable contact angle but identical chemistry. In 2011, such a system was presented by Spencer and coworkers.[10] By varying the crosslink density within a poly(acrylamide) (PAAm) hydrogel brush layer the static water contact angle could be adjusted from 22° to complete wetting. With this system it would be possible to control the surface wetting and thus the flow inside these 3D open porous structures. In addition, It would be of interest to reversibly switch the surface energy of the brush layer. For instance by grafting a poly(*N*-isopropyl acrylamide) (PNIPAM) brush layer. PNIPAM is a well-known polymer that can change its hydrophilicity at temperatures below and above the lower critical solution temperature (LCST). Bunker and coworkers showed that the advancing contact angle of PNIPAM changes from around 85° above to around 67° below the LCST.[11]

References

1 Tugulu, S.; Silacci, P.; Stergiopulos, N.; Klok, H.-A., *Biomaterials* **2007,** *28,* 2536-2546.

2 Yoshikawa, C.; Goto, A.; Tsujii, Y.; Fukuda, T.; Kimura, T.; Yamamoto, K.; Kishida, A., *Macromolecules* **2006,** *39,* 2284-2290.

3 Liu, L.; Ratner, B. D.; Sage, E. H.; Jiang, S., *Langmuir* **2007,** *23,* 11168-11173.

4 Kisiel, M.; Martino, M. M.; Ventura, M.; Hubbell, J. A.; Hilborn, J.; Ossipov, D. A., *Biomaterials* **2013,** *34,* 704-712.

5 Hollister, S. J., *Nature Materials* **2005,** *4,* 518-524.

6 Dimitrov, D. I.; Milchev, A.; Binder, K.; Heermann, D. W., *Macromolecular Theory and Simulations* **2006,** *15,* 573-583.

7 Dimitrov, D. I.; Milchev, A.; Binder, K., *The Journal of Chemical Physics* **2006,** *125,* 1-15.

8 Wijmans, C. M.; Zhulina, E. B., *Macromolecules* **1993,** *26,* 7214-7224.

9 Kobayashi, M.; Terayama, Y.; Yamaguchi, H.; Terada, M.; Murakami, D.; Ishihara, K.; Takahara, A., *Langmuir* **2012,** *28,* 7212-7222.

10 Li, A.; Benetti, E. M.; Tranchida, D.; Clasohm, J. N.; Schönherr, H.; Spencer, N. D., *Macromolecules* **2011,** *44,* 5344-5351.

11 Huber, D. L.; Manginell, R. P.; Samara, M. A.; Kim, B.-I.; Bunker, B. C., *Science* **2003,** *301,* 352-354.

Summary

The aim of this PhD Thesis was the development of polymer brush-based multi-dimensional gradient platforms for tissue engineering. This objective was achieved through the fabrication and application of different coatings “grafted-from” biodegradable polyester-based supports featuring both 2D and 3D scaffolds. A specific focus was devoted to the preparation of brush coatings with controllable properties (e.g. cell adhesion, flexibility and bioactivity) synthesized by surface-initiated atom transfer radical polymerization (SI-ATRP). Thermoresponsive poly(*N*-isopropyl acrylamide) (PNIPAM) layers were applied to thermally control cell adhesion, while poly(oligo(ethylene glycol) methacrylate) (POEGMA)-coated supports were used to vary the bioactivity of the coating via fibronectin (FN) and growth factors (GFs) conjugation.

Chapter 1 provided a short introduction to the topics discussed in this Thesis and the motivation for the reported research. The scope of this Thesis is also presented in this first section.

In **Chapter 2** a literature overview on the application of polymer brush platforms for controlling adhesion and differentiation of different cell types was reported. The fabrication of thermoresponsive and bio-conjugated brush coatings were highlighted as supports for tissue engineering. In the last section, the application of these polymer brush coatings for the fabrication of supports for tissue engineering was presented.

As an additional introductory Chapter, a literature overview on 2D and 3D supports presenting gradients in protein concentration was discussed in **Chapter 3**. The fabrication methods to produce protein gradients on flat substrates and on hydrogel surfaces were reviewed followed by the formation of protein gradients within 3D hydrogel supports and other porous polymeric scaffolds. Additionally, the employment of protein gradients for cell adhesion, migration and differentiation applications was discussed.

In **Chapter 4** surface-initiated polymerization of NIPAM from poly(ε-caprolactone) (PCL) flat films was presented. The surface of PCL was activated by

aminolysis and subsequent initiator coupling which allowed surface-initiated atom transfer radical polymerization (SI-ATRP) of NIPAM. Cells showed to attach, spread and grow on PNIPAM modified surface at 37°C. Cooling the media to 25°C released the cells in the form of sheets and showed to be viable after being harvested when cultured on tissue culture plates. Additionally, free-standing PCL films with a PNIPAM coating on one side proved the thermoresponsive activity by the bending and stretching behavior.

Chapter 5 focused on SI-ATRP of POEGMA from thin PCL films presenting different semicrystalline structures. By varying PCL thermal processing, spherulitic size and density was controlled between sub-micron (up to 1 μm) to several hundreds of microns. The different micro-/nano-topologies obtained were shown to alter the behavior of hMSCs upon attachment and spreading. Sub-100 nm, FN-functionalized POEGMA brush coatings grafted from the different PCL films were finally demonstrated to efficiently decouple substrate topology and cell adhesion. Namely, cells showed to respond irrespective to the underlying PCL topology when different spherulite size/density were uniformly coated with sub-100 nm thick POEGMA-FN brush coatings.

Chapter 6 focused on the behavior of stem cells adhering on a POEMGA brush layer with various grafting densities and chain lengths (molecular weight) grafted from PCL. These substrates were obtained by spin-coating PCL and varying the initiator coverage or the polymerization time. Cell shape analysis showed that cells attached to these POEGMA coatings adopted different morphologies responding to variations in grafting density and brush thickness. Brush layers with low thicknesses (sub-20 nm) or low densities (0.035 chains/nm^2) were shown to allow hMSCs adhesion, while thicker (60 nm) or dense (0.341 chains/nm^2) layers showed cell-repulsive properties due to the efficient resistance by dense and long brushes against protein adsorption. Linear gradients of POEGMA brush thickness were conjugated with fibronectin (FN) to obtain cell adhesive films. Cells adhered uniformly on the gradient and the cell shape showed to be independent of the POEGMA thickness. On the contrary, differences in formation and morphology of focal adhesion (FA) complexes were related to the different brush-ligand flexibilities across the gradient samples.

In **Chapter 7**, a novel method to introduce multi-directional variations of (bio)chemical environments inside 3D porous structures is presented. The hydrophilic nature and the high functionality of POEGMA was coupled to a structured scaffold to trigger diffusion and subsequent covalent immobilization of proteins from solutions. This allowed the fabrication of 3D axial and radial protein gradients with tailored morphologies. Gradients of brush-supported FN controlled the immobilization of human mesenchymal stem cells (hMSCs) in spatially determined cultures. Furthermore, the application of growth factors coupled to POEGMA-coated PCL scaffolds proved as an effective strategy to induce hMSCs differentiation within these 3D environments. The application of multidirectional gradients of brush-supported GFs on these 3D porous scaffolds will have the potential to regenerate complex interfaces between different tissue types, such as bone and cartilage.

Samenvatting

Het doel van dit Proefschrift was het ontwikkelen van multidimensionale gradiënt platforms voor weefsel engineering, gebaseerd op polymeerborstels. Dit werd bereikt door de fabricage en het toepassen van verschillende coatings gegroeid van zowel 2D als 3D biologisch afbreekbare structuren van polyester. Specifiek werd er aandacht besteed aan het produceren van coatings met controleerbare eigenschappen (bijvoorbeeld celadhesie, flexibiliteit, en bio-activiteit) via 'Surface-Initiated Atom Transfer Radical Polymerization' (SI-ATRP). Thermoresponsieve poly(*N*-isopropyl acrylamide) (PNIPAM) borstels werden toegepast voor het reguleren van celadhesie via temperatuurverandering, terwijl poly(oligo(ethylene glycol) methacrylate) (POEGMA)-gecoate structuren werden toegepast voor het variëren van de bio-activiteit door middel van het toevoegen van fibronectine (FN) en verschillende groeifactoren (GF).

Hoofdstuk 1 geeft zowel een korte introductie over de onderwerpen die worden besproken in dit Proefschrift als de motivatie voor het onderzoek. De context en de inhoud van dit Proefschrift worden ook in het eerste deel gepresenteerd.

In **Hoofdstuk 2** wordt een literatuuroverzicht gegeven over het toepassen van polymeerborstels voor het sturen van de adhesie en differentiatie van verschillende celtypes. Het fabriceren van thermoresponsieve en bio-geconjugeerde lagen als coatings voor weefsel engineering wordt met name besproken. In het laatste gedeelte wordt de toepassing van polymeerborstels als coating voor weefsel engineering gepresenteerd.

Als extra inleidend hoofdstuk wordt een literatuuroverzicht over 2D en 3D gradiënten in eiwitconcentratie besproken in **Hoofdstuk 3**. De fabricagemethoden om eiwitgradiënten te produceren op vlakke substraten en hydrogel oppervlakken worden beschreven, gevolgd door de vorming van eiwitgradiënten in 3D hydrogel dragers en andere poreuze polymere structuren. Daarnaast wordt de toepassing van deze eiwit- gradiënten voor celadhesie, -migratie en -differentiatie besproken.

In **Hoofdstuk 4** wordt de oppervlakte-geïnitieerde polymerisatie van NIPAM vanaf vlakke poly(ε-caprolacton) (PCL) films gepresenteerd. Het oppervlak van PCL werd geactiveerd door middel van aminolyse en initiatorkoppeling waarna SI-ATRP van NIPAM kon worden uitgevoerd. Cellen hechten, verspreiden en groeien op PNIPAM gemodificeerde oppervlakken bij 37°C. Door afkoelen van het medium tot 25°C worden de cellen als complete levensvatbare films verwijderd. Daarnaast vertoonden vrijstaande PCL films met aan één kant een PNIPAM coating thermoresponsief gedrag zoals bleek uit het buigen en strekken van de film.

Hoofdstuk 5 richt zich op de SI-ATRP van POEGMA vanaf dunne PCL films met verschillende semikristallijne structuren. Door het variëren van de thermische verwerking van PCL kon de sferulietgrootte en -dichtheid worden ingesteld tussen sub-micrometer (tot 1 µm) en enkele honderden micrometers. De verschillende verkregen micro-/nano structuren veranderden de celadhesie en spreiding. Echter, sub-100 nm, FN-gefunctionaliseerde POEGMA coatings, gegroeid vanaf de verschillende PCL films, maakten het mogelijk om substraat topologie en celadhesie te ontkoppelen. Wanneer de PCL films gelijkmatig werden bedekt met sub-100 nm dikke POEGMA-FN coatings, bleken cellen niet meer te reageren op variaties in topologie van de onderliggende PCL films, ongeacht sferulietgrootte en -dichtheid van deze films.

Hoofdstuk 6 richt zich op het gedrag van stamcellen die zich hechten op POEGMA coatings met verschillende borsteldichtheden en ketenlengtes (molecuulgewicht) gegroeid vanaf PCL. Deze substraten werden verkregen door het spin-coaten van PCL en door de initiatordichtheid of de polymerisatietijd te variëren. Analyse van de celvorm toonde aan dat de morfologie van de cellen afhankelijk is van de borsteldichtheid en -dikte. Borstels met een lage dikte (sub-20 nm) of met lage dichtheden (0,035 ketens/nm^2) toonden aan dat hMSCs adhesie mogelijk is, terwijl de dikkere (60 nm) of dichte (0,341 ketens/nm^2) polymeerborstels cel-afstotende eigenschappen bezaten wat toe te schrijven is aan de hoge weerstand van de dichte en lange borstels tegen eiwitadsorptie.

Lineaire gradiënten in POEGMA borsteldikte werden gefunctionaliseerd met fibronectine (FN) om coatings te verkrijgen waaraan cellen kunnen hechten. Cellen hechtten zich gelijkmatig op de gradiënten en de celvorm bleek onafhankelijk te zijn van de POEGMA dikte. Echter, verschillen in de vorming en morfologie van

focale adhesie (FA) complexen hingen samen met de verschillende borstel-ligand flexibiliteiten over de gradiënt substraten.

In **Hoofdstuk 7** werd een methode gepresenteerd voor het introduceren van multi-directionele variaties in (bio)chemische omgeving in 3D poreuze structuren. De hydrofiele aard en de hoge functionaliteit van POEGMA werd gekoppeld aan een gestructureerde support wat leidde tot de diffusie en de daaropvolgende covalente immobilisatie van eiwitten uit oplossingen. Hierdoor werd de fabricage van 3D-axiale en radiale eiwitgradiënten mogelijk gemaakt. Gradiënten van FN-gemodificeerde borstels stuurden de adhesie van menselijke mesenchymale stamcellen (hMSCs) in deze ruimtelijke structuren. Bovendien werd bewezen dat het gebruik van groeifactoren gekoppeld aan POEMGA-coatings een effectieve strategie is om hMSCs te differentiëren binnen deze 3D structuren. De toepassing van multi-directionele gradiënten van GF gemodificeerde borstels in deze 3D poreuze structuren maakt het mogelijk om complexe grensvlakken tussen verschillende weefsels, zoals bot en kraakbeen, te regenereren.

Acknowledgements

After 14 years of different studies, an "*Unexpected Journey*" has finally come to an end. A journey that has been marked by choosing the road I said I never anticipated. However, by meeting the right people at the right moment, I managed to achieve something which I never expected. So here, on these additional few pages of the Thesis, I would like to express my gratitude to those how made this journey possible and a success.

Firstly, I would like to thank my promotor, Prof. G. Julius Vancso, who gave me the chance to work at MTP. Dear Julius, thank you very much for your confidence, and the freedom you gave me to find my own way. You also managed to challenge me from time to time. A few months in my PhD, you trusted me to supervise a student and after a year you send me to a conference for a lecture. All this allowed me to build my self-confidence and made me the researcher I am today. I also would like to thank you for all your help and support to find my way after the PhD.

The second person I want to thank is Dr. Edmondo Benetti, who supervised me during these last 4 years. Dear Eddy, my friend, thank you very much for everything. When Julius told me that you, the *Master of Polymer Brushes*, would join the team, I was already enthusiastic. And by working with you, my respect even increased, as our collaboration seemed natural and it felt like we were equal, instead of you being my supervisor. The many beer/sambuca/limonchello nights in the city center I will never forget and I sincerely hope we will be working together again, someday in the future.

Another person I want to thank is, Dr. Lorenzo Moroni. Dear Lorenzo, thank you very much for all your support these years. From our first meeting, you managed to trigger my biological interest, which was lost after a lot of years working solely in chemistry. Just by talking to you that day, I knew that this project would fit me perfectly. I also would like to thank you for your open door policy, which allowed me to pass by whenever there were problems.

These last years I had the opportunity to collaborate with some inspiring scientists. Firstly, I would like to thank Prof. Lucio Isa for his help and support with the fluorescent microscopy measurements. I would like to thank Gerard Kip for his help with the XPS measurements and both Dr. Stefan Kooij and Dr. Wojciech Ogieglo for their support with the ellipsometry measurements. A special thanks to Dr. Xiaofeng Sui. Dear Xiaofeng, one week in my PhD you dragged me into the lab and within a few months there was the first manuscript. I thank you for all your help in the first months of the PhD.

I would like to thank my paranymfs and friends, Andrea Di Luca and Lionel Dos Ramos. It is an honor to have you both there on the stage with me. Dear Andrea, you were my partner in crime on this journey as we started and we'll finish this project together. During the ups and downs of a PhD life and the project, you were always the one I could go to and ventilate my thoughts. Dear Lionel, you were my first student to supervise, while I was not ready for it. And afterwards you became my office mate. You were always there to help me and talk about everything. You also managed to improve my idea about the "French" cuisine and food in general by your amazing cooking skills. Dear Andrea and Lionel, I sincerely value your friendships and I wish you both all the best for the future.

Additionally I would like to thank my other office mate, Andreas Schulz. Dear Andy, my friend, you brought another dimension to the group and especially to the office. I will never forget the evening I had to "open" the front door of your apartment with a paperclip. I wish you all the best for the last years of your PhD and for the future.

Office CR4251 deserves a very special thank you. Clemens Padberg, you are the engine of the group and without you, the group would be lost. You were able to fix and arrange everything. Thank you very much for all your support, both scientifically and personally. Dr. Joost Duvigneau, you were my supervisor during my Master project and you managed to convince me to think about a PhD. You were always there to talk to. Thank you very much Joost for everything.

I'm very grateful to Dr. Mark Hempenius. Dear Mark, you are the chemical master mind of the group and I thank you very much for all the help in the lab and for correcting my Dutch summary. A special thank you for Geneviève Rietveld, who

designed the beautiful cover of this Thesis. Dear Gen, thank you for all the small chats in the morning and for finding the perfect apartment where I live now.

During the last 4 years, I had the opportunity to collaborate with multiple students; Thomas van der Horst, Hermannes Z. Bollemaat, Marta Da Pian and Marco Cirelli. Dear Thomas, your contributions to the variations in brush lengths and grafting density in chapter 6 laid the foundation for all the other research. Dear Hermen, your contributions to chapter 7 are exceptional and you deserve the Cum Laude. I will always remember our table soccer matches, as you were the one to make me loose, every time. Dear Marta, you were only for a few month in Enschede, but you managed to drag me out of my house and visit the Netherlands. Master Cire! Your drive to achieve the best in the lab and in life is inspiring. I will never forgot our whisky nights in the Vestingbar. I wish all of you, all the luck for the future and all the best in life.

I would like to especially thank all the other MTP colleagues for their support and for making the PhD life relatively easy. The staff members, Sissi de Beer and Peter Schön. Bram Zoetebier, Bart Kieviet, Xueling Feng, Hairong Wu, Anne Corine IJzer, Kaihuan Zhang, Shanqiu Liu, Yunlong Yu, Aysegul Cumurcu, Wilma de Groot, Edit Kutnyánszky, Anika Embrechts and Qi Chen. And all the bachelor and master students who past the group during these years. Dear Bram and Bart, thank you both for making the life in the lab a blast and of course for letting me win at table soccer (this really boosted my ego ☺). Dear Xueling, thank you for all the small talks these last months about finishing the Thesis and the PhD.

A special thank you goes out to my previous supervisors and colleagues at Artecs B.V.: Dr. Wilco Zuiderduin, Dr. Ype van der Zijpp, Niels Kolkman and Kai Braspenning. I did my MBO internship at their company and they were the first to introduce me to the world of polymer science. Thank you very much for being the initiators of this long and interesting journey.

Many thanks to all the other friends that contributed these years, one way or another, in making this PhD a success. Bas ten Donkelaar, thank you for all the coffee/beer/whisky moments. Kaspar Groot Kormelinck, thank you for keeping me with both feed on the ground. Jan Geert Bruggink, thank you for the awesome road trip. And of course, my gratitude goes out to everybody who I got to know over the years and who I might have forgotten to mention.

Als laatste en als meest belangrijke wil ik graag mijn familie bedanken. Paps, Mams, Marleen, Bart en de klein Laure. Jullie onvoorwaardelijk steun tijdens deze lange en soms moeizame reis hebben mij er doorheen gesleept. Ik kon altijd langskomen om mijn vreugde en frustraties met jullie te delen. Paps en Mams, mijn lieve ouders, zonder jullie steun en liefde was ik nooit zo ver gekomen! Marleen, mijn lieve grote zus, jij bent mijn grote voorbeeld! Laure, mijn lieve kleine nichtje, blijf voor altijd zo lief! Ik weet dat ik het niet zo vaak zeg, maar ik hou van jullie.

Michel

About the author

Michel Klein Gunnewiek was born on the 16th of May, 1985 in Eibergen, the Netherlands. He obtained his MBO degree in June 2005 as a chemical laboratory assistant from the ROC institute in Hengelo. As part of the internships, he worked for 5 months both at Thales Nederland and at Artecs B.V.

In September 2005 he started at the Saxion Hogescholen in Enschede to obtain a Bachelor's degree in Chemistry. In September 2007 he continued his Bachelor project at Vernay Europe B.V. The subject of his Bachelor Thesis was on Low temperature gas plasma surface modification of fluorosilicone rubber.

After obtaining his Bachelor degree, he continued with his Master in chemical engineering in the direction of Chemistry and Technology of Materials (CTM) at the university of Twente. His research project was performed in the Materials Science and Technology of Polymer (MTP) group headed by Prof. G.J. Vancso. He worked on Nanoscale thermal analysis of thin polymer films which was issued as a chapter in the PhD Thesis of Dr. Joost Duvigneau.

Starting from January 2011, Michel continued as a PhD student under supervision of Prof. G.J. Vancso, Dr. L. Moroni and Dr. E.M. Benetti. His research project was funded by the Dutch Technology Foundation STW, which is part of the Netherlands Organisation for Scientific Research (NWO).

In 2014, he got the opportunity to do research at the Eidgenössische Technische Hochschule (ETH) Zürich in Switzerland. During this period he worked together with Prof. Dr. Lucio Isa on fluorescent imaging of labeled proteins which were attached to and flowing through polymer brush modified 3D porous structures. Parts of the obtained results are presented in this Thesis.

List of publications:

X. Sui, A. Di Luca, M. Klein Gunnewiek, E. S. Kooij, C. A. van Blitterswijk, L. Moroni, M. A. Hempenius, G. J. Vancso; Stability and Cell Adhesion Properties of Poly(N-isopropylacrylamide) Brushes with Variable Grafting Densities, *Australian Journal of Chemistry* **2011**, *64*, 1259-1266.

M. Klein Gunnewiek, A. Di Luca, X. Sui, C. A. van Blitterswijk, L. Moroni, G. J. Vancso; Controlled Surface Initiated Polymerization of N-Isopropylacrylamide from Polycaprolactone Substrates for Regulating Cell Attachment and Detachment, *Israel Journal of Chemistry* **2012**, *52*, 339-346.

N. Sanandaji, L. Ovaskainen, M. Klein Gunnewiek, G.J. Vancso, M.S. Hedenqvist, S. Yu, L. Eriksson, S.V. Roth, U.W. Gedde; Unusual crystals of poly(ε-caprolactone) by unusual crystallisation: the effects of rapid cooling and fast solvent loss on the morphology, crystal structure and melting, *Polymer* **2013**, 54, 1497-1503.

M. Klein Gunnewiek, E.M Benetti, L. Moroni, G.J. Vancso; Thin Polymer Brush Decouples Biomaterial's Micro-/Nano-Topology and Stem Cell Adhesion, *Langmuir* **2013**, 29, 13843-13852.

L. Moroni, M. Klein Gunnewiek, E.M Benetti; Polymer brush coatings regulating cell behavior: Passive interfaces turn into active, *Acta Biomaterialia* **2014**, 10, 2367-2378

M. Klein Gunnewiek, A. Di Luca, Hermen Z. Bollemaat, C.A. van Blitterswijk, G.J. Vancso, L. Moroni, E.M Benetti; Creeping Proteins in Microporous Structures: Polymer Brush-Assisted Fabrication of 3D Gradients for Tissue Engineering, *Advanced Healthcare Materials* **2015**, ACCEPTED